# INVESTIGATION OF PLASMONIC GOLD NANOSTRUCTURES FOR ENHANCEMENT OF ORGANIC SOLAR CELLS

**SOPIT PHETSANG**

**DOCTORAL PROGRAM IN ELECTRICAL AND INFORMATION ENGINEERING**

**GRADUATE SCHOOL OF SCIENCE AND TECHNOLOGY**

**NIIGATA UNIVERSITY**

**ABSTRACT**

Organic solar cells (OSCs) are particularly promising candidates for next-generation renewable power sources. Although the OSCs provide excellent power conversion efficiency (PCE), a short carrier diffusion length limits the photoactive layer thickness, resulting in a low light absorption and efficiency in the devices. Light management plays an important role for light harvesting enhancement in OSCs. The utilization of advanced nanomaterials and the design of device structures for broadening light absorption have gained attraction in order to achieve great photovoltaic performances in OSCs. Additionally, plasmonic nanostructures have been extensively used to increase light trapping and broaden optical absorption in photovoltaic devices. In this study, gold nanoparticles (AuNPs) with different sizes and shapes, consisting of gold quantum dots (AuQDs), gold nanospheres (AuNSs), and gold nanorods (AuNRs) were included within the devices to improve the photovoltaic performances and the synergistic effects from the combination of plasmonic nanostructures (AuQDs/AuNPs, AuQDs/metallic grating, and AuNSs:AuNRs/metallic grating) on the OSCs performances were also investigated.

Three work chapters are demonstrated. Firstly, the incorporation of AuQDs and plasmonic AuNPs for OSCs enhancement is described. An important challenge in this part is to apply AuQDs to organic light harvesting systems. AuQDs absorb the UV light and generate visible light as fluorescence emission while AuNPs provide the localized surface plasmon resonance effect. The combination of AuQDs and AuNPs into the OSCs system can enhance the photovoltaic performances due to the absorption of the fluorescence from the AuQDs and energy/electron transfer from the AuQDs to the AuNPs, leading to a 13% improvement in the PCE. Secondly, an enhancement of OSCs performances by incorporating AuQDs together with metallic grating nanostructure is demonstrated. Extending absorption in UV regions by AuQDs is proposed and the fluorescence originated from AuQDs could act as

additional light source, enhancing a high photocurrent in the developed device. Moreover, grating-coupled surface plasmon resonance (GCSPR) can increase the optical absorption path length of the devices. Interestingly, the synergistic effect of AuQDs and GCSPR in the developed OSCs exhibited better electrical and optical properties, leading to an enhancement of photocurrent with PCE improvement of approximately 20%. Finally, effect of AuNSs/AuNRs hybrid with metallic grating nanostructure for OSCs enhancement is investigated. The synergistic effect of the multi-LSPR and GCSPR is expected to enhance the optical path length within the devices. AuNSs/AuNRs hybrid were added in a hole transport layer. As compared to reference cell, the developed OSCs exhibited higher photovoltaic performances by increasing both of short-circuit current density ($J_{sc}$) and PCE with large enhancements of *ca*. 16.23% and 14.06%, respectively. The results suggest that the incorporation of metallic nanostructures inside the developed photovoltaic devices can improve the OSCs efficiency by increasing broadband absorption and improving electrical property. Therefore, the proposed OSCs could be further developed in practical application.

KEYWORDS: Organic solar cells, Photovoltaic devices, Gold nanoparticles, Gold quantum dots, Plasmonic nanostructures, Grating-coupled surface plasmon resonance, Nanoimprinting

# ACKNOWLEDGEMENTS

The author would like to express her deepest sincere gratitude to Assoc. Prof. Dr. Akira Baba, her dissertation advisor, and Asst. Prof. Dr. Kontad Ounnunkad for their giving great opportunity, kind-precious supervision, insightful suggestion, practical training, continual encouragement, assistance and financial support throughout this research work and helping her to succeed in this dissertation.

She is sincerely grateful to Prof. Dr. Keizo Kato, Prof. Dr. Kazunari Shinbo, Asst. Prof. Dr. Chutiparn Lertvachirapaiboon, and Prof. Dr. Futao Kaneko from Niigata University for impressive encouragement, valuable suggestion, practical training, and assistance. She also would like to thank Asst. Prof. Dr. Pitchaya Mungkornasawakul from Chiang Mai University for valuable suggestions, impressive encouragement, and kind supervision.

She gratefully acknowledges Center for Transdisciplinary Research, Niigata University, Global Circus Program from Japan Society for the Promotion of Science (JSPS), Graduate School of Science and Technology Niigata University, and Human Resource Development in Science Project (Science Achievement Scholarship of Thailand, SAST) for financial supports.

She would like to thank her friends and colleagues for their help and warm friendship. Finally, the author also gratefully acknowledges her beloved family for their unconditional love, understanding, encouragements and supporting throughout the period of her study. She would like to thank those whose names are not listed here, who have contributed to the success of this study.

Sopit Phetsang

## CONTENTS


Page

ABSTRACT ii
ACKNOWLEDGMENTS iv
CONTENTS v
LIST OF TABLES vii
LIST OF FIGURES viii
LIST OF ABBREVIATIONS xiv

**CHAPTER I**
**INTRODUCTION** 1

1.1 RESEARCH BACKGROUND 2
1.1.1 Organic solar cells (OSCs) 2
1.1.2 Enhancement of light-harvesting in OSCs 6
1.1.2.1 Plasmonic nanostructures 6
1.1.3 Fluorescence emission of gold quantum dots 9
1.2 OBJECTIVES 10
1.3 SCOPE OF THE DISSERTATION 10
1.4 REFERENCES 11

**CHAPTER II**
**Investigation of Gold Quantum Dot/Plasmonic Gold Nanoparticle System Incorporated into Organic Solar Cells**

ABSTRACT 17
2.1 INTRODUCTION 18
2.2 EXPERIMENTAL SECTION 20
2.3 RESULTS AND DISCUSSION 21
2.4 SUMMARY 37
2.5 REFERENCES 38

**CHAPTER III**

**Investigation of Gold Quantum Dots/Metallic Grating System Incorporated into Organic Solar Cells**

ABSTRACT 44
3.1 INTRODUCTION 45
3.2 EXPERIMENTAL SECTION 47
3.3 RESULTS AND DISCUSSION 50
3.4 SUMMARY 69
3.5 REFERENCES 69

**CHAPTER IV**

**Investigation of Gold Nanospheres-Gold Nanorods Hybrid/Metallic Grating Incorporated into Organic Solar Cells**

ABSTRACT 79
4.1 INTRODUCTION 80
4.2 EXPERIMENTAL SECTION 82
4.3 RESULTS AND DISCUSSION 85
4.4 SUMMARY 101
4.5 REFERENCES 102

**CHAPTER V**

**CONCLUSIONS** 107
RECOMENDATION FOR FUTURE WORK 108

**APPENDICES**

APPENDIX A 110
APPENDIX B 114
APPENDIX C 118
VITAE 120

## LIST OF TABLES

Page

**CHAPTER II**

**Investigation of Gold Quantum Dot/Plasmonic Gold Nanoparticle System Incorporated into Organic Solar Cells**

Table 2.1 Photovoltaic parameters of the developed OSCs 29

**CHAPTER III**

**Investigation of Gold Quantum Dots/Metallic Grating System Incorporated into Organic Solar Cells**

Table 3.1 Photovoltaic parameters of the OSCs incorporated different types of AuQDs with and without metallic grating nanostructures under solar light illumination 59

**CHAPTER IV**

**Investigation of Gold Nanospheres-Gold Nanorods Hybrid/Metallic Grating Incorporated into Organic Solar Cells**

Table 4.1 Photovoltaic parameters of the OSCs 93

Table 4.2 Photovoltaic parameters of the hybrid plasmonic OSCs with and without metallic grating nanostructures under solar light illumination 97

## LIST OF FIGURES

Page

**CHAPTER I**
**INTRODUCTION**


Figure 1.1 The structures of donor and acceptor materials for OSCs 3

Figure 1.2 Band diagram and main processes in OSCs; (1) Absorption of photon followed by exciton formation, (2) Exciton diffusion, (3) Charge separation, and (4) Charge extraction 4

Figure 1.3 Standard solar spectra for space and terrestrial use 6

Figure 1.4 Plasmonic light-harvesting pathways for OSCs, (a) light scattering, (b) light absorption by LSPR, and (c) light trapping by SPPs 8

Figure 1.5 Absorption (dashed) and emission (solid) spectra of AuQDs 9


**CHAPTER II**
**Investigation of Gold Quantum Dot/Plasmonic Gold Nanoparticle System Incorporated into Organic Solar Cells**


Figure 2.1 (a) UV–vis absorption spectra and (b) fluorescence spectra of AuQDs and AuQDs:AuNPs aqueous solution 22

Figure 2.2 Fluorescence emission characters of AuQDs films (a) B-AuQDs, (b) G-AuQDs, and (c) R-AuQDs on glass substrates under UV illumination 23

Figure 2.3 UV-visible spectra of (a) AuQDs/PEDOT:PSS:AuNPs films and (b) AuQDs/PEDOT:PSS:AuNPs/P3HT:PCBM films on ITO glass substrates 24

Figure 2.4 AFM images of AuQDs films after directly spin coated on glass substrates, (a) B-AuQDs, (b) G-AuQDs, (c) R-AuQDs with a concentration of 5.0 μM 25

Figure 2.5 Surface morphology of PEDOT:PSS films on (a) ITO substrate (reference cell), (b) B-AuQDs layer, (c) G-AuQDs layer, (d) R-AuQDs layer and of PEDOT:PSS:AuNPs films on (e) ITO substrate, (f) B-AuQDs layer, (g) G-AuQDs layer, and (h) R-AuQDs layer 26

Figure 2.6 (a) Schematic of the fabricated OSCs and (b) J-V characteristics of the OSCs compared with the reference cell 28

Figure 2.7 (a) %IPCE and (b) E.F. profiles for only AuQDs layer system and (c) %IPCE and (d) E.F. profiles for the AuQDs/plasmonic AuNPs OSCs 32

Figure 2.8 Nyquist plots of the OSCs based on (a) individual AuQDs layers and (b) the AuQDs/plasmonic AuNPs systems under solar light illumination 34

Figure 2.9 Bode phase plots of the OSCs with (a) individual AuQDs layer and (b) the AuQDs/plasmonic AuNPs system under solar light illumination 36

**CHAPTER III**

**Investigation of Gold Quantum Dots/Metallic Grating System Incorporated into Organic Solar Cells**

Figure 3.1 Fluorescent emission of the mixing solution of 0.003 mM AuQDs and dilution of PEDOT:PSS at ratio 6:1, 10-fold dilution of PEDOT:PSS (a), mixing solution of PEDOT:PSS (10-fold dilution) with B-AuQDs (b), 10-fold dilution of PEDOT:PSS (c), mixing solution of PEDOT:PSS (100-fold dilution) with B-AuQDs (d), G-AuQDs (e), and R-AuQDs (f) under UV illumination 50

Figure 3.2 AFM images of PEDOT:PSS film (reference cell) (a), PEDOT:PSS:B-AuQDs film (b), PEDOT:PSS:G-AuQDs film (c), PEDOT:PSS:R-AuQDs film (d) on ITO glass substrate 52

Figure 3.3 Surface morphology of P3HT:PCBM layer on PEDOT:PSS layer of reference cell (a,e), the cell contained B-AuQDs (b,f), G-AuQDs (c,g), and R-AuQDs (d,h) of flat cell and BD-R imprinting cell, respectively. Surface morphology of reference cell (i), contained B-AuQDs (j), G-AuQDs (k), and R-AuQDs (l), after Al coating with grating pattern 53

Figure 3.4 Schematic of the fabricated OSCs with/without BD-R imprinting (a), surface morphology of P3HT:PCBM films without BD-R imprinting or flat (b) and with BD-R imprinting (c) 54

Figure 3.5 SPR reflectivity curves of the fabricated OSCs adding G-AuQDs without BD-R grating (flat cell) (a,b) and with BD-R grating (imprinting cell) (c,d) under p-pol or s-pol illumination, measured at fixed incident angles from $20^{o}$ to $60^{o}$ 55

Figure 3.6 SPR reflectivity curves of the fabricated OSCs adding B-AuQDs without BD-R grating (flat cell) (a,b) and with BD-R grating (imprinting cell) (c,d) under p-pol or s-pol illumination, measured at fixed incident angles from $20^{o}$ to $60^{o}$ 56

Figure 3.7 SPR reflectivity curves of the fabricated OSCs adding R-AuQDs without BD-R grating (flat cell) (a,b) and with BD-R grating (imprinting cell) (c,d) under p-pol or s-pol illumination, measured at fixed incident angles from $20^{o}$ to $60^{o}$ 57

Figure 3.8 *J-V* characteristics of the developed photovoltaic devices compared to the reference flat cell 58

Figure 3.9 IPCE spectra and E.F. spectra of AuQDs; B-AuQDs (a, d), G-AuQDs (b, e), and R-AuQDs (c, f) loaded photovoltaic devices with/without BD-R imprinting as compared to the reference OSCs, measured at fixed incident angles $30^{o}$ under irradiation of non-polarized light 62

Figure 3.10 IPCE E.F. spectra of flat devices and patterning devices incorporated AuQDs. Flat devices; B-AuQDs (a), G-AuQDs (b), and R-AuQDs (c), patterning devices; reference (d), B-AuQDs (e), G-AuQDs (f), and R-AuQDs (g), performed at fixed incident angles from $20^o$ to $60^o$ under irradiation of normal light 64

Figure 3.11 IPCE E.F. spectra; (p-pol/s-pol) of reference cell (flat cell) (a), and BD-R imprinting cell incorporated with B-AuQDs (b), G-AuQDs (c), R-AuQDs (d), performed at fixed incident angles from 20o to 60o under irradiation of s- or p-polarized light 65

Figure 3.12 Impedance spectroscopy of photovoltaic device, Nyquist plots of flat devices (a), BD-R imprinting device (b) incorporating with three types of AuQDs 66

Figure 3.13 Bode phase plots of flat devices (a) and BD-R imprinting device (b) incorporating with three types of AuQDs under solar light illumination 68

**CHAPTER IV**

**Investigation of Gold Nanospheres-Gold Nanorods Hybrid/Metallic Grating Incorporated into Organic Solar Cells**

Figure 4.1 Schematic illustration of the fabrication of hybrid plasmonic OSCs incorporated with metallic grating nanostructure 84

Figure 4.2 UV-vis absorption spectra, (A) the solution of AuNSs, AuNRs and the mixture solution of AuNSs and AuNRs , (B) the photoactive layer film of fabricated solar cell:glass/AuNPs:PEDOT:PSS/P3HT:PCBM 85

Figure 4.3 AFM images of PEDOT:PSS films, pristine PEDOT:PSS (without AuNPs) (A), and PEDOT:PSS:AuNSs:AuNRs films containing different total concentrations of mixture AuNSs:AuNRs (1:1); 0.030 mM (B), 0.050 mM (C), 0.070 mM (D), and 0.100 (E) on ITO glass substrate 87

Figure 4.4 Surface morphology of P3HT:PCBM layer coated on PEDOT:PSS layer after imprinting process, reference cell (A), AuNSs (B), AuNRs (C) and mix AuNSs:AuNRs (D) 88

Figure 4.5 SPR reflectivity curves of the plasmonic OSCs adding AuNSs:AuNRs, (A and B) without BD-R grating (flat device) and (C and D) with BD-R grating under p-pol or s-pol illumination, measured at fixed incident angles from $10^{o}$ to $60^{o}$ 90

Figure 4.6 SPR reflectivity curves of the fabricated OSCs (A) reference flat, (B) reference BD-R, (C) AuNSs flat, (D) AuNSs BD-R, (E) AuNRs flat, and (F) AuNRs BD-R. The reflectivity curves were recorded at various incident angles under illumination of p-pol light 91

Figure 4.7 SPR reflectivity curves of the fabricated OSCs (A) reference flat, (B) reference BD-R, (C) AuNSs flat, (D) AuNSs BD-R, (E) AuNRs flat, and (F) AuNRs BD-R. The reflectivity curves were recorded at various incident angles under illumination of s-pol light 92

Figure 4.8 *J-V* characteristics of the developed photovoltaic devices with different concentrations and the reference cell 94

Figure 4.9 Impedance spectroscopy of photovoltaic device, Nyquist plots of flat devices incorporating with AuNSs:AuNRs 95

Figure 4.10 J-V characteristics of the developed photovoltaic devices; flat and BD-R imprinting cells 96

Figure 4.11 IPCE spectra compared to the reference cell, (A) Flat OSCs and (B) BD-R imprinting OSCs incorporated with AuNSs, AuNRs, and mix AuNSs:AuNRs, respectively, measuring under irradiation of non-pol light 98

Figure 4.12 IPCE E.F. spectra of patterning devices, reference imprinting cell without the insertion of AuNPs (A), the developing cell incorporated AuNSs (B), AuNRs (C), and mixed AuNSs:AuNRs (D), performed at fixed incident angles from $30^{o}$ to $50^{o}$ under irradiation of normal light 100

Figure 4.13 IPCE E.F. spectra of different patterning devices including reference cell, AuNSs, AuNRs, and mixed AuNSs:AuNRs at the incident angle of $0^o$ (A), $30^o$ (B), $40^o$ (C) and $50^o$ (D), respectively. The experiment was measured at fixed incident angles from 0o to 50o under irradiation of non-polarized light 101

# LIST OF ABBREVIATIONS

| | |
|---|---|
| AM | Air mass |
| AFM | Atomic force microscope |
| AgNPs | Silver nanoparticles |
| AuNPs | Gold nanoparticles |
| AuNSs | Gold nanospheres |
| AuNRs | Gold nanorods |
| AuQDs | Gold quantum dot |
| BD-R | Blu-ray disc recordable |
| CPE | Constant phase element |
| DI-water | Deionized water |
| E.F. | Enhancement Factor |
| EIS | Electrochemical impedance spectroscopy |
| FF | Fill factor |
| GCSPR | Grating-coupled surface plasmon resonance |
| HOMO | Highest occupied molecular orbital |
| HTL | Hole transport layer |
| ITO | Indium-tin-oxide |
| IPCE | Photo to current conversion efficiency |
| *J-V* | Current-voltage |
| $J_{sc}$ | Short-circuit current density |
| LSPR | Localized surface plasmon resonance |
| LUMO | Lowest unoccupied molecular orbital |

| | |
|---|---|
| NPs | Nanoparticles |
| OSCs | Organic solar cells |
| P3HT | Poly(3-hexylthiophene) |
| PCBM | Phenyl-$C_{61}$-butyric acid methyl ester |
| PEDOT:PSS | Poly(3,4-ethylenedioxythiophene) polystyrene sulfonate |
| p-pol | p-polarize |
| PCE | Power conversion efficiency |
| $R_s$ | Series resistance |
| $R_{ct}$ | Charge transfer resistance |
| SPR | Surface plasmon resonance |
| SPP | Surface plasmon polaritron |
| SP | Surface plasmon |
| s-pol | s-polarize |
| UV | Ultraviolet |
| $V_{oc}$ | Open-circuit voltage |
| V | Volt |
| Z | Impedance |
| $^{o}C$ | Degree celsius |
| Ω | Ohm |

# CHAPTER I

# INTRODUCTION

According to increasing of population and economic growth, the energy demanding has been rapidly increased worldwide and the predicted electrical power demands will reach 28 terawatts by 2050 and 46 terawatts by 2100 [1]. Fossil fuels, including coal, gas, and oil, are the main sources of energy, which are less available, more expensive and consumable. Moreover, the burning of fossil fuels, producing the carbon dioxide in the atmosphere, is the major causes of environmental problem, i.e. global climate change. In contrast, the global warming emissions are minimal with use of renewable energy [2-6]. Therefore, the alternative energy plays a significant role for the energy production in the future. Solar energy is one of renewable energy sources, which is the most important clean energy source to produce the thermal or electrical energy for many years. Solar technologies can utilize the sunlight to many energy forms such as photovoltaic, solar heating, and solar thermal energy. Photovoltaic devices or solar cells can generate electricity directly from the sunlight via the photovoltaic effect without the pollution and moving parts [7]. Thus, photovoltaic devices have been considered as promising candidates for electrical power production nowadays. Although solar cell technologies have been successfully developed as commercial devices, they are still limited with high material usage, the module manufacturing cost, and the weighty crystalline silicon. Hence, organic solar cells (OSCs) have attracted much attention for the solar production of electricity because of their cost-effectiveness, simplistic fabrication, solution processing, flexibility and lightweight [5, 8-10]. Development of advanced nanomaterials and design of device for broadening light absorption in OSCs has been demonstrated in solar cell research by several research groups worldwide in order to decrease the cost, increase the reliability, and increase the efficiency of photovoltaic

performance. This work aims to enhance photovoltaic performances of the OSCs by the incorporation of plasmonic metallic nanostructures for the light harvesting enhancement.

## 1.1 RESEARCH BACKGROUND

### 1.1.1 Organic solar cells (OSCs)

Organic solar cells (OSCs), photovoltaic devices, are promising technologies due to their unique properties including, low cost, light weight, mechanical flexibility, and ease of processing. Due to the solution-based processing, the OSCs are suitable for the large scale fabrication in which the solution of organic semiconductors can be sprayed or printed onto flexible substrates namely, flexible glass, metal foils, and plastic films [6]. The solar cells, electronic devices, directly convert the solar light into electricity by photovoltaic effect. The photovoltaic effect is a process of the conversion of sunlight to voltage or electric current in the solar cells. When the light, pure energy composed of photons, is absorbed by a solar cell. The energy from the photon is transferred to electrons or atoms of the semiconducting material in the p-n junction. This effect induces the electrons to jump to a higher energy state from the valence band to the conduction band. The movement of the electron creates two charge carriers, an electron-hole pair, giving a photovoltage to drive a current through an external circuit [11].

The principle of OSCs operation is different from the traditional inorganic solar cells. The photoactive layers in OSCs are polymers, consisting of electron donors (semiconducting polymers) and electron acceptors (fullerene derivatives or semiconductor nanoparticles). Some of donor and acceptor materials for OSCs are shown in Figure 1.1.

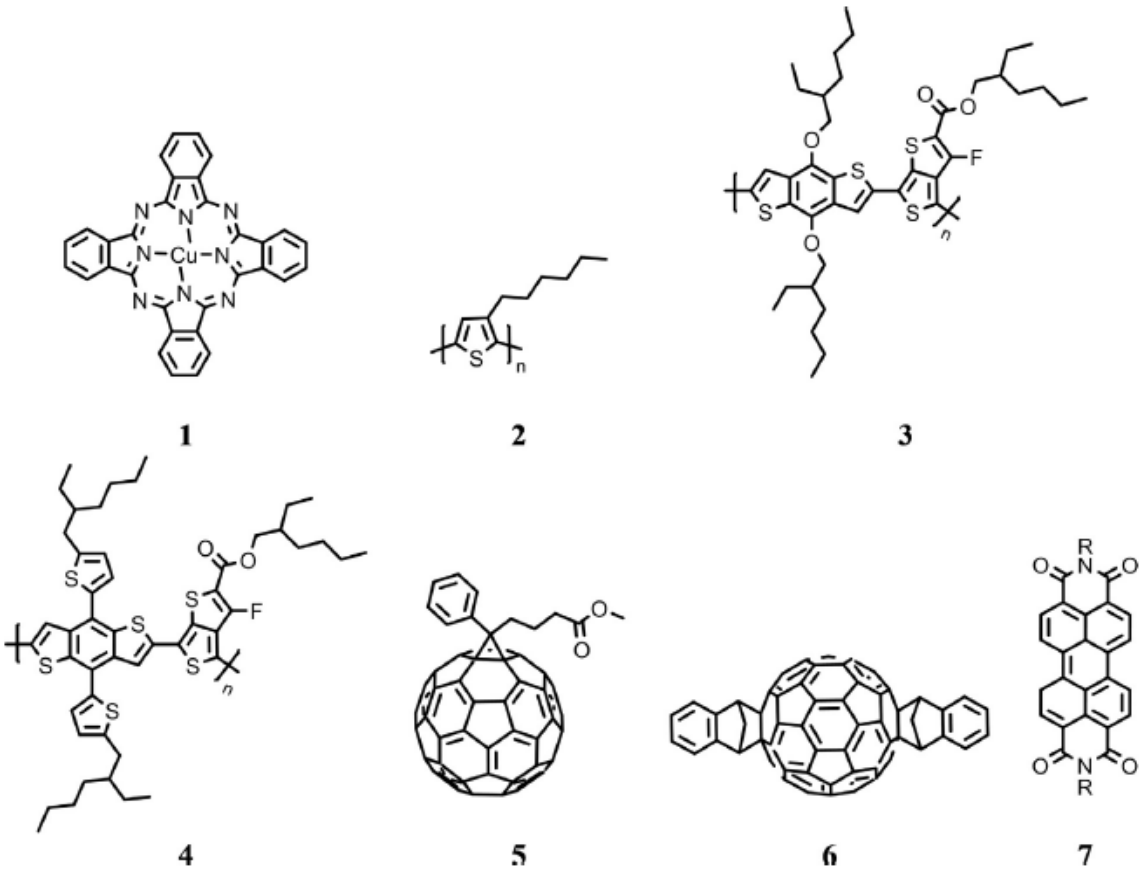


**Figure 1.1** The structures of donor and acceptor materials for OSCs, (1) copper-phthalocyanine, (2) poly (3-hexylthiophene) (P3HT), (3) benzodithiophene and thieno[3,4-b]thiophene (PTB7), (4) poly[4,8-bis(5-(2-ethylhexyl)thiophen-2-yl)benzo[1,2-b; 4,5-b'] dithiophene-2,6-diyl-alt-(4-(2-ethylhexyl)-3-fluorothieno[3,4-b]thiophene-)-2-carboxylate-2 6-diyl)] (PTB7-Th), (5) [6,6]-phenyl-$C_{61}$-butyric acid methyl ester ($PC_{61}BM$), (6) indene-C60 bisadduct (ICBA), and (7) perylene tetracarboxylic derivative (PDI). (Reprinted from N. Marinova *et al*. [12], Copyright (2017), with permission from Elsevier).

These polymers provide broadband absorption of sunlight with the optimized highest occupied molecular orbital (HOMO) and lowest unoccupied molecular orbital (LUMO) levels and high hole mobilities. HOMO and LUMO are similar to be the valence bands and conduction bands in inorganic devices, respectively.

The LUMO of acceptors are energetically low that promotes them high electron affinity and allows them to accept electrons from the donors [2, 13]. The diagram and main processes in OSCs is presented in Figure 1.2.

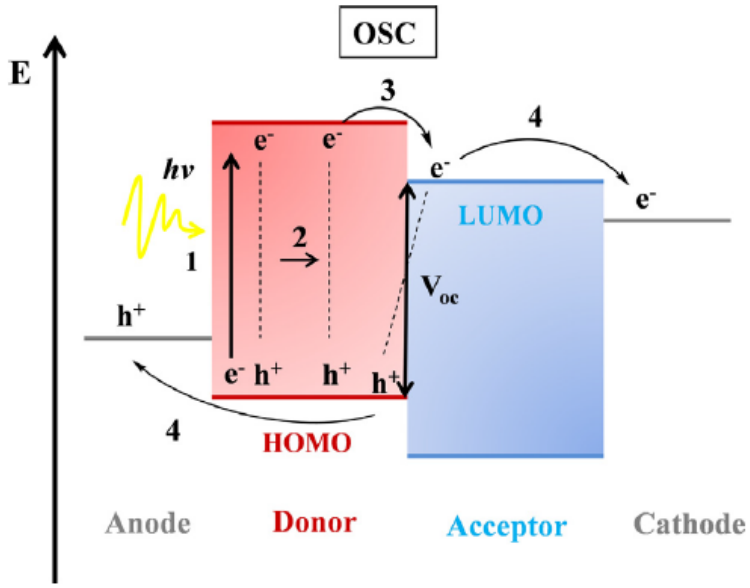


**Figure 1.2** Band diagram and main processes in OSCs; (1) Absorption of photon followed by exciton formation, (2) Exciton diffusion, (3) Charge separation, and (4) Charge extraction. (Reprinted from N. Marinova *et al*. [12], Copyright (2017), with permission from Elsevier).

When the polymeric molecules absorb the solar light electrons are excited from the HOMO to the LUMO. The mechanism of reaction is similar the promotion of electron from the valence band to the conduction band in inorganic semiconductors. The optical excitations of organic semiconductors generate a tightly bound electron-hole pair, namely excitons [6]. In order to produce photocurrent, the exciton needs to overcome the binding energy (0.3–1 eV) and dissociate into free charges electrons and holes [12]. The diffusive process of exciton migration is achieved at the interface between an electron donor and an electron acceptor of semiconductors. Organic semiconductors typically exhibit small exciton diffusion lengths (1-10 nm), which limits the thickness of photoactive layer [14, 15].

In practice, the efficiency of the OSCs is usually lower than the theoretical maximum due to optical and electrical losses. Disadvantages from incomplete absorption, reflection, and shading can decrease the efficiency. Also, the series and shunt resistances cause the electrical loss, resulting in lower performances. Solar cell efficiency is limited by the following parameters, including non-absorption of low-energy photons, thermalization losses from the absorption of high-energy photons, and extraction losses due to unavoidable charge carrier recombination. The problem is from the mismatch of spectral between the incident solar spectrum and absorption profile in the devices [16]. Therefore, an effective absorption in the wide solar spectral range covering 350–1250 nm has been an important aspect of solar cell research [7]. The standard solar spectrum is shown in Figure 1.3. Sunlight at the outer fringes of the earth's atmosphere (AMO) covers a broad range of wavelengths (350-2500 nm). The atmosphere affects many parts of the spectrum such as absorption of X-rays before reaching the ground, elimination of ultraviolet radiation, reflection and scattering of some radiation back into space, resulting in chinks in the spectral distributions AM1 and AM10 [11]. The sunlight provides many different colors that combined as a white light. Each of the visible and invisible radiations of the spectrum obtains different energy. Within the visible regions, red is at the low-energy while violet is at the high-energy. Light in the infrared region has less energy than that in the visible region. The light from ultraviolet region gives the highest energy [11].

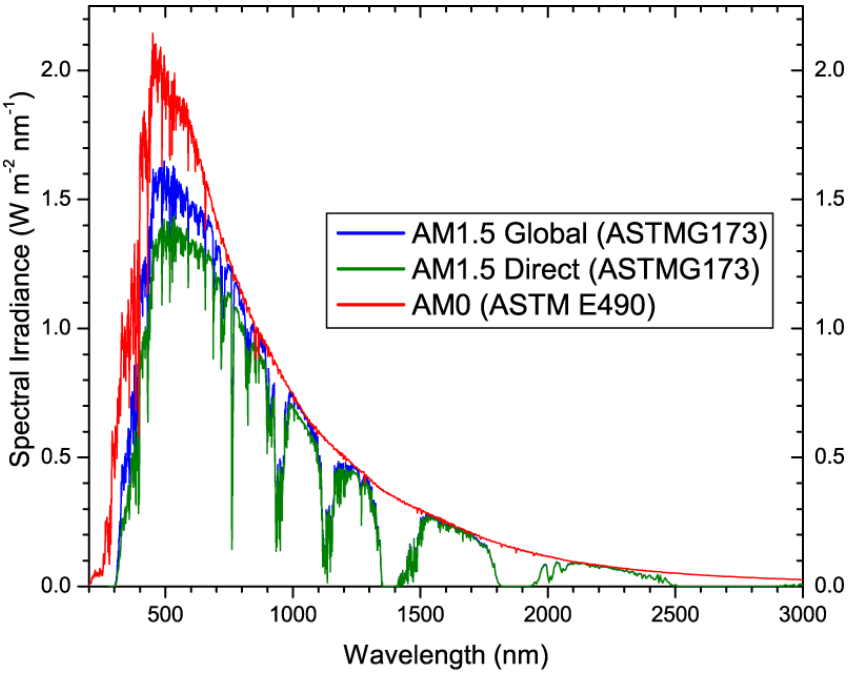


**Figure 1.3** Standard solar spectra for space and terrestrial use (Reprinted from P. Mandal and S. Sharma [7], Copyright (2016), with permission from Elsevier).

### 1.1.2 Enhancement of light-harvesting in OSCs

#### 1.1.2.1 Plasmonic nanostructures

OSCs have been promising candidates for a cost-effective and lightweight solar energy conversion device, giving high power conversion efficiency (PCE) up to 10% [3]. However, the OSCs are limited by the low charge-carrier mobility and small exciton diffusion length of polymeric materials, limiting the thickness of photoactive layer in OSCs [3, 17]. Although increasing of the active layer thickness enhance the light absorption, larger thickness can cause a higher recombination of free charge carriers in OSCs, which possibly affect high resistance and low PCE [8, 18, 19]. Therefore, the increasing of light harvesting of active layer film without thickness enlargement is challenge. Advanced nanomaterials or nanostructures have been extensively incorporated into the OSCs in order to improve the light trapping for achieving high photovoltaic efficiencies. Metallic nanostructures, providing surface plasmons, offered effective light trapping inside the photovoltaic devices. Surface

plasmons, excitations of the conduction electrons at the interface between a metal and a dielectric, promote the light harvesting and concentrating in active layer, thereby increasing the absorption in OSCs [20].

Plasmonic nanostructures can enhance the light trapping of the photoactive layer in OSCs by three ways, including light scattering and light concentration by metallic nanoparticles and light trapping by surface plasmon polaritons (SPPs). Metallic nanoparticles (NPs), gold nanoparticles (AuNPs) and silver nanoparticles (AgNPs), can be used as subwavelength scattering elements to couple and trap freely propagating plane waves from sunlight into photoactive film. When the metallic NPs are located close to the interface between two dielectrics, the light will scatter into the dielectric with the larger permittivity that effectively increases the optical path length (Figure 1.4a) [3, 20, 21]. Moreover, metallic NPs, particularly small particles with diameter of 5-20 nm, offer a strong localized surface plasmon resonance (LSPR). The plasmonic near-field is coupled to the semiconductor, increasing its effective absorption cross-section (Figure 1.4b). In addition, a corrugated metallic film on the back surface can couple sunlight into SPP modes, which are electromagnetic waves that travel along the interface between a metal back contact and the photoactive layer (Figure 1.4c) [20]. This can generate photocarriers within photovoltaic devices. Metallic NPs with different materials, concentrations, sizes, and shapes have been widely inserted in hole transport layer (HTL), photoactive layer, and interfaces within the devices in order to enhance optical absorption of OSCs [3, 22].

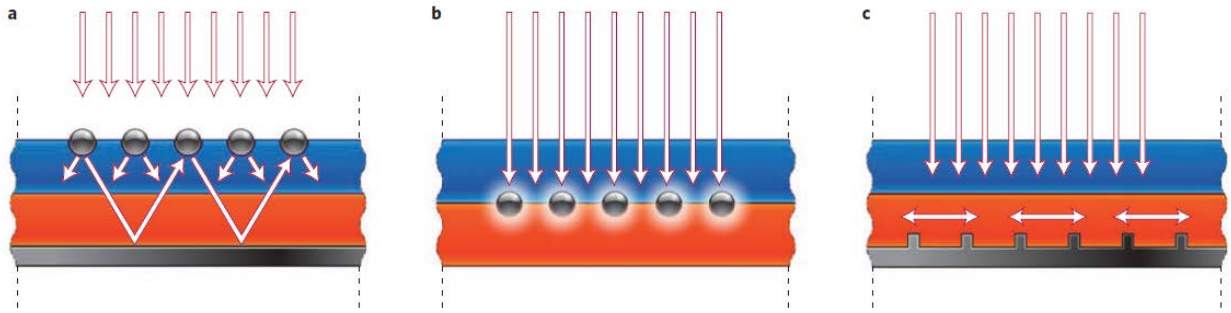


**Figure 1.4** Plasmonic light-harvesting pathways for OSCs, (a) light scattering, (b) light absorption by LSPR, and (c) light trapping by SPPs (Reprinted from H.A. Atwater and A. Polman [20], Copyright (2010), with permission from Springer Nature).

AuNPs, giving a strong LSPR, have been extensively introduced into hole transport layers or photoactive layers of OSCs to achieve high photovoltaic performances [22-24]. Additionally, incorporation of mixed nanoparticles such as AgNPs and AuNPs [25, 26], gold nanodots (AuNDs) and AuNPs [24], or gold nanospheres (AuNSs) and gold nanorods (AuNRs) [27] into photovoltaic devices showed the PCE enhancement. Furthermore, nanoimprinting technique is a useful in the nanotechnology field, giving the nanostructure of the photoactive layer in OSCs [28]. Several corrugated metallic nanostructures including, nanohole, honeycomb, nanopillar, and grating nanostructure have been fabricated on the surface to increase the optical property [28]. Periodic grating nanostructures provide the SPP modes that the resonance wavelength can be tuned within the visible to near-infrared regions [5]. The fabrication of grating nanostructures on the top of OSCs can improve the photovoltaic property due to waveguide modes and plasmonic effect [3]. The grating nanostructures also produce a larger interfacial surface area, facilitating efficient exciton dissociation [2]. In addition, dual plasmonic nanostructures consist of metallic NPs and metallic nanograting obviously enhanced both optical and electrical properties in OSCs [8].

### 1.1.3 Fluorescence emission of gold quantum dots

Typically, the color of AuNPs depends on their shapes and sizes and the particles sizes in the ranges of 2-100 nm provide the plasmonic property. When the particles sizes are very small (less than 2 nm) known as gold quantum dots (AuQDs), the band gap energy increases and the valence and conduction bands break into quantized energy levels [29]. The fluorescence emission of AuQDs is resulted from the electronic transition and the shift of fluorescent emission wavelength of AuQDs is influenced by quantum confinement effects. The smallest cluster ($Au_5$) has a high quantum yield, illustrating blue emission, and the emission wavelength of larger cluster is in a redshift. This suggesting that increment of nanocluster size leads to lower energy emission [29-31]. The absorption and emission spectra of different sizes of AuQDs is shown in Figure 1.5.

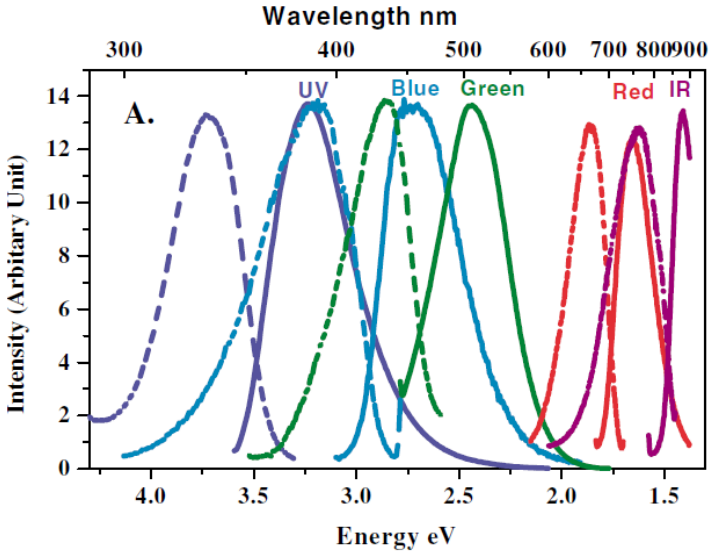


**Figure 1.5** Absorption (dashed) and emission (solid) spectra of AuQDs. (Reprinted from J. Zheng *et. al* [31], Copyright (2004), with permission from American Physical Society).

The characteristic of the AuQDs can be implied that AuQDs can harvest the light from ultraviolet (UV) regions and convert it into the fluorescence in visible regions. Different sizes of AuQDs can tune the fluorescence emission, matching with the absorption spectrum of several kinds of plasmonic NPs and the photoactive layer [32]. Therefore, AuQDs give new

opportunity for light emitting sources which can increase the light management within the developed OSCs.

## 1.2 OBJECTIVES

This work aims to broaden the solar light harvesting in OSCs using plasmonic nanostructures. AuNPs, AuQDs, and grating nanostructures were incorporated into the developed OSCs for light management. The addition of AuQDs into the device are necessary to extend light absorption in UV region while the combination of AuNPs and grating structure are required to enhance the light harvesting in the visible region. Therefore, the objectives of this work are:

1. To fabricate and characterize the OSCs with high photovoltaic performances
2. To study the effect of AuQDs/AuNPs for light harvesting in developed OSCs
3. To study the effect of AuQDs incorporated with GCSPR in photovoltaic performances
4. To study the effect of the mixture AuNPs (gold nanospheres (AuNSs) and gold nanorods (AuNRs)) incorporated with GCSPR in light trapping enhancement

## 1.3 SCOPE OF THE DISSERTATION

The enhancement of the photovoltaic properties of OSCs was investigated by introduction of plasmonic nanostructures into OSCs. AuNPs; AuNSs and AuNRs and AuQDs with blue-, green-, and red-emission were used. The incorporation of AuQDs and plasmonic AuNPs for OSCs enhancement was studied. An important challenge in this part is to apply AuQDs to organic light harvesting systems. AuQDs absorb the UV light and generate visible light as fluorescence emission while AuNPs provide the localized surface plasmon resonance effect. Moreover, the incorporation of AuQDs with GCSPR and AuNPs with GCSPR were investigated. The poly(3- hexylthiophene) (P3HT) and phenyl-$C_{61}$-butyric acid methyl ester

(PCBM) were used as active layer, while poly(3,4-ethylenedioxythiophene) doped with poly(styrene sulfonate) (PEDOT:PSS) were used as hole transport layer of OSCs. AuNPs or AuQDs were introduced into PEDOT:PSS and the grating pattern was constructed onto active layer surface. In addition, UV-visible spectra, surface morphology, current density versus voltage characteristics, the impedance spectra, and the incident photon-to-current efficiency of the fabricated devices were evaluated.

Three works are included as follows:

1. Investigation of Gold Quantum Dot/Plasmonic Gold Nanoparticle System Incorporated into Organic Solar Cells

2. Investigation of Gold Quantum Dots/Metallic Grating System Incorporated into Organic Solar Cells

3. Investigation of Gold Nanospheres-Gold Nanorods Hybrid/Metallic Grating Incorporated into Organic Solar Cells

## 1.4 REFERENCES


[1] Hoffert, M.I., K. Caldeira, A.K. Jain, E.F. Haites, L.D.D. Harvey, S.D. Potter, M.E. Schlesinger, S.H. Schneider, R.G. Watts, T.M.L. Wigley, and D.J. Wuebbles, *Energy implications of future stabilization of atmospheric $CO_2$ content*. Nature, 1998. **395**(6705): p. 881-884.

[2] Jonas, W., D.R. B., H.H. C., W. Wolfgang, and S.-M. Lukas, *Nanostructured organic and hybrid solar cells*. Advanced Materials, 2011. **23**(16): p. 1810-1828.

[3] Qiaoqiang, G., B.F. J., and K.Z. H., *Plasmonic-enhanced organic photovoltaics: breaking the 10% efficiency barrier*. Advanced Materials, 2013. **25**(17): p. 2385-2396.

[4] Kang, M.-G., M.-S. Kim, J. Kim, and L.J. Guo, *Organic solar cells using nanoimprinted transparent metal electrodes*. Advanced Materials, 2008. **20**(23): p. 4408-4413.

[5] Chou, C.-H. and F.-C. Chen, *Plasmonic nanostructures for light trapping in organic photovoltaic devices*. Nanoscale, 2014. **6**(15): p. 8444-8458.

[6] McGehee, M.D. and C. Goh, *Organic semiconductors for low-cost solar Cells*. AIP Conference Proceedings, 2008. **1044**(1): p. 322-330.

[7] Mandal, P. and S. Sharma, *Progress in plasmonic solar cell efficiency improvement: a status review*. Renewable and Sustainable Energy Reviews, 2016. **65**: p. 537-552.

[8] Li, X., W.C.H. Choy, L. Huo, F. Xie, W.E.I. Sha, B. Ding, X. Guo, Y. Li, J. Hou, J. You, and Y. Yang, *Dual Plasmonic nanostructures for high performance inverted organic solar cells*. Advanced Materials, 2012. **24**(22): p. 3046-3052.

[9] Choy, W.C.H., *The emerging multiple metal nanostructures for enhancing the light trapping of thin film organic photovoltaic cells*. Chemical Communications, 2014. **50**(81): p. 11984-11993.

[10] Leever, B.J., C.A. Bailey, T.J. Marks, M.C. Hersam, and M.F. Durstock, *In situ characterization of lifetime and morphology in operating bulk heterojunction organic photovoltaic devices by impedance spectroscopy*. Advanced Energy Materials, 2012. **2**(1): p. 120-128.

[11] Hersch, P. and K. Zweibel, *Basic photovoltaic principles and methods*. 1982.

[12] Marinova, N., S. Valero, and J.L. Delgado, *Organic and perovskite solar cells: working principles, materials and interfaces*. Journal of Colloid and Interface Science, 2017. **488**: p. 373-389.

[13] Srivastava, A., D.P. Samajdar, and D. Sharma, *Plasmonic effect of different nanoarchitectures in the efficiency enhancement of polymer based solar cells: a review*. Solar Energy, 2018. **173**: p. 905-919.

[14] Sauvé, G. and R. Fernando, *Beyond fullerenes: designing alternative molecular electron acceptors for solution-processable bulk heterojunction organic photovoltaics*. The Journal of Physical Chemistry Letters, 2015. **6**(18): p. 3770-3780.

[15] Feron, K., W.J. Belcher, C.J. Fell, and P.C. Dastoor, *Organic solar cells: understanding the role of Förster resonance energy transfer*. International journal of molecular sciences, 2012. **13**(12): p. 17019-17047.

[16] Day, J., S. Senthilarasu, and T.K. Mallick, *Improving spectral modification for applications in solar cells: a review*. Renewable Energy, 2019. **132**: p. 186-205.

[17] Yang, J., J. You, C.-C. Chen, W.-C. Hsu, H.-r. Tan, X. W. Zhang, Z. Hong, and Y. Yang, *Plasmonic polymer tandem solar cell*. ACS Nano, 2011. **5**(8): p. 6210-6217.

[18] Notarianni, M., K. Vernon, A. Chou, M. Aljada, J. Liu, and N. Motta, *Plasmonic effect of gold nanoparticles in organic solar cells*. Solar Energy, 2014. **106**: p. 23-37.

[19] Nootchanat, S., A. Pangdam, R. Ishikawa, K. Wongravee, K. Shinbo, K. Kato, F. Kaneko, S. Ekgasit, and A. Baba, *Grating-coupled surface plasmon resonance enhanced organic photovoltaic devices induced by Blu-ray disc recordable and Blu-ray disc grating structures*. Nanoscale, 2017. **9**(15): p. 4963-4971.

[20] Atwater, H.A. and A. Polman, *Plasmonics for improved photovoltaic devices*. Nature Materials, 2010. **9**: p. 205.

[21] Xuanhua, L., W.C.H. Choy, H. Lu, W.E.I. Sha, and A.H.P. Ho, *Efficiency enhancement of organic solar cells by using shape-dependent broadband plasmonic absorption in metallic nanoparticles*. Advanced Functional Materials, 2013. **23**(21): p. 2728-2735.

[22] Stratakis, E. and E. Kymakis, *Nanoparticle-based plasmonic organic photovoltaic devices*. Materials Today, 2013. **16**(4): p. 133-146.

[23] Ng, A., W.K. Yiu, Y. Foo, Q. Shen, A. Bejaoui, Y. Zhao, H.C. Gokkaya, A.B. Djurišić, J.A. Zapien, W.K. Chan, and C. Surya, *Enhanced performance of PTB7:$PC_{71}$BM solar cells via different morphologies of gold nanoparticles*. ACS Applied Materials & Interfaces, 2014. **6**(23): p. 20676-20684.

[24] Liu, C.-M., C.-M. Chen, Y.W. Su, S.-M. Wang, and K.-H. Wei, *The dual localized surface plasmonic effects of gold nanodots and gold nanoparticles enhance the performance of bulk heterojunction polymer solar cells*. Organic Electronics, 2013. **14**(10): p. 2476-2483.

[25] Lu, L., Z. Luo, T. Xu, and L. Yu, *Cooperative plasmonic effect of Ag and Au nanoparticles on enhancing performance of polymer solar cells*. Nano Letters, 2013. **13**(1): p. 59-64.

[26] Sharma, M., P.R. Pudasaini, F. Ruiz-Zepeda, E. Vinogradova, and A.A. Ayon, *Plasmonic effects of Au/Ag bimetallic multispiked nanoparticles for photovoltaic applications*. ACS Applied Materials & Interfaces, 2014. **6**(17): p. 15472-15479.

[27] Hsiao, Y.-S., S. Charan, F.-Y. Wu, F.-C. Chien, C.-W. Chu, P. Chen, and F.-C. Chen, *Improving the light trapping efficiency of plasmonic polymer solar cells through photon management*. The Journal of Physical Chemistry C, 2012. **116**(39): p. 20731-20737.

[28] Yang, Y., K. Mielczarek, M. Aryal, A. Zakhidov, and W. Hu, *Nanoimprinted polymer solar cell*. ACS Nano, 2012. **6**(4): p. 2877-2892.

[29] Eustis, S. and M.A. El-Sayed, *Why gold nanoparticles are more precious than pretty gold: noble metal surface plasmon resonance and its enhancement of the radiative and nonradiative properties of nanocrystals of different shapes*. Chemical Society Reviews, 2006. **35**(3): p. 209-217.

[30] Chen, L.-Y., C.-W. Wang, Z. Yuan, and H.-T. Chang, *Fluorescent gold nanoclusters: recent advances in sensing and imaging*. Analytical Chemistry, 2015. **87**(1): p. 216-229.

[31] Zheng, J., C. Zhang, and R.M. Dickson, *Highly fluorescent, water-soluble, size-tunable gold quantum dots*. Physical Review Letters, 2004. **93**(7): p. 077402.

[32] Cohen-Hoshen, E., G.W. Bryant, I. Pinkas, J. Sperling, and I. Bar-Joseph, *Exciton-plasmon interactions in quantum dot-gold nanoparticle structures*. Nano Letters, 2012. **12**(8): p. 4260-4264.

# CHAPTER II

## Investigation of Gold Quantum Dot/Plasmonic Gold Nanoparticle System Incorporated into Organic Solar Cells

This chapter adapted from the article published in Nanoscale Advances, 2019, 1, 792.

**Citation:** Phetsang, S., A. Phengdaam, C. Lertvachirapaiboon, R. Ishikawa, K. Shinbo, K. Kato, P. Mungkornasawakul, K. Ounnunkad, and A. Baba, "Investigation of a gold quantum dot/plasmonic gold nanoparticle system for improvement of organic solar cells," Nanoscale Advances, 1, 2019, 792-798.

**ABSTRACT**

Light management allows enhancement of light harvesting in organic solar cells (OSCs). An improvement in performances of OSCs has been achieved by employing promising plasmonic nanoparticles or others. This work described the investigation of enhanced OSCs by incorporating with gold quantum dots (AuQDs) layer and plasmonic gold nanoparticles (AuNPs) blended in hole-transport layer (HTL). Different AuQDs with blue-, green-, and red-fluorescent emissions were examined in this study. OSCs were demonstrated with a structure of ITO-coated glass substrate/AuQDs/PEDOT:PSS:AuNPs/ P3HT:PCBM/Al. UV-visible spectra, current density versus voltage characteristics, the impedance spectra, and the incident photon-to-current efficiency of the fabricated devices were evaluated. The results showed an enhancement of photovoltaic efficiency observed by increasing the short circuit current density ($J_{SC}$) and power conversion efficiency (PCE) in comparison with the reference OSCs. The best synergetic benefit was found with OSCs consisted of green-emission AuQDs layer and HTL containing well-dispersed AuNPs, leading to the greatest power conversion efficiency of 3.66 (improved 13.0%). This indicated that the increase in light harvesting in the developed devices was induced by extended light absorption in the UV region resulting from absorption by the AuQDs layer and emission of visible fluorescence from the AuQDs layer to the photoactive layers. Moreover, the localized surface plasmon effect of AuNPs, which also contributed to an increase in light trapping in the proposed OSCs, was enhanced by the effect of the AuQDs.

## 2.1 INTRODUCTION

Organic thin film solar cells (OSCs) have been considered as promising an alternative ways for renewable energy sources due to their great potentials, such as light in weight, high flexibility, low temperature processing, solution-based fabrication and cost-effective production [1-3]. Although the bulk heterojunction (BHJ) OSCs obtained several advantages and improved the performance of photovoltaic device, the short carrier diffusion length of polymer materials limits the film thickness of the active layer in the OSCs, lowering the power conversion efficiency (PCE) compared with the traditional solar cells based crystalline Si [1, 4]. Metallic nanostructures supported plasmonic properties have been used to improve the light harvesting in the photovoltaic device; in particularly, the introduction of gold nanoparticles (AuNPs) into OSCs enhanced the photocurrent and power conversion efficiency [5-10]. Moreover, our group reported the utilization of AuNPs to improve the performance on OSCs [5, 11]. Plasmonic nanoparticles (NPs) are usually dispersed into the photoactive and hole transport buffer layers as well being deposited at the interfaces of organic layers in photovoltaic devices [12, 13]. AuNPs with a particle size from 2 to 100 nm typically enhance an electric field and optical absorption through the excitation of localized surface plasmon resonance (LSPR) which depends on the particle size, shape and the surrounding environment. When the size of gold nanoparticles further becomes very small (< 2 nm), they are called gold nanoclusters (AuNCs) or gold quantum dots (AuQDs), on which localized plasmons cannot be excited. Instead, due to the quantum confinement effect, electrons in AuQDs are excited from the ground state by absorbing near-UV light, and the AuQDs emit fluorescence in the visible range. The size of the AuQDs, i.e. the number of gold atoms, determines the wavelength of the fluorescence emission [14-16]. This implies that AuQDs can harvest light from the UV region and convert it into visible light. From the previous studies, AuQDs were effective in the operation of dye-sensitized solar cells (DSSCs), and they were employed as a

photosensitizer and catalyst in the system. AuQDs deposited on $TiO_2$ electrode improved the light absorption capability, increased the photocurrent, and enhanced charge transport [17-20]. Because most organic photoelectric-converting materials harvest light mostly in the visible range, an important challenge is to apply AuQDs to organic light harvesting systems, which absorb light in the near-UV region and convert it to visible light as fluorescence emission. In combining AuQDs and AuNPs, synergistic effects are expected because the fluorescence from AuQDs enhances the localized plasmon effect of the AuNPs, and simultaneously the enhanced electric field on AuNPs enhances the fluorescence of AuQDs by localized plasmon excitation [21].

This work demonstrates the synergistic effect of AuNPs/AuQDs system on the OSCs performance. The enhancement of the photovoltaic properties of plasmonic OSCs by introducing AuNPs and AuQDs (blue, green, and red) was investigated. AuQDs/plasmonic solar cells with an Aluminium (Al)/poly(3-hexylthiophene-2,5-diyl) (P3HT): [6,6]-phenyl C61 butyric acid methyl ester (PCBM) AuNP:poly(3,4-ethylene dioxythiophene): poly(styrene sulfonate) (PEDOT:PSS)/ AuQDs/indium tin oxide (ITO) glass substrate structure exhibited an improved performance. The results demonstrated that the AuQDs/AuNPs in the OSCs played an important role in improving its photovoltaic properties due to the fluorescence from the AuQDs and energy/electron transfer from the AuQDs to the AuNPs, leading to a 13% increase in the PCE.

## 2.2 EXPERIMENTAL SECTION

### 2.2.1 Chemicals and materials

Three types of gold quantum dots (AuQDs) with different fluorescence emission wavelengths; Blue-AuQDs (mixed $Au_5$ and $Au_8$ nanoclusters), Green-AuQDs ($Au_{13}$ nanoclusters), and Red-AuQDs ($Au_{25}$ nanoclusters) (B-AuQDs, G-AuQDs, and R-AuQDs, respectively) were purchased from Dai Nippon Toryo Co. Ltd. (Japan). Poly(3,4-ethylenedioxythiophene): poly(styrene sulfonate) (PEDOT:PSS) (Clevios$^{TM}$ HTL Solar) was obtained from Heraeus (Germany). Poly(3-hexylthiophene-2,5-diyl) (P3HT), [6,6]-Phenyl $C_{61}$ butyric acid methyl ester (PCBM), 1,2-dichlorobenzene, and gold nanoparticles solution (AuNPs, an average of 5.0 nm) were purchased from Sigma-Aldrich (Japan). An indium tin oxide (ITO)-coated glass substrate with a conductivity of 10 Ω/cm$^2$ was purchased from Furuuchi chemical (Japan). Concentrated hydrochloric acid (HCl, 37%) and analytical grade acetone were purchased from Sigma-Aldrich (Japan).

### 2.2.2 Fabrication of AuQDs/plasmonic AuNPs OSCs

In this work, the photovoltaic devices were constructed on ITO-coated glass substrates (area of 1.0 cm$^2$). After cleaning process, the ITO glass substrate was dried and treated with UV ozone for 20 min in order to improve the wettability of the ITO surface. To prepare the PEDOT:PSS:AuNPs composite buffer layer, 0.10 mM solution of AuNPs with a particle size of 5.0 nm was mixed with PEDOT:PSS solution (ratio of 1:6 v/v) using sonication for 1 h. The aqueous solution of AuQDs (B-AuQDs, G-AuQDs, or R-AuQDs) with an optimized concentration (Table A1.1, appendix A) was first deposited on an ITO glass substrate by spin-coating technique, subsequently annealed at 120 $^oC$ for 30 min. The PEDOT:PSS:AuNPs solution was next spin-coated at 1000 rpm on the top of the layer of AuQDs and annealed at 120 $^oC$ for 30 min. The thickness of this layer was approximately 100 nm (Appendix A, Figure A2.1). The P3HT:PCBM blended solution with a mass ratio of 1:0.8 in

dichlorobenzene was spin-coated on the PEDOT:PSS surface, followed by annealing at 120 $^{o}$C for 30 min. The P3HT:PCBM played as a photoactive layer with a thickness of 100 nm. (Appendix A, Figure A2.2). Finally, a 150 nm thick layer of Al electrode was deposited onto the P3HT:PCBM layer through a thermal evaporation under vacuum. Then, all of devices were annealed at 150 $^{o}$C for 45 min under a vacuum chamber before further characterization.

### 2.2.3 Characterization

The photovoltaic properties and impedance spectra of the fabricated devices were measured by a precision source/measure unit (B2901A, Agilent) and a potentiostat (PARSTAT 4000, Princeton Applied Research), respectively, and the solar cell was performed under illumination from a solar simulator (HAL-C100, 100W compact xenon light source, Asahi Spectra) with a light intensity of 75 mW/cm$^2$. The UV–visible absorption spectra of the AuQDs/PEDOT:PSS:AuNPs films and the AuQDs/PEDOT:PSS:AuNPs/ P3HT:PCBM films on TIO glasses were evaluated by a UV–vis spectrometer (V-650, Jasco). The surface morphologies of the AuQDs films and PEDOT:PSS:AuNP films were characterized using an atomic force microscope (AFM, SPM-9600, Shimadzu, Japan).

## 2.3 RESULTS AND DISCUSSION

### 2.3.1 Optical properties and surface morphology of the AuQDs/plasmonic AuNPs systems

Three types of AuQDs with different fluorescence emissions; B-AuQDs (mixture of $Au_5$ and $Au_8$ nanoparticles), G-AuQDs ($Au_{13}$ nanoparticles), and R-AuQDs ($A_{25}$ nanoparticles), were used in this study. The emission visible lights from AuQDs layers would be expected to govern more light trapping available in the solar cells. The characteristic absorption of AuQDs greatly depended on their size which would influence on the performances of plasmonic AuNPs solar cells. AuQDs stabilized by pepsin molecules in an

aqueous solution form exhibit strong absorptions at the wavelength below 400 nm and emit the fluorescence at the longer wavelength in the visible region [14]. The absorption spectra of the three AuQDs solutions (5.0 μM) are presented in Figure 2.1(a) and their fluorescence spectra under UV light illumination ($\lambda_{ext}$ = 350 nm) are shown in Figure 2.1(b).

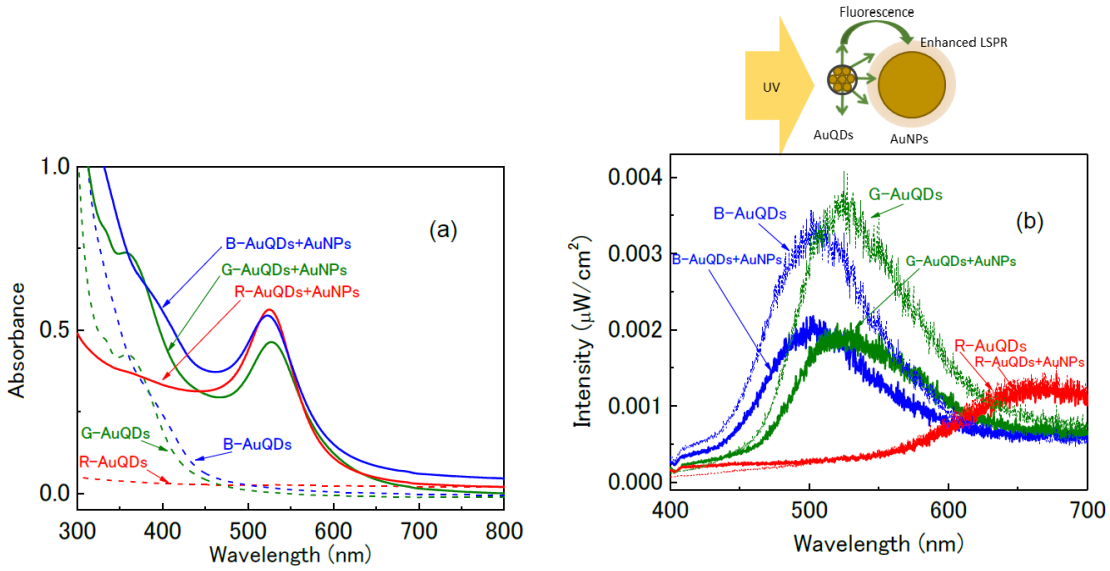


**Figure 2.1** (a) UV–vis absorption spectra and (b) fluorescence spectra of AuQDs and AuQDs:AuNPs aqueous solution. The figure reproduced from Ref. [22] Copyright 2019 with permission from the Royal Society of Chemistry.

In this measurement, deionized water was added to the AuQDs to maintain the same concentration (5.0 μM) as in the AuQDs/AuNPs complex system in deionized water, as the added AuNPs were dissolved in deionized water. The absorption spectra of the AuQDs/AuNPs complex exhibit a localized plasmon peak at around 525 nm in addition to the absorption baseline of AuQDs. It should be noted that the fluorescence peaks of B-AuQDs and G-AuQDs decreased considerably when they were mixed with the AuNPs. This result clearly indicates that the fluorescence emission of AuQDs is quenched by AuNPs. Especially, significant quenching was observed in the G-AuQDs/AuNPs complex. Because the fluorescence peak of G-AuQDs and the localized plasmon peak overlap significantly, the quenching can be considered mainly as an energy transfer, which should enhance localized

plasmon excitation [19]. This is expected to enhance photocarrier generation in the active layer when the G-AuQDs/AuNPs complex system is used in OSC devices. However, almost no fluorescence quenching was observed for R-AuQDs/AuNPs. This is reasonable because the overlap between the absorption of AuNPs and the fluorescence emission wavelength of R-AuQDs is very small, resulting in almost no energy transfer in this system.

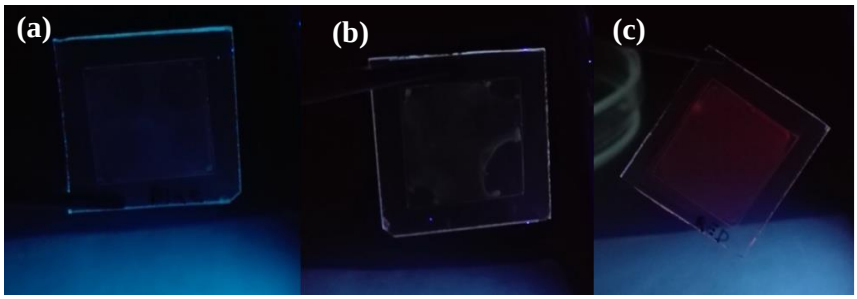


**Figure 2.2** Fluorescence emission characters of AuQDs films (a) B-AuQDs, (b) G-AuQDs, and (c) R-AuQDs on glass substrates under UV illumination.

In addition, the fluorescence emission of dried AuQDs films could be clearly observed by naked eyes under irradiating UV light (Figure 2.2), observable characteristic colors emitted from these AuQDs in dried state are similar to those in the solution form, suggesting that excited electrons of AuQDs would be promoted by a UV absorption and then the visible light was generated into the system when the AuQDs films are employed to construct the devices.

The UV-visible absorption studies of AuQDs/AuNPs: PEDOT:PSS and AuQDs/AuNPs:PEDOT:PSS/P3HT:PCBM films are shown in Figures 2.3(a) and 2.3(b), respectively.

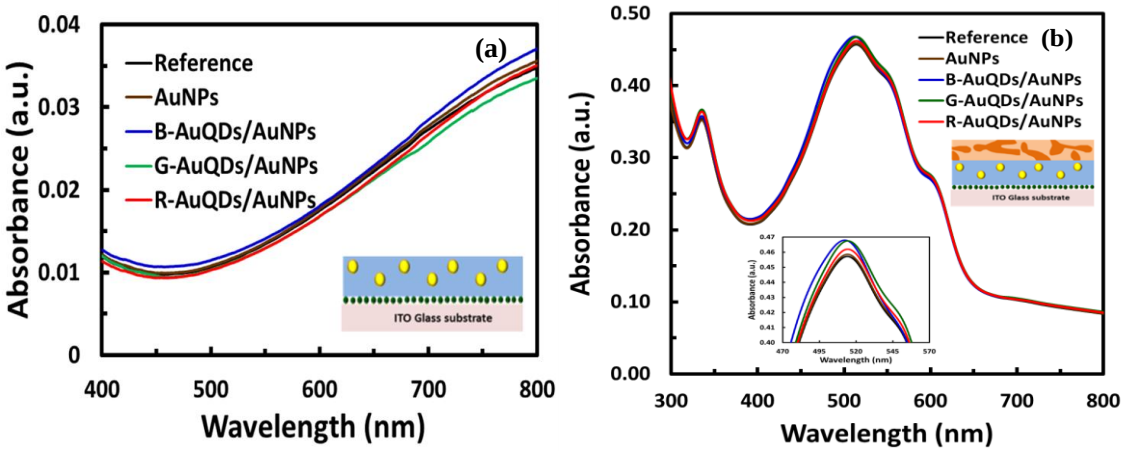


**Figure 2.3** UV-visible spectra of (a) AuQDs/PEDOT:PSS:AuNPs films and (b) AuQDs/PEDOT:PSS:AuNPs/P3HT:PCBM films on ITO glass substrates.

The absorption spectrum of PEDOT:PSS film exhibited a higher absorption after loading metal nanoparticle into the device, indicating that AuNPs could enhance the optical absorption within the film by localized surface plasmon resonance (LSPR) effects [9, 23, 24]. By contrast, incorporation of G-AuQDs into the plasmonic AuNPs:PEDOT:PSS film obtained the lowest absorption at longer wavelength compared to the others. In general, the decrease in this case might be induced from a strong fluorescence emission in longer wavelength region of AuQDs [25]. G-AuQDs demonstrated a photoluminescence at a maximum wavelength of 510 nm which is longer than that of B-AuQDs (402 nm). Although, R-AuQDs emitted the fluorescence at longer wavelength (maximum peak of 670 nm), it still exhibited weak emission compared to that of G-AuQDs [14, 25]; therefore, this phenomenon might cause reduction of the absorption in PEDOT:PSS film when combined with G-AuQDs layer [14, 25]. Furthermore, the UV-visible absorption spectra of photoactive layer films with and without the plasmonic AuNPs systems have been also investigated. The P3HT:PCBM blend was used as a light absorber in the solar cell which revealed two strong absorption regions; an absorption peak at *ca*. 350 nm and an absorption broad peak between 400 and 700 nm [23]. At the second adsorption region, no significant change in the adsorption intensity in

AuNPs:PEDOT:PSS/P3HT:PCBM film was found as compared to that of the reference PEDOT:PSS/P3HT:PCBM film whilst the absorption intensities of AuQDs/AuNPs: PEDOT:PSS/P3HT:PCBM film slightly increased. From the results above, it is plausible that the absorption enhancement in the devices is resulted from LSPR effect of AuNPs and agglomerated AuNPs/AuQDs [5, 23, 25].

The surface morphologies of AuQDs and AuQD/AuNP:PEDOT:PSS films were studied using atomic force microscopic (AFM) measurement. In this experiment, the aqueous solution of AuQDs was deposited onto the substrate by spin coating technique as the first step. The surfaces of AuQDs films revealed irregular shape of Au nanoparticles as bright spots as shown in Figure 2.4. The appearance of bright spots on the surface was originated from the large aggregation of AuQDs with a size of *ca.* 5 nm. As a result, the increase in light adsorption of the AuQDs/AuNPs:PEDOT:PSS/P3HT:PCBM film would be contributed from LSPR of such agglomerated particles.

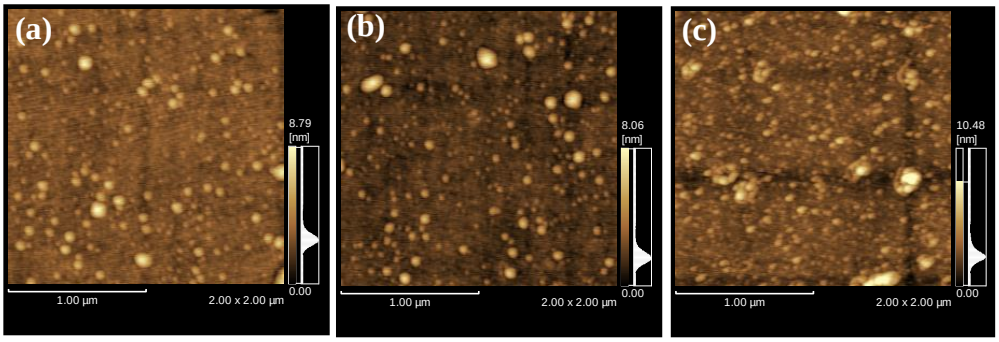


**Figure 2.4** AFM images of AuQDs films after directly spin coated on glass substrates, (a) B-AuQDs, (b) G-AuQDs, (c) R-AuQDs with a concentration of 5.0 µM.

Although aggregation of AuQDs was observed on the film surface, a photograph of AuQDs under UV irradiation indicated homogeneous fluorescence (see Figure 2.2), indicating that the non-aggregated AuQDs were uniformly deposited on the substrate together with the aggregated AuQDs. It should be noted that aggregated AuQDs with a size of 5 nm are

expected to exhibit a plasmonic-like effect because the size of Au becomes similar to that of plasmonic AuNPs [20]. The AFM images of a variety of PEDOT:PSS films are presented in Figure 2.5. A similar surface morphology was observed after spin coated a pristine PEDOT:PSS solution on the tops of all the AuQDs layers (Figure 2.5(a-d)). In addition, no significant difference in the morphology of PEDOT:PSS in AuNPs:PEDOT:PSS film sitting on all AuQDs films was observed and the surface exhibited some aggregation of AuNPs as bright spots (supporting information, Figure 2.5 (e-h)). This suggests that the AuQDs-AuNPs plasmonic system strongly affects the device performances. Moreover, the distributions of various sized metal nanoparticles in PEDOT:PSS layer could increase the surface roughness as the particles size increases. High surface roughness can enlarge the interface area between anode and photoactive layer, providing a short route for holes to reach the anode and leading to enhance the holes collection efficiency [8].

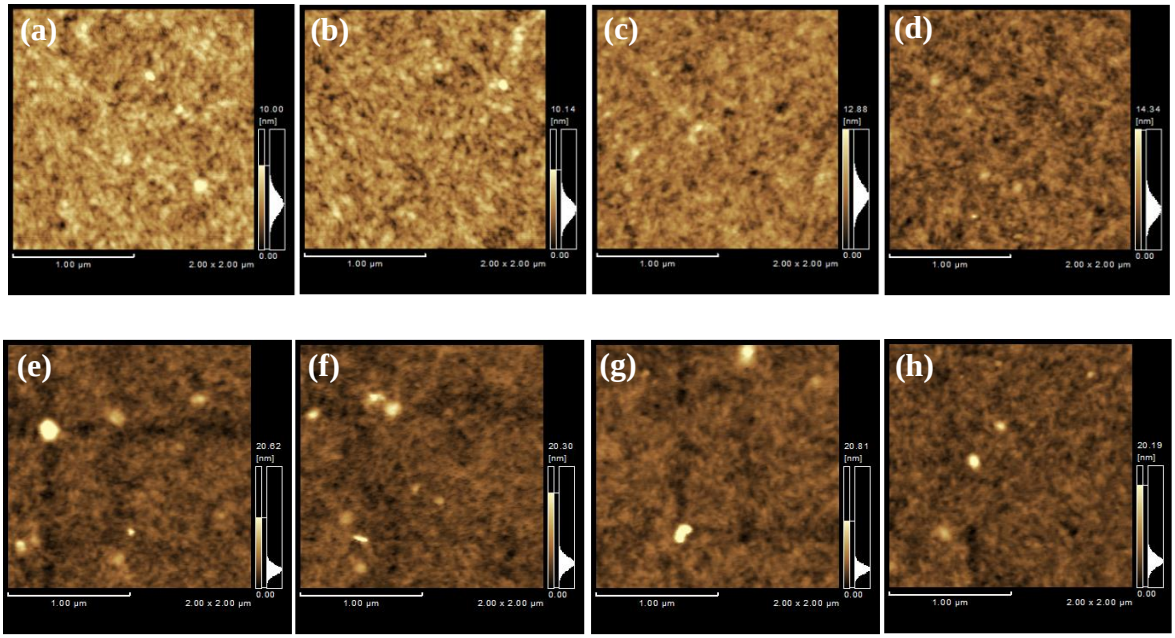


**Figure 2.5** Surface morphology of PEDOT:PSS films on (a) ITO substrate (reference cell), (b) B-AuQDs layer, (c) G-AuQDs layer, (d) R-AuQDs layer and of PEDOT:PSS:AuNPs films on (e) ITO substrate, (f) B-AuQDs layer, (g) G-AuQDs layer, and (h) R-AuQDs layer.

An aggregation of AuQDs is normally formed as various particle sizes. In this case, it is expected that the insertion of AuQDs layer with different aggregated sizes and the incorporation of AuNPs into PEDOT:PSS layer could increase surface roughness within the device, which can improve the holes collection efficiency and enhance the solar cell performances.

### 2.3.2 Photovoltaic performances of AuQDs/plasmonic AuNPs solar cells

The proposed device structure of AuQDs/plasmonic AuNPs solar cells is Al/P3HT:PCBM/PEDOT:PSS:AuNPs/AuQDs/ITO glass substrate as shown in Figure 2.6(a). Different florescence emissions of AuQDs: B-AuQDs, G-AuQDs, and R-AuQDs are used to improve the properties in plasmonic AuNPs-enhanced photovoltaic devices. Under the same experimental conditions, AuNPs are added into the hole-transport PEDOT:PSS layer for photon trapping and each AuQDs layer is used for UV light harvesting. It is found that AuQDs/plasmonic AuNPs system shows the synergistic benefit in the light management of the developed OSCs. The current density-voltage (*J*-*V*) characteristics of different AuQDs/plasmonic AuNPs fashions in fabricated solar cells are presented in Figure 2.6(b), and the important photovoltaic parameters of the devices are illustrated in Table 2.1.

Especially, AuNPs induce localized surface plasmonic effect which can enhance the optical path lengths via light scattering, as well as increasing the light absorption into a photoactive layer [5, 26, 27]. Moreover, AuQDs layer inserted into the plasmonic AuNPs OSCs can increase the light absorption in UV region and convert it into visible light [25] available in the cells, in which the higher photogenerated carrier would be obtained due to higher absorption of visible light by active layer.

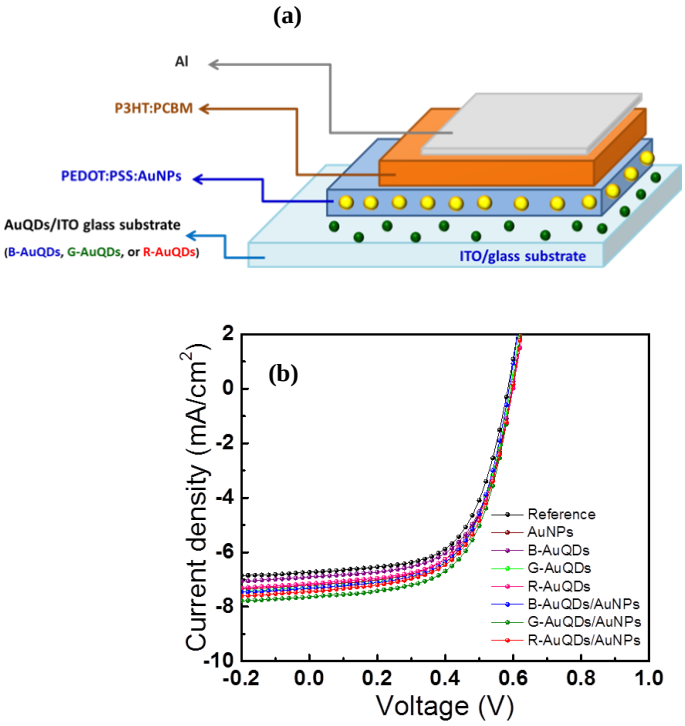


**Figure 2.6** (a) Schematic of the fabricated OSCs and (b) *J-V* characteristics of the OSCs compared with the reference cell. The figure reproduced from Ref. [22] Copyright 2019 with permission from the Royal Society of Chemistry.

The device without loading metal nanoparticles was used as a reference cell. After incorporation of a AuQDs layer; B-AuQDs, G-AuQDs, or R-AuQDs, and/or a AuNPs:PEDOT:PSS layer into the polymer solar cells, values of open-circuit voltage ($V_{oc}$) and the fill factor (FF) are found to be similar while short-circuit current density ($J_{sc}$) increase from 2.92 to 11.1 % and power conversion efficiency (PCE) enhance from 2.47 to 13.0 % in comparison with those of the reference cell. Among three AuQDs, putting G-AuQDs layer in the solar cell with no addition of the plasmonic AuNPs reveal the best performances which gave a $J_{sc}$ value of 7.33 mA·cm$^{-2}$ and PCE of 3.50 %. Comparative *J-V* curves for all the OSCs are clearly shown in Figure A2.3 (a), Appendix A. Interestingly, the AuQDs/plasmonic AuNPs embedded in the devices offered great photovoltaic performances.

**Table 2.1** Photovoltaic parameters of the developed OSCs

| Devices | Parameters | | | | |
|---|---|---|---|---|---|
| | $J_{sc}$ (mA·cm$^{-2}$) | $V_{oc}$ (V) | FF (%) | PCE (%) | Enhancement (%) |
| Reference | 6.85±0.08 | 0.59 | 0.59 | 3.24±0.03 | - |
| AuNPs | 7.28±0.05 | 0.59 | 0.60 | 3.42±0.02 | 5.56 |
| B-AuQDs | 7.05±0.15 | 0.59 | 0.59 | 3.32±0.02 | 2.47 |
| G-AuQDs | 7.33±0.02 | 0.59 | 0.60 | 3.50±0.01 | 8.02 |
| R-AuQDs | 7.21±0.07 | 0.60 | 0.60 | 3.45±0.04 | 6.48 |
| B-AuQDs/AuNPs | 7.20±0.11 | 0.59 | 0.60 | 3.44±0.04 | 6.17 |
| G-AuQDs/AuNPs | 7.61±0.04 | 0.60 | 0.60 | 3.66±0.03 | 13.0 |
| R-AuQDs/AuNPs | 7.38±0.05 | 0.60 | 0.60 | 3.54±0.01 | 9.26 |

The results clearly indicated that the $J_{sc}$ and PCE of all AuQDs/plasmonic AuNPs devices were additionally enhanced from those of the solar cells without plasmonic AuNPs in the HTL. Their *J-V* curves are shown in Figure A2.3 (b), Appendix A. The presence of both G-AuQDs layer under and AuNPs in PEDOT:PSS film actually reveals the greatest ability to increase the $J_{sc}$ from 6.85 to 7.61 mA·cm$^{-2}$ and enhance the PCE from 3.24 to 3.66 %, followed by those of R-AuQDs/plasmonic AuNPs and B-AuQDs/plasmonic AuNPs OSCs, respectively. The latter two solar cell systems obtained the $J_{sc}$ values of 7.38 and 7.20 mA·cm$^{-2}$ and the PCE values of 3.54 and 3.44 %, respectively. As observed with the fluorescence measurements are shown in Figure 2.1, UV harvesting by AuQDs and energy/electron transfer to plasmonic AuNPs should play an important role in enhancing the device performance. Therefore, light management, namely a fluorescent plasmonic system, should play an important role in developing photovoltaics. By comparing the efficiencies of the

AuQDs/AuNPs-OSCs and AuQDs-OSCs (without AuNPs), we can determine how much synergistic enhancement is obtained from each AuQDs/AuNPs system. The enhancement of the G-AuQDs/AuNPs-OSCs (η = 3.66%) compared to G-AuQDs-OSCs (η = 3.50%) was found to be 4.6%, while the enhancement of B-AuQDs/AuNPs (η = 3.44%) compared to B-AuQDs-OSCs (η = 3.32%) was 3.6%, and for R-AuQDs/AuNPs-OSCs (η = 3.54%) it was 2.6% compared to R-AuQDs-OSCs (η = 3.45%).The enhancement of the G-AuQDs/AuNPs combination was much more than that of the R-AuQDs/AuNPs, indicating that the best synergistic effect was obtained in this system. This is reasonable because the energy transfer, which enhances the localized surface plasmon excitation, can be obtained in the G-AuQD/AuNP system due to the overlap of the wavelength between the fluorescence of G-AuQDs and the localized plasmon peak of AuNPs. For the B-AuQDs/AuNPs-OSCs, the enhancement was greater than that of the R-AuQDs/AuNPs-OSCs, although not as high as for G-AuQDs/AuNPs-OSCs. This could be due to the significant aggregation of B-AuQDs observed in the AFM images and also due to the reduced energy/electron transfer compared to that of the G-AuQDs/AuNPs system observed in Figure 2.1.

To study the cooperative effects between AuQDs and AuNPs in the OSCs property, especially photocurrent responses or $J_{sc}$, the incident photon-to-current efficiency (IPCE) was measured at incident light wavelength of 300-800 nm. The fabricated solar cells with individual metal quantum dots demonstrated with an improvement in the IPCE spectra as shown in Figure 2.7(a) (Here, the V-shape dip at around 470 nm was originated from the light source characteristic, which was not related to the device performance). These developed devices dramatically enhanced the IPCE values over the broad wavelength range of 300-800 nm. Incorporating G-AuQDs into OSCs produced the greatest IPCE improvement as same as increases in $J_{sc}$ and PCE values, following by those of R-AuQDs and B-AuQDs, respectively. Additionally, the IPCE enhancement factors (E.F.), obtained by dividing the IPCE values of

the developed OSCs by the IPCE values of the reference solar cell, were plotted against the incident light wavelength as presented in Figure 2.7(b). An enhancement of IPCE values could be clearly observed for all OSCs based on only AuQDs layer. It is noted that the effect of AuQDs layer on OSCs could be described as follows. The E.F. in the near UV wavelength region, particularly around 300-500 nm, were induced from the absorption of AuQDs within the device. Via a quantum effect, these absorbed UV and emitted fluorescence at longer wavelengths, especially in the visible light region, to be absorbed by photoactive materials in the OSCs. Therefore, an increase in the enhancement factors from 300-500 nm was found, by which AuQDs generated a strong fluorescence in visible regions (420-680 nm, 450-700 nm, and 550-780 nm for B-AuQDs, G-AuQDs, and R-AuQDs, respectively) [25], that could promote the higher number of photocarriers in the photoactive layer. Over a region of 420-680 mm, it was found that G-AuQDs offers the highest improvement due to its highest intensity of fluorescence, which would be available for the absorptions of photoactive layer, plasmonic AuNPs, aggregated AuNPs, and/or aggregated AuQDs [25], as well as by a plasmonic-like effect associated with the aggregated AuQDs.

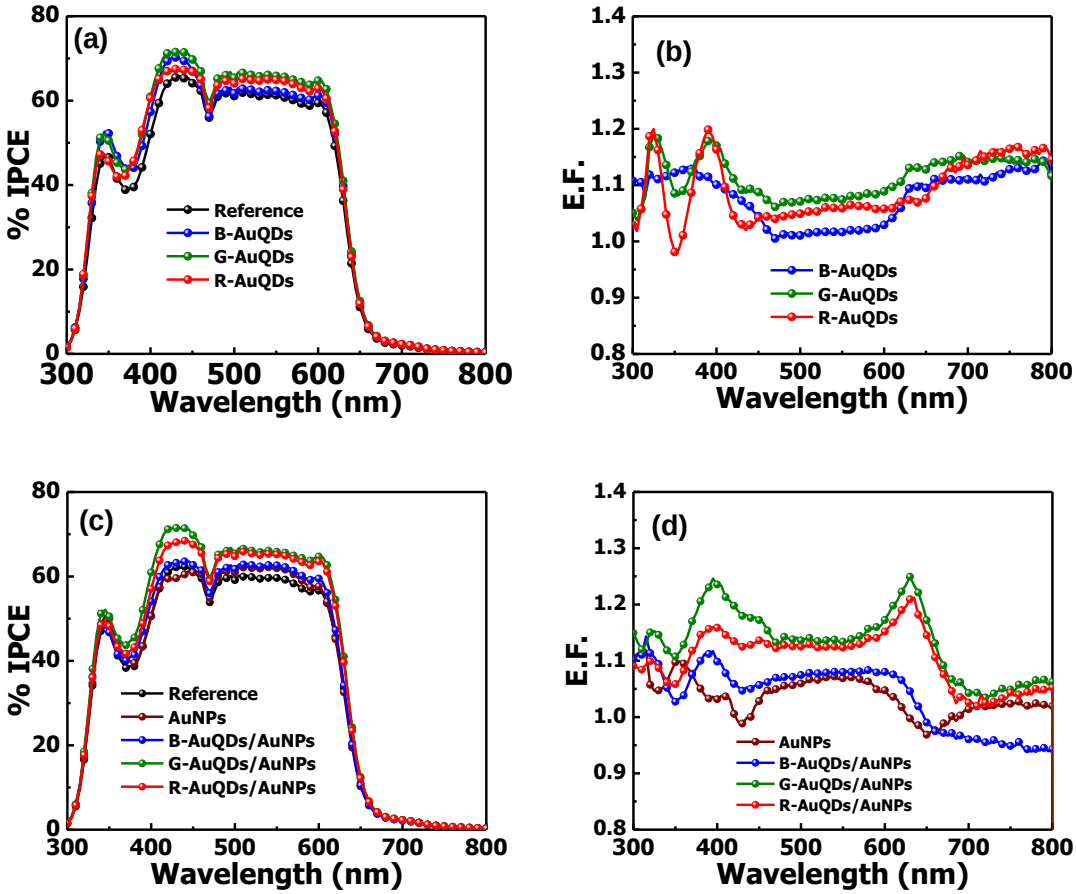


**Figure 2.7** (a) %IPCE and (b) E.F. profiles for only AuQDs layer system and (c) %IPCE and (d) E.F. profiles for the AuQDs/plasmonic AuNPs OSCs. The figure reproduced from Ref. [22] Copyright 2019 with permission from the Royal Society of Chemistry.

In IPCE at the wavelength range of 700-800 nm, R-AuQDs provided the highest enhancement due to its fluorescence. In the region 450–800 nm, the E.F. for B-AuQDs-OSCs were lower than those for the other two OSCs, even while presenting strong fluorescence emission. This might be caused by significant aggregation, which generally occurs with small high-surface-area nanoparticles [25, 28], thus lowering fluorescent intensity in our OSCs. Furthermore, the combination of AuQDs layer and dispersion of AuNPs in HTL for construction of OSCs has been studied. Again, the IPCE spectra and enhancement factor of AuQDs/plasmonic AuNPs OSCs were investigated as shown in Figures 2.7(c) and 2.7(d), respectively. A greater improvement in IPCEs over a similar wavelength region for all OSCs

is observed. Figure 2.7(d) presents the larger IPCE enhancement and G-AuQDs/plasmonic AuNPs system showed the best improvement in IPCEs, which is correlated to its photovoltaic performances. It was found that the combination benefits our device improvement as seen at the full wavelength range. In the region from 375-650 nm, the plasmonic OSC or the device incorporated with AuNPs into HTL obtained a lower IPCE enhancement than those performed with the AuQDs/plasmonic AuNPs OSCs but it is higher than that of the reference OSC. The G-AuQDs/plasmonic AuNPs OSC showed an increase the IPCE for a recorded whole range. In this case, an enhancement in the AuQDs/plasmonic AuNPs OSCs could result from a variety of unique properties of AuQDs and AuNPs within the devices. This could be explained mainly according to two phenomena. Firstly, the plasmonic effect (LSPR excitation) can induce at AuNPs that contributed to enhance the light trapping and the optical absorption cross-section of the device, leading to a higher efficiency improvement [1, 27]. Mixing the AuNPs into the PEDOT:PSS or HTL could promote the absorption possibility of the photoactive layer and they also increased the exciton generation rate and probability of exciton dissociation [29]. Secondly, when the size of AuNPs becomes less than 2 nm, the LSPR phenomenon cannot be observed but they exhibit a fluorescence emission which is depending on the quantum size effect [30]. B-AuQDs, G-AuQDs, or R-AuQDs layer not only enhance the light harvesting from the UV region but also generates the specific fluorescent lights inside fabricated devices [14]. In this study, incorporating AuQDs layer into the plasmonic AuNPs devices can improve their efficiencies as well. In particular, the best G-AuQDs/plasmonic AuNPs-OSCs demonstrated UV absorption and generated strong fluorescence emission (a maximum wavelength of *ca*. 525 nm), with energy that matched localized plasmon excitation, facilitating energy transfer from the AuQDs to the plasmonic AuNPs; therefore, this contributed to the largest increase in absorption and photocarrier generation in the P3HT:PCBM active layer.

### 2.3.3 Impedance spectroscopy of AuQDs/plasmonic AuNPs OSCs

The electrochemical impedance spectroscopy (EIS) was usually used for analysis the internal resistances and the electron transport kinetics in the organic solar cell [31, 32]. In this work, the interfacial properties of the developed photovoltaic devices consisting of AuQDs and AuQDs/plasmonic AuNPs configurations were investigated. The Nyquist plots of the impedance spectra under solar light illumination for the developed OSCs including AuQDs and AuQDs/plasmonic AuNPs systems are shown in Figures 2.8(a) and 2.8(b), respectively. The results indicate that all studied devices provide single semicircular curves in the Nyquist plots and the significant difference among impedance spectra of each device is clearly observed. The simple equivalent circuit model is shown in the inset of Figures 2.8(a) and 2.8(b). In this model, the $R_s$ value or a contact resistance in series represents the resistive loss in the ITO and PEDOT:PSS, corresponding to the intersection of the semicircles [27].

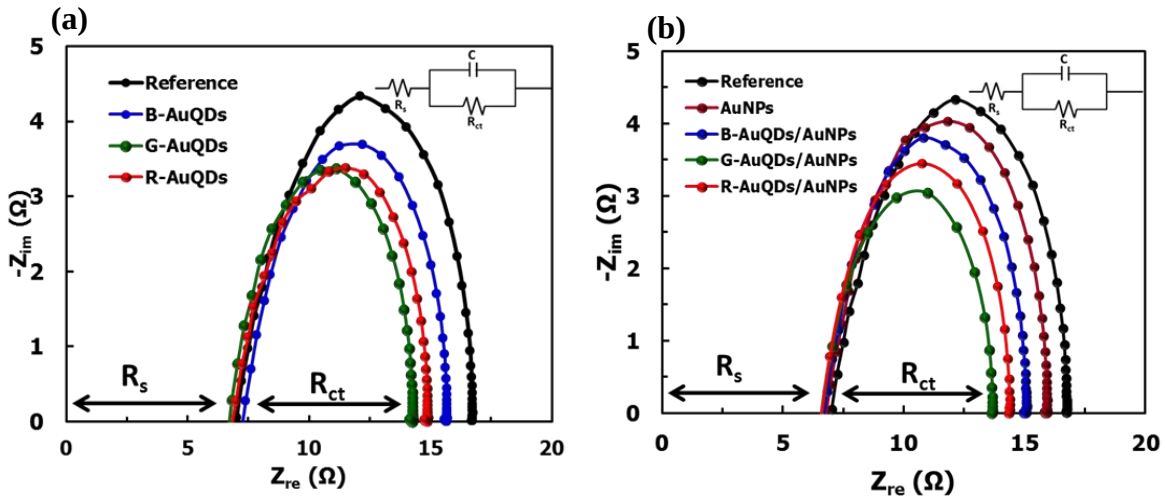


**Figure 2.8** Nyquist plots of the OSCs based on (a) individual AuQDs layers and (b) the AuQDs/plasmonic AuNPs systems under solar light illumination. The figure reproduced from Ref. [22] Copyright 2019 with permission from the Royal Society of Chemistry.

It was found that the $R_s$ values of the both AuQDs and AuQDs/plasmonic AuNPs devices are slightly smaller than that of the reference cell (Figure 2.8(a)). This described that the interfacial contact resistance of the fabricated devices was decreased by insertion of AuQDs layer, loading AuNPs into PEDOT:PSS film or combination of AuQDs and AuNPs:PEDOT:PSS layers. On the other hand, the constant phase element (CPE) in parallel with a charge transfer resistance ($R_{ct}$) is corresponding to the chemical capacitance which is used to describe a distribution of relaxation times at the donor/acceptor interfaces [33]. The charge transfer resistance of the photoactive layer in the fabricated plasmonic solar cells was decreased with incorporation of the plasmonic layers. The bulk resistances of the devices are derived as follows: the cells with no plasmonic nanoparticles (9.8 Ω), only AuNPs:PEDOT:PSS layer (8.9 Ω), only B-AuQDs layer (8.3 Ω), only R-AuQDs layer (7.9 Ω), and only G-AuQDs layer (7.3 Ω). Interestingly, the incorporation of both AuNPs:PEDOT:PSS and AuQDs layers into OSCs resulted in lower $R_{ct}$ values compared to those of individual systems, which were 8.1, 7.4, and 6.7 Ω for plasmonic B-AuQDs, R-AuQDs, and G-AuQDs systems, respectively. This indicated that the introductions of AuNPs into HTL and the layer of AuQDs into OSCs could induce an enhancement of the charge transport in the P3HT:PCBM layer [27]. Adding AuQDs layer could increase the number of photocarriers in the device via its fluorescence properties, which is consistent with the results obtained from *J-V* measurements. These photogenerated carriers in the P3HT:PCBM layer should result from absorption of UV and visible light fluorescence emission in the AuQDs layer. Furthermore, the combination of AuQDs and AuNPs further increased the photocarriers. This could be due to an enhanced localized plasmon field at the AuNPs caused by the fluorescence emission of AuQDs and energy/electron transfer from the AuQDs to AuNPs, which corresponded to the fluorescence quenching shown in Figure 2.1.

The characteristic frequency peaks of Bode phase plots for AuQDs and AuQDs/plasmonic AuNPs OSCs are shown in Figures 2.9(a) and 2.9(b), respectively. The characteristic frequency peaks are related to electron lifetime in the photoactive film [11, 31, 34]. Figure 2.9(a) showed that Bode phase plots of the devices incorporated with only AuQDs layer; B-AuQDs, G-AuQDs, or R-AuQDs. It could be seen that after adding AuQDs layer into the devices, the frequency peaks slightly shifted to higher frequency peaks in comparison with that of the reference cell. As found with the same behavior, the OSCs cooperating with AuQDs/plasmonic AuNPs systems obviously exhibited higher frequency peaks compared to that of an individual AuNPs cell (Figure 2.9(b)).

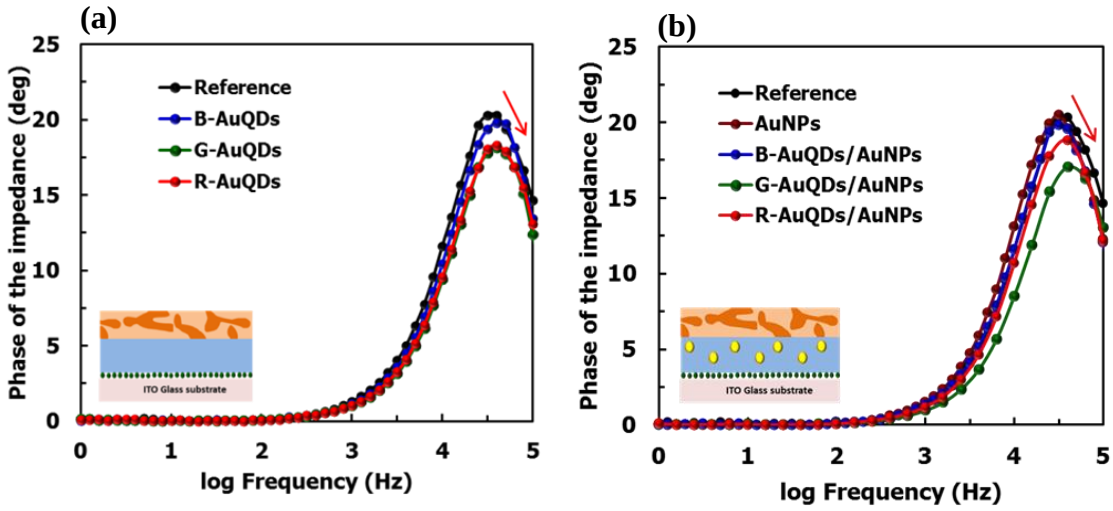


**Figure 2.9** Bode phase plots of the OSCs with (a) individual AuQDs layer and (b) the AuQDs/plasmonic AuNPs system under solar light illumination. The figure reproduced from Ref. [22] Copyright 2019 with permission from the Royal Society of Chemistry.

The results could imply that the developed devices had lower resistances which are correlated to the Nyquist plots, leading to higher performances. The specific fluorescence emission from AuQDs and the LSPR behavior from AuNPs induced a decrease in the bulk resistance and improved the charge transport in the P3HT:PCBM layer as well as along the

devices, thus contributed to a higher power conversion efficiency (PCE) [33]. The determination of the average electron lifetime in organic solar cell can be investigated using impedance spectroscopy [33, 35, 36]. The characteristic frequency peak of each photovoltaic device in Bode phase plots was employed for calculation of the average electron lifetime ($\tau_{avg}$) [11, 36]. In our study, the average carrier lifetimes are summarized in Table A2.2 (Appendix A). The results are not significantly different, suggesting that AuNPs:PEDOT:PSS and/or AuQDs layers would not affect the carrier lifetime. Therefore, the modification of OSCs configuration with AuNPs:PEDOT:PSS and/or AuQDs layers could improve the device performances by their virtues such as plasmonic and fluorescence effects.

## 2.4 SUMMARY

Novel design of AuQDs/plasmonic AuNPs system to manage photon for enhanced OSCs was illustrated. AuQDs layer with green fluorescence light emission and AuNPs:PEDOT:PSS HTL with LSPR excitation delivered the best light harvesting of OSCs. G-AuQDs exhibited a great enhancement of photovoltaic performances ($J_{sc}$ of 7.61 mA/cm$^2$ and a PCE of up to 3.66% (13% improvement), as compared to those of reference OSCs. AuQDs could broaden light harvesting in the UV region and emit light in the visible region, which could be absorbed in the active layer as well as inducing energy/electron transfer to the plasmonic AuNPs, resulting in more light harvesting in OSCs. Hence, the AuQDs/AuNPs complex system designed for OSCs has the potential to synergistically enhance OSCs performances. Our strategy for light manipulation in OSCs using AuQDs and AuNPs is promising and could be applied to the development of other types of solar cells.

## 2.5 REFERENCES


[1] Arinze, E.S., B. Qiu, G. Nyirjesy, and S.M. Thon, *Plasmonic nanoparticle enhancement of solution-processed solar cells: practical limits and opportunities*. ACS Photonics, 2016. **3**(2): p. 158-173.

[2] Chou, C.-H. and F.-C. Chen, *Plasmonic nanostructures for light trapping in organic photovoltaic devices.* Nanoscale, 2014. **6**(15): p. 8444-8458.

[3] Yang, J., J. You, C.-C. Chen, W.-C. Hsu, H.W. Zhang, Z. Hong, and Y. Yang, *Plasmonic polymer tandem solar cell*. ACS Nano, 2011. **5**(8): p. 6210-6217.

[4] Lim, E.L., C.C. Yap, M.A.M. Teridi, C.H. Teh, A.R.M. Yusoff, and M.H.H. Jumali, *A review of recent plasmonic nanoparticles incorporated P3HT: PCBM organic thin film solar cells*. Organic Electronics, 2016. **36**: p. 12-28.

[5] Pangdam, A., S. Nootchanat, R. Ishikawa, K. Shinbo, K. Kato, F. Kaneko, C. Thammacharoen, S. Ekgasit, and A. Baba, *Effect of urchin-like gold nanoparticles in organic thin-film solar cells*. Physical Chemistry Chemical Physics, 2016. **18**(27): p. 18500-18506.

[6] Hsiao, Y.-S., S. Charan, F.-Y. Wu, F.-C. Chien, C.-W. Chu, P. Chen, and F.-C. Chen, *Improving the light trapping efficiency of plasmonic polymer solar cells through photon management.* The Journal of Physical Chemistry C, 2012. **116**(39): p. 20731-20737.

[7] Wang, C.C.D., W.C.H. Choy, C. Duan, D.D.S. Fung, W.E.I. Sha, F.-X., Xie, F. Huang, and Y. Cao, *Optical and electrical effects of gold nanoparticles in the active layer of polymer solar cells*. Journal of Materials Chemistry, 2012. **22**(3): p. 1206-1211.

[8] Chen, X., L. Zuo, W. Fu, Q. Yan, C. Fan, and H. Chen, *Insight into the efficiency enhancement of polymer solar cells by incorporating gold nanoparticles*. Solar Energy Materials and Solar Cells, 2013. **111**: p. 1-8.

[9] Nagamani, S., G. Kumarasamy, M. Song, C.S. Kim, D.-H. Kim, S.Y. Ryu, J.-W. Kang, and S.-H. Jin, *Optical absorption and electrical properties of enhanced efficiency in organic solar cells as interfacial layer with Au NPs*. Synthetic Metals, 2016. **217**: p. 117-122.

[10] Notarianni, M., K. Vernon, A. Chou, M. Aljada, J. Liu, and N. Motta, *Plasmonic effect of gold nanoparticles in organic solar cells*. Solar Energy, 2014. **106**: p. 23-37.

[11] Nootchanat, S., H. Ninsonti, A. Baba, S. Ekgasit, C. Thammacharoen, K. Shinbo, K. Kato, and F. Kaneko, *Investigation of localized surface plasmon/grating-coupled surface plasmon enhanced photocurrent in $TiO_2$ thin films*. Physical Chemistry Chemical Physics, 2014. **16**(44): p. 24484-24492.

[12] Stratakis, E. and E. Kymakis, *Nanoparticle-based plasmonic organic photovoltaic devices*. Materials Today, 2013. **16**(4): p. 133-146.

[13] Liu, C.-M., C.-M. Chen, Y.-W. Su, S.-M. Wang, and K.-H. Wei, *The dual localized surface plasmonic effects of gold nanodots and gold nanoparticles enhance the performance of bulk heterojunction polymer solar cells*. Organic Electronics, 2013. **14**(10): p. 2476-2483.

[14] Kawasaki, H., K. Hamaguchi, I. Osaka, and R. Arakawa, *ph-Dependent synthesis of pepsin-mediated gold nanoclusters with blue green and red fluorescent emission*. Advanced Functional Materials, 2011. **21**(18): p. 3508-3515.

[15] Stamplecoskie, K.G. and P.V. Kamat, *Synergistic effects in the coupling of plasmon resonance of metal nanoparticles with excited gold clusters*. The Journal of Physical Chemistry Letters, 2015. **6**(10): p. 1870-1875.

[16] Kamat, P.V., *Quantum dot solar cells. semiconductor nanocrystals as light harvesters.* The Journal of Physical Chemistry C, 2008. **112**(48): p. 18737-18753.

[17] Kogo, A., Y. Takahashi, N. Sakai, and T. Tatsuma, *Gold cluster-nanoparticle diad systems for plasmonic enhancement of photosensitization*. Nanoscale, 2013. **5**(17): p. 7855-7860.

[18] Sakai, N. and T. Tatsuma, *Photovoltaic properties of glutathione-protected gold clusters adsorbed on $TiO_2$ electrodes*. Advanced Materials, 2010. **22**(29): p. 3185-3188.

[19] Choi, H., Y.-S. Chen, K.G. Stamplecoskie, and P.V. Kamat, *Boosting the photovoltage of dye-sensitized solar cells with thiolated gold nanoclusters*. The Journal of Physical Chemistry Letters, 2015. **6**(1): p. 217-223.

[20] Abbas, M.A., T.-Y. Kim, S.U. Lee, Y.S. Kang, and J.H. Bang, *Exploring interfacial events in gold-nanocluster-sensitized solar cells: insights into the effects of the cluster size and electrolyte on solar cell performance*. Journal of the American Chemical Society, 2016. **138**(1): p. 390-401.

[21] Stamplecoskie, K.G., Y.-S. Chen, and P.V. Kamat, *Excited-state behavior of luminescent glutathione-protected gold clusters*. The Journal of Physical Chemistry C, 2014. **118**(2): p. 1370-1376.

[22] Phetsang, S., A. Phengdaam, C. Lertvachirapaiboon, R. Ishikawa, K. Shinbo, K. Kato, P. Mungkornasawakul, K. Ounnunkad, and A. Baba, *Investigation of a gold quantum dot/plasmonic gold nanoparticle system for improvement of organic solar cells*. Nanoscale Advances, 2019. **1**(2): p. 792-798.

[23] Chen, X., L. Zuo, W. Fu, Q. Yan, C. Fan, and H, Chen, *Insight into the efficiency enhancement of polymer solar cells by incorporating gold nanoparticles*. Solar Energy Materials and Solar Cells, 2013. **111**: p. 1-8.

[24] Liu, C.-M., C.-M. Chen, Y.-W. Su, S.-M. Wang, and K.-H. Wei, *The dual localized surface plasmonic effects of gold nanodots and gold nanoparticles enhance the performance of bulk heterojunction polymer solar cells*. Organic Electronics, 2013. **14**(10): p. 2476-2483.

[25] Pangdam, A., S. Nootchanat, C. Lertvachirapaiboon, R. Ishikawa, K. Shinbo, K. Kato, F. Kaneko, S. Ekgasit, and A. Baba, *Investigation of Gold Quantum Dot Enhanced Organic Thin Film Solar Cells*. Particle & Particle systems Characterization, 2017. **34**(11): p.1-8.

[26] Atwater, H.A. and A. Polman, *Plasmonics for improved photovoltaic devices*. Nature Material, 2010. **9**(3): p. 205-213.

[27] Ng, A., W.K. Yiu, Y. Foo, Q. Shen, A. Bejaoui, Y. Zhao, H.C. Gokkaya, A.B. Djurišić, J.A. Zapien, W.K. Chan, and C. Surya, *Enhanced performance of PTB7:$PC_{71}BM$ solar cells via different morphologies of gold nanoparticles*. ACS Applied Materials & Interfaces, 2014. **6**(23): p. 20676-20684.

[28] Xia, Y., Y. Xiong, B. Lim, and S.E. Skrabalak, *Shape-controlled synthesis of metal nanocrystals: simple chemistry meets complex physics?*, Angewandte Chemie International Edition, 2009. **48**(1): p. 60-103.

[29] Chen, F.-C., J.-L. Wu, C.-L. Lee, Y. Hong, C.-H. Kuo, and M.H. Huang, *Plasmonic-enhanced polymer photovoltaic devices incorporating solution-processable metal nanoparticles*. Applied Physics Letters, 2009. **95**(1): p. 013305.

[30] Zheng, J., C. Zhang, and R.M. Dickson, *Highly fluorescent, water-soluble, size-tunable gold quantum dots*. Physical Review Letters, 2004. **93**(7): p. 077402.

[31] Hsu, C.-P., K.-M. Lee, J.T.-W. Huang, C.-Y. Lin, C.-H. Lee, L.-P. Wang, S.-Y. Tsai, and K.-C. Ho, *EIS analysis on low temperature fabrication of $TiO_2$ porous films for dye-sensitized solar cells*. Electrochimica Acta, 2008. **53**(25): p. 7514-7522.

[32] Hara, K., C. Lertvachirapaiboon, R. Ishikawa, Y. Ohdaira, K. Shinbo, K. Kato, F. Kaneko, and A. Baba, *Inverted organic solar cells enhanced by grating-coupled surface plasmons and waveguide modes*. Physical Chemistry Chemical Physics, 2017. **19**(4): p. 2791-2796.

[33] Leever, B.J., C.A. Bailey, T.J. Marks, M.C. Hersam, and M.F. Durstock, *In situ characterization of lifetime and morphology in operating bulk heterojunction organic photovoltaic devices by impedance spectroscopy*. Advanced Energy Materials, 2012. **2**(1): p. 120-128.

[34] Wang, Q., J.-E. Moser, and M. Grätzel, *Electrochemical impedance spectroscopic analysis of dye-sensitized solar cells*. The Journal of Physical Chemistry B, 2005. **109**(31): p. 14945-14953.

[35] Bisquert, J., F. Fabregat-Santiago, I. Mora-Seró, G. Garcia-Belmonte, and S. Giménez, *Electron lifetime in dye-sensitized solar cells: theory and interpretation of measurements*. The Journal of Physical Chemistry C, 2009. **113**(40): p. 17278-17290.

[36] Jiang, W., H. Liu, L. Yin, and Y. Ding, *Fabrication of well-arrayed plasmonic mesoporous $TiO_2$/Ag films for dye-sensitized solar cells by multiple-step nanoimprint lithography*. Journal of Materials Chemistry A, 2013. **1**(21): p. 6433-6440.

# CHAPTER III

## Investigation of Gold Quantum Dots/Metallic Grating System Incorporated into Organic Solar Cells

**ABSTRACT**

Development of advanced nanomaterials and device design play an important role for broadening light absorption in organic solar cells (OSCs). The incorporation of metallic nanostructures into photovoltaic devices provides a great potential for the light harvesting enhancement. This study demonstrates the fabrication of OSCs using novel dual function of gold quantum dots (AuQDs) together with metallic grating nanostructures. The combination of AuQDs and grating-couple surface plasmon resonance (GCSPR) into developed device in a structure of ITO/PEDOT:PSS:AuQDs/P3HT:PCBM/Al grating electrode was proposed as a new strategic concept to extend the light absorption in the UV regions by AuQDs (Blue: B-AuQDs, Green: G-AuQDs, and Red: R-AuQDs). Additionally, the fluorescent emission in visible regions originated from AuQDs can enhance the light harvesting of photoactive layer, resulting in a higher photocurrent in the solar cells. Furthermore, the GCSPR can increase the optical absorption path length of the devices. As a result, significant enhancements on the short circuit photocurrent ($J_{SC}$) and power conversion efficiency (PCE) of the developed photovoltaic devices were observed. Both single and dual systems improved the light harvesting of the OSCs. The incorporation of G-AuQDs and GCSPR showed the best photovoltaic performances compared to that of the reference device, resulting in the highest $J_{SC}$ of 8.41 mA/cm$^2$ and the greatest PCE of 3.91% with 19.57% enhancement. The synergetic effect between AuQDs and GCSPR benefit the remarkable enhancement of OSCs efficiency. This proposed platform could be further developed in practical application for next generation of solar cells.

**Keywords:** gold quantum dots, plasmonic solar cells, fluorescence, localized surface plasmon resonance, grating-coupled surface plasmon resonance

## 3.1 INTRODUCTION

Alternative energy technologies play an important role in the energy production because of the population growth and more energy demanding. Since, fossil fuel resources, a major source of energy in the world, are less available, more expensive and consumable. Additionally, the use of fossil fuels is the main cause of environmental problem like global climate change. Consequently, renewable energy sources are becoming a promising candidate to be an alternative clean energy and sustainable sources [1-4]. Sunlight is one interesting renewable free energy sources which is directly converted to electricity by photovoltaic devices. Although solar cell technologies have been successfully fabricated as a commercial device, the module manufacturing cost and the weighty crystalline silicon device are still concerned and needed to develop. Organic solar cells (OSCs) have a great potential, providing the cost-effective and simplistic fabrication. Because of the solution processing, it offers a flexible larger area process to fabricate lightweight solar cell platforms [4-7]. Although the bulk heterojunction OSCs offer a higher of charge generation efficiency, the short diffusion length of the photogenerated excitons (typically 10 nm) limits the photoactive layer thickness in the range of 30-100 nm, resulting in a decrease in optical absorption with a consequently low photocurrent [6, 8-10]. An increasing of the active layer thickness may enhance the light absorption but larger thickness can induce an increment of the recombination of free charge carriers within the OSCs, which possibly affect a higher resistance and a lower power conversion efficiency [5, 8, 9]. In order to increase the OSCs efficiency without the thickness enlargement, an enhancement of broadband absorption using advanced nanomaterials is from the good cell design. Recently, surface plasmon resonance is a promising way to improve the light trapping in photovoltaic devices by increasing the optical path length [11-15]. Periodic metallic nanostructures offer a propagating surface plasmon, resulting in an enhancement of the optical absorption of photoactive layers in OSCs

[5, 6, 14, 16-19]. Additionally, grating-coupled surface plasmon resonance (GCSPR) have been enhanced the photovoltaic performances with remarkable improvement in the photocurrent of the device [8, 20-23]. Metallic nanoparticles such as silver and gold nanoparticles (AgNPs and AuNPs) provide a strong localized surface plasmon resonance (LSPR); therefore, the introduction of AgNPs and AuNPs into the hole transport or the photoactive layers of OSCs can promote an efficient light harvesting in the visible range [13, 24-29]. Moreover, the incorporation of dual metallic nanostructure has been investigated to enhance the OSCs performances [5, 26, 27, 30, 31]. Many researchers have widely used AuNPs to take advantage from the SPR excitation in OSCs enhancement because AuNPs are not suffered from oxidation effects, maintaining a great stability into device [9, 26, 30, 32, 33]. The color of AuNPs depends on various shapes, sizes, and surrounding environment of the NPs and small particles sizes in the ranges of 2-100 nm typically provide the LSPR property [34]. When the particles size of gold becomes very small (less than 2 nm), they are called gold quantum dots (AuQDs) or gold nanocluster (AuNCs). Unlike the most popular of AuNPs, AuQDs do not give LSPR property but they exhibit electronic transitions in light absorption similar to molecules, which can generate the fluorescence in the visible region [35-38]. The shift of fluorescent emission wavelength of AuQDs is influenced by quantum confinement effects. The smallest cluster ($Au_5$) has a high quantum yield, illustrating blue emission, and the emission wavelength of larger cluster is in a redshift [34, 39, 40]. This characteristic can be implied that AuQDs can harvest the light from ultraviolet (UV) regions and convert it into the fluorescence in visible regions. Therefore, AuQDs are interesting material, used for broadening of light absorption especially in UV ranges. Also, AuQDs would be performed as a photosensitizer within OSCs. A few reports demonstrated the utilization of AuQDs for light harvesting improvement in the OSCs. The introduction of AuQDs into photovoltaic device can improve the solar cell performances, leading to increase

a short circuit current density and achieve power conversion efficiency up to 13% improvement [41]. Furthermore, AuQDs were effective in the operation of dye-sensitized solar cells (DSSCs), and they were employed as a photosensitizer and catalyst in the system. The deposited AuQDs at $TiO_2$ electrode improved the light absorption capability and increased the photocurrent and charge transport [35, 42-44].

This work demonstrates a novel design of OSCs by incorporation of AuQDs (Blue; B-, Green; G-, and Red; R- AuQDs) and BD-R metallic grating nanostructures into the device with a structure of ITO/PEDOT:PSS:AuQDs/P3HT:PCBM/Al nanograting electrode. AuQDs were directly introduced into the hole transport layer while the photoactive layer was patterned with BD-R grating structure in order to increase the efficiency. According to the optical property, this concept proposed to extend the light absorption over abroad range especially in UV regions by AuQDs and increase the optical path length of the device via GCSPR. Additionally, the fluorescence from AuQDs could act as a photosensitizer, enhancing a high photocurrent in the developed device. The synergistic effects between AuQDs and GCSPR in the fabricated OSCs exhibited better electrical and optical properties, leading to an enhancement of photocurrent and power conversion efficiency with approximately 20% improvement.

## 3.2 EXPERIMENTAL SECTION

### 3.2.1 Chemicals and materials

In this work, Poly(3-hexylthiophene-2,5-diyl) (P3HT), [6,6]-Phenyl $C_{61}$ butyric acid methyl ester (PCBM), 1,2-dichlorobenzene, and nitric acid ($HNO_3$) were purchased from Sigma-Aldrich (Singapore). The analytical grade of ethanol and acetone were obtained from Kanto Chemical Co. Ltd (Japan). Poly(3,4-ethylenedioxythiophene): poly(styrenesulfonate) or PEDOT:PSS (Clevios$^{TM}$ HTL Solar) was purchased from Heraeus (Germany). Three types of gold quantum dot (AuQDs) with different fluorescent emission wavelengths consisting of

Blue-AuQDs: B-AuQDs (mixture of $Au_5$ and $Au_8$ (mixture 5 and 8 Au atoms)), Green-AuQDs: G-AuQDs ($Au_{13}$ (13 Au atoms)), and Red-AuQDs: R-AuQDs ($A_{25}$ (25 Au atoms)) were purchased from Dai Nippon Toryo Co. Ltd. (Japan). An indium tin oxide (ITO)-coated glass substrate with a conductivity of 10 $\Omega.cm^{-2}$ was purchased from Furuuchi chemical (Japan).

### 3.2.2 Preparation of PDMS molds

The master templates of periodic BD-R pattern were prepared using the polydimethylsiloxane (PDMS). Firstly, the BD-R was cut into small rectangular pieces (2.5 cm x 4.0 cm) and immersed in conc. $HNO_3$ for 20 min to remove the dye coating layer on the polycarbonate grating side. Secondly, the BD-R substrates were sequentially cleaned with liquid detergent, tap water, and DI-water using an ultrasonic bath for 15 min of each step and these substrates were dried under $N_2$ stream. The liquid PDMS was casted on the cleaned BD-R grating substrates and removal of air bubbles by placing in a vacuum chamber before curing at 80 $^oC$ for 3 h. Finally, the PDMS molds with negative BD-R pattern were obtained.

### 3.2.3 Fabrication of organic solar cells

The photovoltaic devices were performed on an ITO-coated glass substrate (area of 1.0 $cm^2$). ITO glass substrates were cleaned using ultrasonic treatment with a detergent, DI water, and acetone to eliminate the impurity. The prepared ITO glass substrates were treated with UV ozone for 20 min in order to improve the wettability of the surface before the deposition of PEDOT:PSS or hole transport layer (HTL). To prepare the mixture of PEDOT:PSS and AuQDs, 0.003 mM of AuQDs (B-AuQDs, G-AuQDs, or R-AuQDs) was added into PEDOT:PSS solution with a ratio of 1:6 v/v and sonicated for 1 h. The nanocomposite of PEDOT:PSS:AuQDs solution was spin-coated on the ITO-coated glass substrate at 1000 rpm for 90 s, subsequently annealed at 120 $^oC$ for 30 min. The thickness of this layer was approximately 80 nm (Appendix B, Figure B3.1). After drying, the polymer

blended solution (P3HT:PCBM, weight ratio of 1:0.8 in dichlorobenzene) was spin-coated on the PEDOT:PSS or PEDOT:PSS:AuQDs layer (1000 rpm, 10 s and 1500 rpm, 60 s) to produce 100 nm-thick photoactive layer of the OSCs device (Appendix B, Figure B3.2). The PDMS mold with BD-R grating pattern was carefully placed onto P3HT:PCBM film and annealing at 100 $^{o}$C for 60 min for the nanoimprinting process. Then, the PDMS mold was peeled off from the substrate after cooling to room temperature. Finally, a 150 nm thick layer of Al electrode was deposited onto the P3HT:PCBM layer through thermal evaporation under vacuum and annealed at 150 $^{o}$C for 45 min under vacuum chamber.

### 3.2.4 Characterizations

The surface morphology and thickness of PEDOT:PSS film and P3HT:PCBM film were investigated using an atomic force microscopic technique (AFM, SPM-9600, Shimadzu, Japan). The photovoltaic performances of the fabricated OSCs were evaluated by a precision source/measure unit (B2901A, Agilent) and the solar cells were then illuminated under a solar simulator (HAL-C100, 100W compact xenon light source, Asahi Spectra, USA Inc.) with a light intensity of 75 mW/cm$^2$. The study of electrochemical impedance spectroscopy (EIS) was performed using a potentiostat (PARSTAT 4000, Princeton Applied Research) at frequencies in the range of 1 Hz - 1 MHz with an excitation of amplitude at 10 mV under the similar solar light intensity. For the reflectivity scan measurement, the fabricated devices were characterized by a homemade reflectrometer, consisting of a $\theta$-2$\theta$ goniometer, a halogen lamp, and ultraviolet-visible spectrometer (Ocean optic USB 2000). The halogen light source was applied for SP excitation and P-polarized (p-pol) light or S-polarized (s-pol) light were generated using an objective lens.

## 3.3 RESULTS AND DISCUSSION

### 3.3.1 Optical property and surface morphology of fabricated OSCs

The incorporation of AuQDs including B-AuQDs, G-AuQDs, or R-AuQDs into PEDOT:PSS layer for light harvesting was investigated in this work. The difference of fluorescent emission from gold nanoclusters is expected to broaden the light absorption in the solar cells. Generally, the particle sizes of metal originate in the tunability of the absorption spectrum due to their plasmonic effect and many metal NPs have been loaded into photovoltaic device to improve the optical and electrical properties [1, 4, 9]. On the other hand, when the particle size is very small (less than 2 nm), the fluorescence can be generated due to their quantum confinement effect [34, 36, 39]. The optical transitions of AuQDs are strongly dependent on the number of gold atoms in the nanoclusters [34]; B-AuQDs (mixture of $Au_5$ and $Au_8$ atoms), G-AuQDs ($Au_{13}$ atoms), and R-AuQDs ($Au_{25}$ atoms). AuQDs including B-, G-, and R-AuQDs are stabilized by pepsin molecules in an aqueous solution exhibit strong absorption in UV regions at the wavelength lower than 500 nm and emit the fluorescence in visible regions at the wavelength of 507, 520, and 650 nm, respectively [41].

In this work, an aqueous solution of 0.003 mM AuQDs; B-AuQDs, G-AuQDs, or R-AuQDs was mixed into PEDOT:PSS solution and then spin coated onto ITO glass substrate. AuQDs display a specific character after mixing process as shown in Figure 3.1.

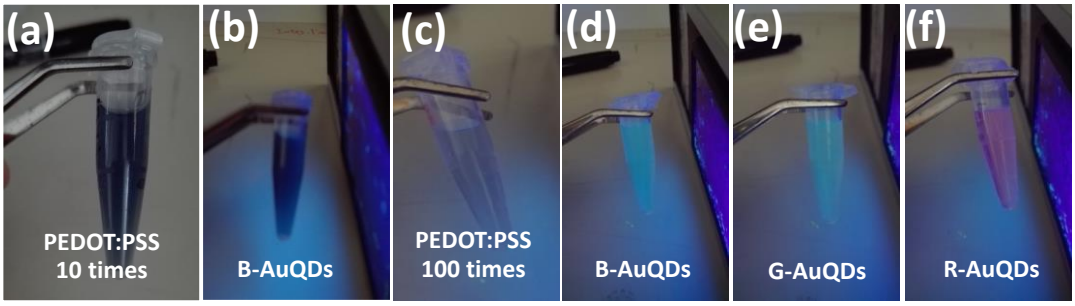


**Figure 3.1** Fluorescent emission of the mixing solution of 0.003 mM AuQDs and dilution of PEDOT:PSS at ratio 6:1, 10-fold dilution of PEDOT:PSS (a), mixing solution of PEDOT:PSS

(10-fold dilution) with B-AuQDs (b), 10-fold dilution of PEDOT:PSS (c), mixing solution of PEDOT:PSS (100-fold dilution) with B-AuQDs (d), G-AuQDs (e), and R-AuQDs (f) under UV illumination.

The results show that the pristine PEDOT:PSS solution do not generate the fluorescence under UV light illumination (Figure 3.1 (a and c)). No light emitting of AuQDs is observed at high concentration and the blue emission from B-AuQDs:PEDOT:PSS (10-fold dilution) appears as shown in Figure 3.1 (b). This phenomenon might be affected by the dark pigments of PEDOT:PSS, they could darken the light emission from AuQDs. Moreover, all of mixing AuQDs with 100-fold dilution of PEDOT:PSS solutions show that the fluorescence of B-AuQDs, G-AuQDs, and R-AuQDs clearly shine and easily observe by naked eyes as blue-, green-, and red-colors, respectively as shown in Figure 3.1 (d-f). From the result, it can be noticed that an introduction of AuQDs into PEDOT:PSS shows the characteristic of AuQDs. Thus, AuQDs are not only homogeneously dispersed in PEDOT:PSS but their optical property are also being. Additionally, the previous report demonstrated that more light absorption in UV region could be observed from AuQDs:PEDOT:PSS films as compared to PEDOT:PSS films and the fluorescence of AuQDs resulted in the slight decrease in the light absorption of PEDOT:PSS at the longer wavelength [41]. Therefore, the characteristic of AuQDs still maintains on the casting PEDOT:PSS:AuQDs films.

The surface morphology of the component films influenced on the optical and electrical properties of the photovoltaic devices [25, 32, 45]. Therefore, the effect of AuQDs on surface morphologies of fabricated organic solar cells was investigated. In this work, the mixture solution, AuQDs:PEDOT:PSS, were directly spin coated onto ITO glass substrate and the AFM images of the PEDOT:PSS film (reference cell) and AuQDs:PEDOT:PSS films are shown in Figure 3.2. A pristine PEDOT:PSS film exhibit a planar surface whereas some bright spots from the aggregation of AuQDs could be observed on the PEDOT:PSS:AuQDs

films as presented in Figure 3.2 (a-d). The results suggest that the incorporation of AuQDs into PEDOT:PSS can increase the surface roughness within the photovoltaic device which might be originated from the agglomeration of AuQDs. High surface roughness can enlarge the interfacial area between PEDOT:PSS and P3HT:PCBM, resulting in a short route for holes transport to the anode and enhancing the holes collection efficiency [25, 32]. Although the agglomeration of AuQDs in AuQDs:PEDOT:PSS film occurred, the photoluminescence of AuQDs still exists within photovoltaic device [41].

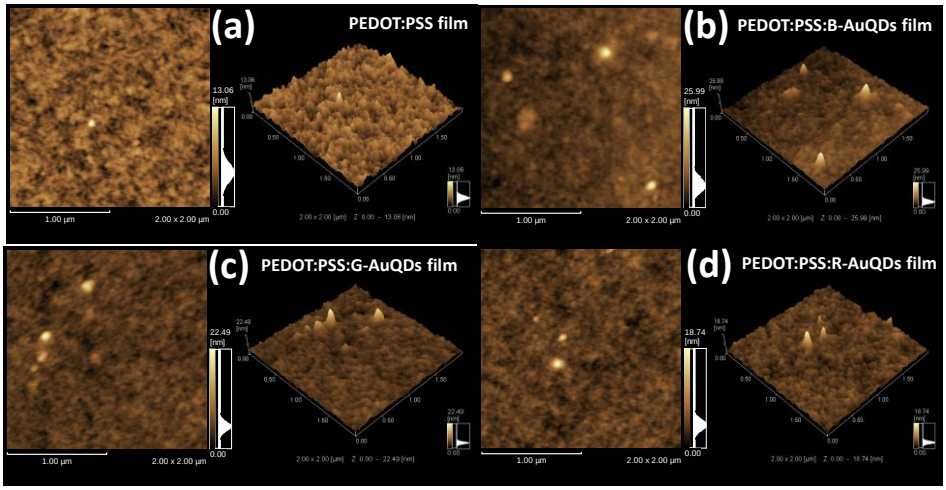


**Figure 3.2** AFM images of PEDOT:PSS film (reference cell) (a), PEDOT:PSS:B-AuQDs film (b), PEDOT:PSS:G-AuQDs film (c), PEDOT:PSS:R-AuQDs film (d) on ITO glass substrate.

In this study, it is expected that the addition of AuQDs into the fabricated OSCs would broaden the light absorption in UV region. Moreover, the aggregation of AuQDs is beneficial to produce small size of AuNPs, which is offering the LSPR, leading to increase the photovoltaic performances of the developed device. In addition, the morphology changes of P3HT:PCBM layer before and after patterning are shown in Figure 3.3. After spin coating of P3HT:PCBM film on the top of PEDOT:PSS layer, all electrodes display smooth surface morphology of the flat films (Figure 3.3 (a-d)). The pattern of the periodic BD-R nanostructure on P3HT:PCBM film is clearly observed after nanoimprinting process. The

results imply that the grating nanostructure is successfully constructed on the surface of photoactive layer as shown in Figure 3.3 (e-h). In the nanoimprinting process, the fluidic blended polymer can flow and align toward the grooves of grating pattern of the PDMS mold by the capillary force and the inverse nanostructure are faithfully transferred to the topography of the polymer film after demolding [8, 46].

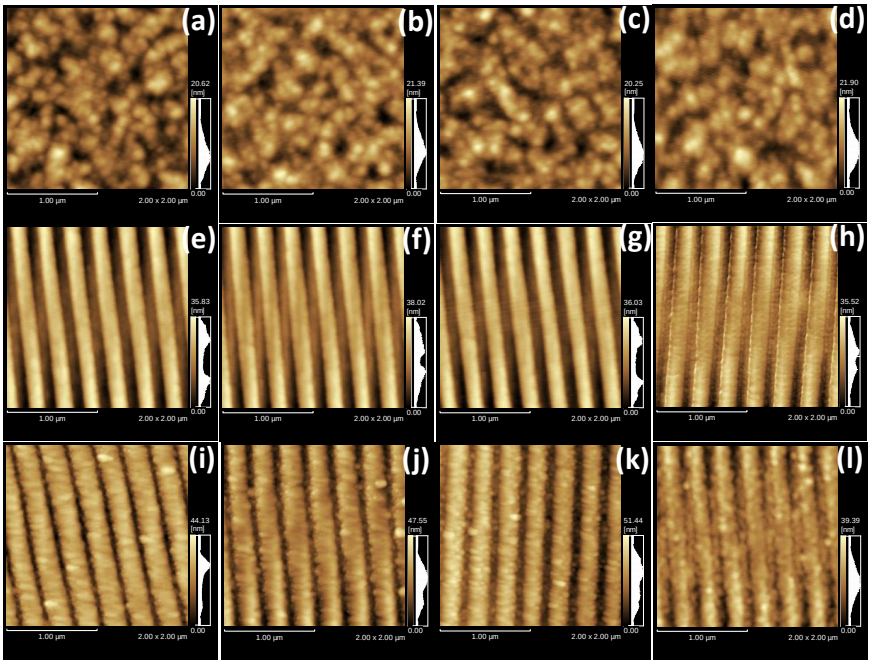


**Figure 3.3** Surface morphology of P3HT:PCBM layer on PEDOT:PSS layer of reference cell (a,e), the cell contained B-AuQDs (b,f), G-AuQDs (c,g), and R-AuQDs (d,h) of flat cell and BD-R imprinting cell, respectively. Surface morphology of reference cell (i), contained B-AuQDs (j), G-AuQDs (k), and R-AuQDs (l), after Al coating with grating pattern

The imprinted pattern can increase a roughness within the OSC device, leading to a relative increase in the interfacial area. This property can promote the exciton dissociation and charge transport enhancement of photovoltaic device [1, 12, 46-48]. Moreover, the corrugated nanopatterns of the device can be observed after Al coating as shown in Figure 3.3 (i-l). Typically, the incorporation of metallic grating nanostructure on the surface of photoactive layer has been carried out for light trapping enhancement without extending the physical

thickness of absorber layer [8, 12, 20, 21]. Several metallic nanostructures such as nanopillar, honeycomb lattice, and periodic grating nanostructure offer the surface plasmons, inducing a highly potential for the absorption property of fabricated OSCs [8, 19-21, 46]. Therefore, the patterning of BD-R grating-nanostructure is required to improve the solar cells efficiency due to their plasmonic effect and the schematic of the OSCs fabrication is shown in Figure 3.4.

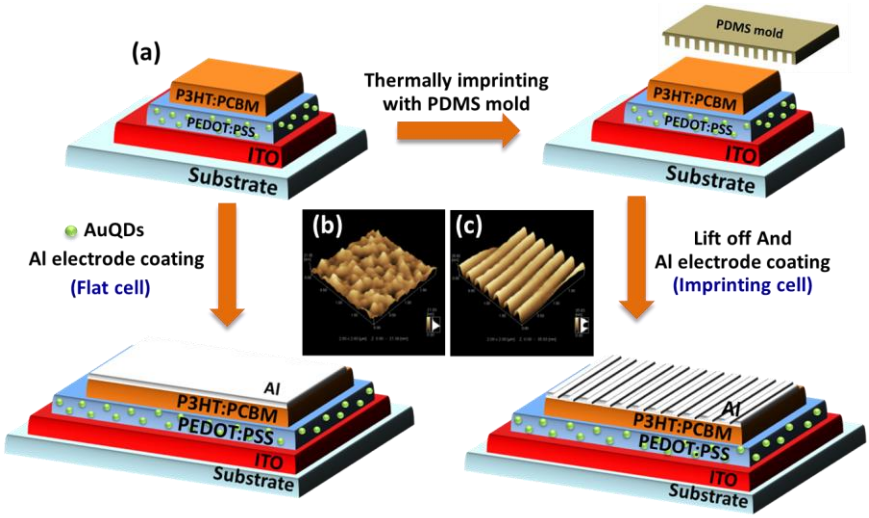


**Figure 3.4** Schematic of the fabricated OSCs with/without BD-R imprinting (a), surface morphology of P3HT:PCBM films without BD-R imprinting or flat (b) and with BD-R imprinting (c).

The surface plasmon resonances (SPR) property was examined from the reflectivity curve. The light absorption peaks enhancement are exactly correlated to the reflection peaks of Al gratings [8]. The excitation of GCSPR can be observed as dip peaks at fixed incident angles in the resonant wavelength and the SPR reflectivity spectra are shown in Figure 3.5. The reflectivity curves were operated by setting the incident angles from $20^{o}$ to $60^{o}$ under p-pol (the excitation of SP) or s-pol (the non-excitation of SP) white light illumination. The comparison between flat device (without grating nanostructure) and the grating device obviously exhibit a difference characteristic.

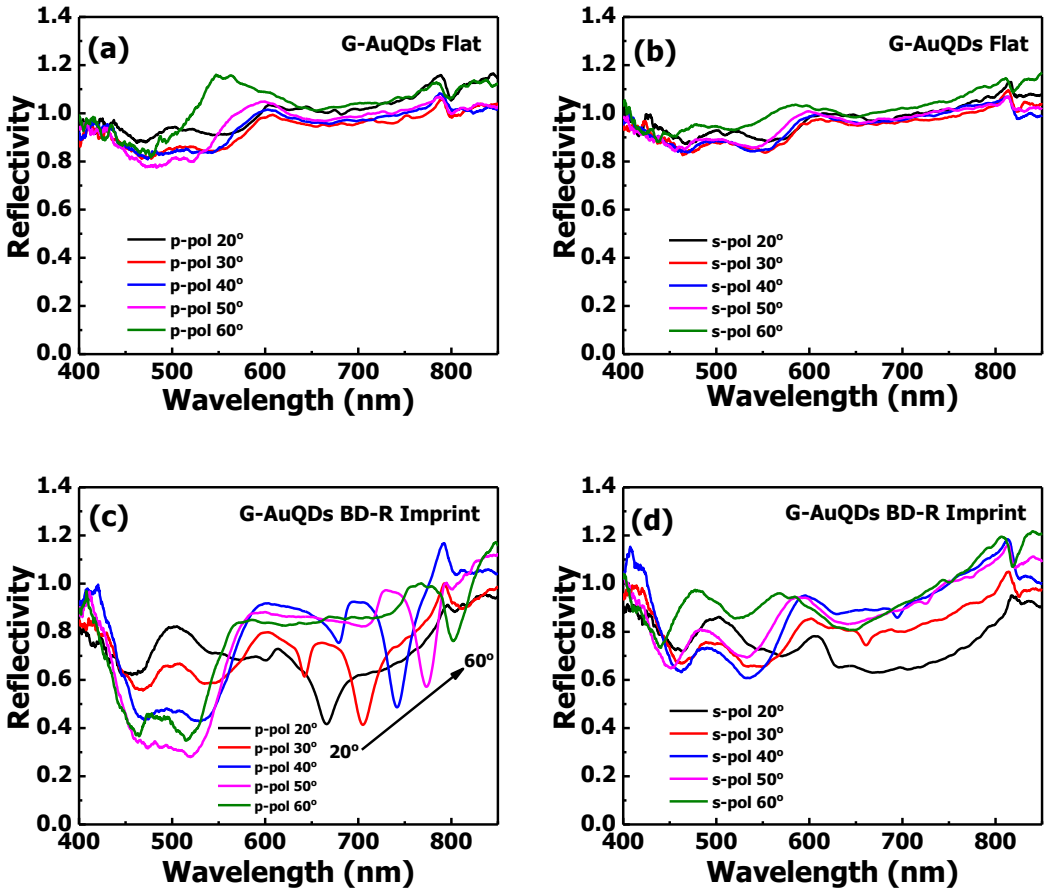


**Figure 3.5** SPR reflectivity curves of the fabricated OSCs adding G-AuQDs without BD-R grating (flat cell) (a,b) and with BD-R grating (imprinting cell) (c,d) under p-pol or s-pol illumination, measured at fixed incident angles from 20° to 60°.

The flat Al films, non-grating structure play like a mirror almost 100% and no dip peaks can be observed after irradiated both polarizations because the planar solar cell not allowed the SPR property [8], Figure 3.5 (a-b). On the other hand, sharp dip peaks are clearly observed from the device incorporated with metallic grating nanopatterns at the reflectivity spectra in the wavelengths above 500 nm under p-pol radiation. The resonant peaks shift toward longer wavelengths from 600 to 850 nm when increase the incident angles from 20 to 60°, respectively as shown in Figure 3.5 (c). Two resonance peaks could be observed for each angle. For example, at an incident angle 30°, the reflection peaks are observed at approximately 640 and 710 nm. As a result can be indicating that the electromagnetic fields

enhancement would obtain, enhancing the photocurrent of the device [8, 20-22]. Additionally, any dips peak did not appear under s-pol irradiating, Figure 3.5 (d). Actually, SPR cannot be excited under s-pol illumination. This result can be noted that the SPR can be originated from the BD-R nanostructure which is contributed to enhance the solar cell efficiency in photovoltaic device. Similarly, the SPR reflectivity of device containing with B-AuQDs and R-AuQDs exhibit the same character of resonant peak as shown in Figure 3.6 and 3.7, respectively.

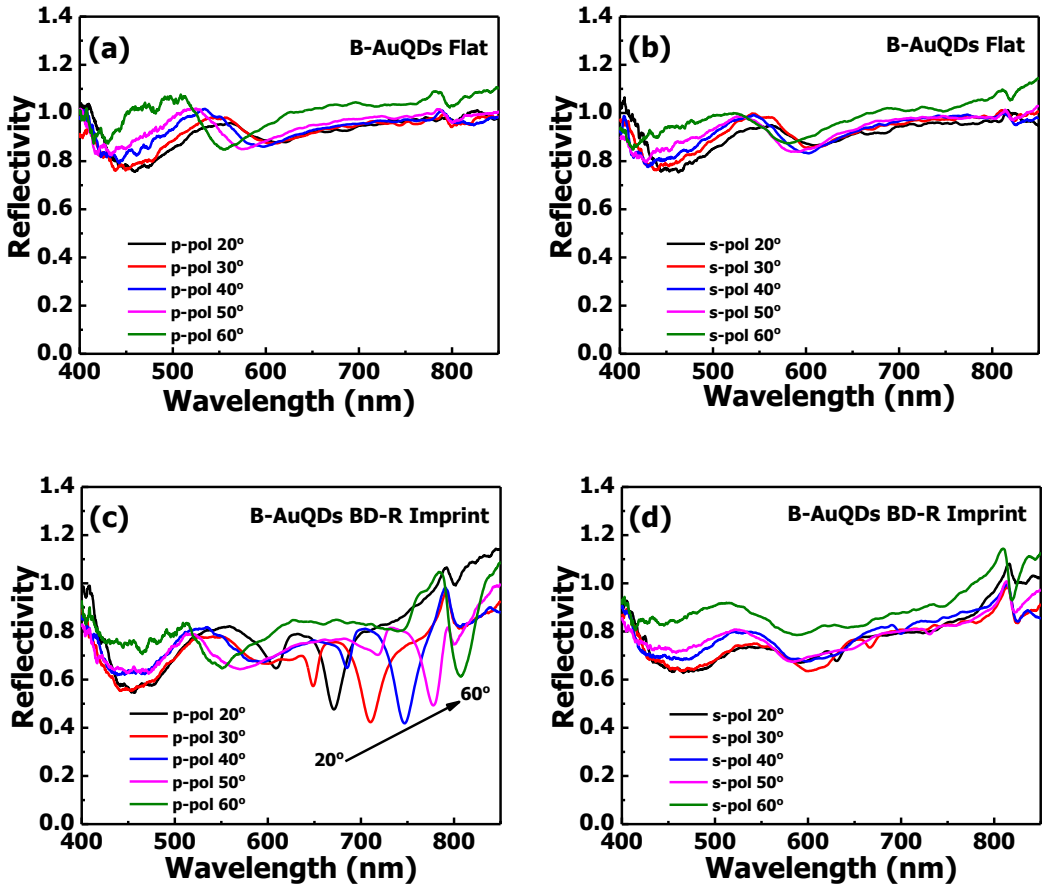


**Figure 3.6** SPR reflectivity curves of the fabricated OSCs adding B-AuQDs without BD-R grating (flat cell) (a,b) and with BD-R grating (imprinting cell) (c,d) under p-pol or s-pol illumination, measured at fixed incident angles from 20° to 60°.

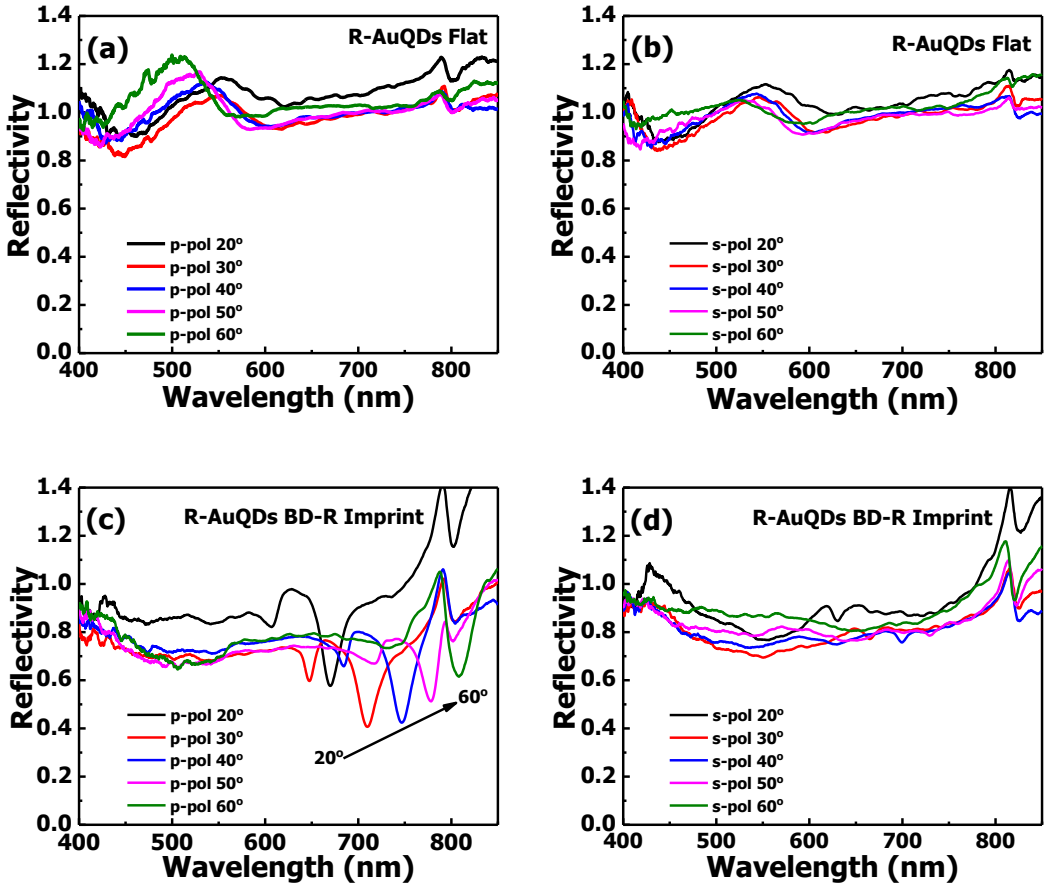


**Figure 3.7** SPR reflectivity curves of the fabricated OSCs adding R-AuQDs without BD-R grating (flat cell) (a,b) and with BD-R grating (imprinting cell) (c,d) under p-pol or s-pol illumination, measured at fixed incident angles from 20$^{o}$ to 60$^{o}$.

### 3.3.2 Photovoltaic performances of fabricated OSCs

The effect of AuQDs and BD-R nanostructure on the photovoltaic device are investigated under solar light irradiation and the current density versus voltage (*J-V*) characteristics of all fabricated solar cell are shown in Figure 3.8

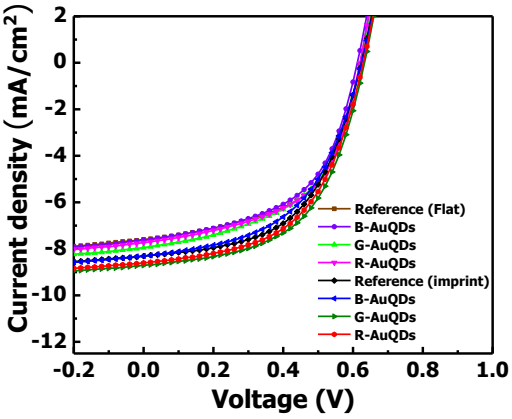


**Figure 3.8** *J-V* characteristics of the developed photovoltaic devices compared to the reference flat cell.

In comparison with the reference cell (a flat cell without AuQDs), the $J_{sc}$ is obviously improved after introduced AuQDs or patterned grating structure into the device. Especially, the incorporation of G-AuQDs with grating-nanostructure provides the highest enhancement. The *J-V* curves of each type of AuQDs; B-AuQDs, G-AuQDs, and R-AuQDs with and without BD-R grating are shown in appendix B Figure B3.3 (a-c). The *J-V* plots clearly exhibit that the devices covered with grating-nanostructure provide more $J_{sc}$ as compared to flat devices because of a high interfacial area. The dual metallic nanostructured devices (AuQDs and grating-nanostructure) have a greatest potential to increase the performances for all of electrodes.

The photovoltaic parameters of each device are listed in Table 3.1. The open circuit voltage ($V_{oc}$) and the fill factor (FF) are insignificant change whereas the $J_{sc}$ and the power conversion efficiency (PCE) increase for all of devices. As a result, the device containing G-AuQDs exhibits the greatest enhancement, followed by the cells included R-AuQDs and B-AuQDs, respectively.

**Table 3.1** Photovoltaic parameters of the OSCs incorporated different types of AuQDs with and without metallic grating nanostructures under solar light illumination.

| Devices | Parameters | | | | |
|---|---|---|---|---|---|
| | $J_{sc}$ (mA·cm$^{-2}$) | $V_{oc}$ (V) | FF (%) | PCE (%) | Enhancement (%) |
| Flat device | | | | | |
| Reference Flat | 7.37±0.08 | 0.61 | 0.54 | 3.27±0.03 | - |
| B-AuQDs Flat | 7.57±0.15 | 0.62 | 0.53 | 3.31±0.02 | 1.22 |
| G-AuQDs Flat | 7.83±0.07 | 0.62 | 0.54 | 3.54±0.04 | 8.26 |
| R-AuQDs Flat | 7.61±0.04 | 0.62 | 0.54 | 3.49±0.03 | 6.73 |
| Imprinting device | | | | | |
| Reference BD-R Imprint | 7.89±0.05 | 0.63 | 0.54 | 3.61±0.02 | 10.40 |
| B-AuQDs BD-R Imprint | 8.35±0.02 | 0.62 | 0.54 | 3.62±0.01 | 10.70 |
| G-AuQDs BD-R Imprint | 8.41±0.11 | 0.62 | 0.55 | 3.91±0.04 | 19.57 |
| R-AuQDs BD-R Imprint | 8.42±0.05 | 0.63 | 0.54 | 3.81±0.01 | 16.51 |

The reference cell exhibits the values of $J_{sc}$ (7.37 mA·cm$^{-2}$), $V_{oc}$ (0.61 V), FF (0.54%), and PCE (3.27%), respectively. The insertion of B-AuQDs into photovoltaic device slightly increases the $J_{sc}$ (7.57 mA·cm$^{-2}$) and PCE (3.31%) with the %improvement of 1.22%. Interestingly, the solar cells including R-AuQDs and G-AuQDs provide an excellent

enhancement of $J_{sc}$ and PCE, the R-AuQDs displays a $J_{sc}$ of 7.61 mA·cm$^{-2}$ and the PCE increases from 3.27 to 3.49% (6.73 % improvement). Additionally, the presence of G-AuQDs significantly enhances the $J_{sc}$ from 7.37 to 7.83 mA·cm$^{-2}$ and the PCE is improved to 3.54% (8.26% enhancement). In this study, aqueous solution of AuQDs was blended directly into the PEDOT:PSS layer because both of them are water solubility; therefore, a good distribution and the uniformity of each AuQDs could be formed. An enhancement of solar cell performances is indeed originated from AuQDs within the device. AuQDs did not only promote the absorption in UV region but they also generated the visible light into the proposed OSCs [41]. In this work, G-AuQDs provide an excellent enhancement of the photovoltaic performances, indicating that G-AuQDs can broaden the UV light absorption within OSCs. Furthermore, the fluorescence in visible regions ($\lambda_{emission}$= 520 nm) [41] completely matched with the absorption range of photoactive layer (300-700 nm) [14], leading to the highest PCE enhancement.

The combination of grating nanostructure on photovoltaic devices exhibits higher $J_{SC}$ and PCE than those of flat devices. Interestingly, the dual metallic nanostructures; AuQDs and BD-R grating-nanostructure give more improvement of the electrical properties. The incorporation of R-AuQDs and G-AuQDs with grating devices show a great $J_{sc}$ value of 8.42 and 8.41 mA·cm$^{-2}$, respectively, which is a higher value than reference flat cell ($J_{SC}$ = 7.37 mA·cm$^{-2}$), indicating a large $J_{sc}$ enhancement percentage of approximately 14%. This improvement attributed to increase the PCE value of 3.81% (R-AuQDs) and 3.91% (G-AuQDs) which is a considerable PCE enhancement percentage of 16.51 and 19.57%, respectively. As a result, it could be indicated that the introduction of AuQDs and grating nanopatterns into photovoltaic devices lead to increase the photocurrent via the efficient light trapping and the reduction of resistance.

To further elucidate the effect of plasmonic absorption enhancement of fabricated device, the incident photon-to-current efficiency (IPCE) were characterized in the wavelength from 300 to 800 nm. IPCE is defined as the ratio between the number of collected charge carriers and the number of incident photons at a given wavelength of the device [49]. Compared to the flat reference cell, the IPCE values of all developed devices display an enhancement of the photocurrent in an overall the broad wavelength at a fixed incident angle of $30^{o}$ as shown in the Figure 3.9 (a-c). It is found that these devices highly depended on the AuQDs and grating nanopatterns, the dual solar cells (B-, G-, and R-AuQDs incorporated grating nanostructures) plainly enhanced the IPCE. In order to understand the metallic nanostructure properties, the enhancement factor (E.F.) of the extracted IPCE between flat reference cell and developing cell was calculated. From the E.F. spectra, all of developing photovoltaic devices clearly exhibit an enhancement over a wide wavelength range and the E.F. tendency of three types of AuQDs seems a similar characteristic (Figure 3.9 (d-f). Considering in figure 3.9e, the addition of G-AuQDs into flat and imprinting device obviously reveals an IPCE E.F. in the UV wavelength regions particularly around 300-500 nm, inducing from the absorption of AuQDs within the device. Moreover, the effect of the BD-R grating on the absorption enhancement could be clearly observed the resonance peaks in visible regions at the wavelength around 550 - 660 nm and 660 - 760 nm. On the other hand, the flat cell cannot observe resonance peak and exhibit the lowest enhancement in the regions.

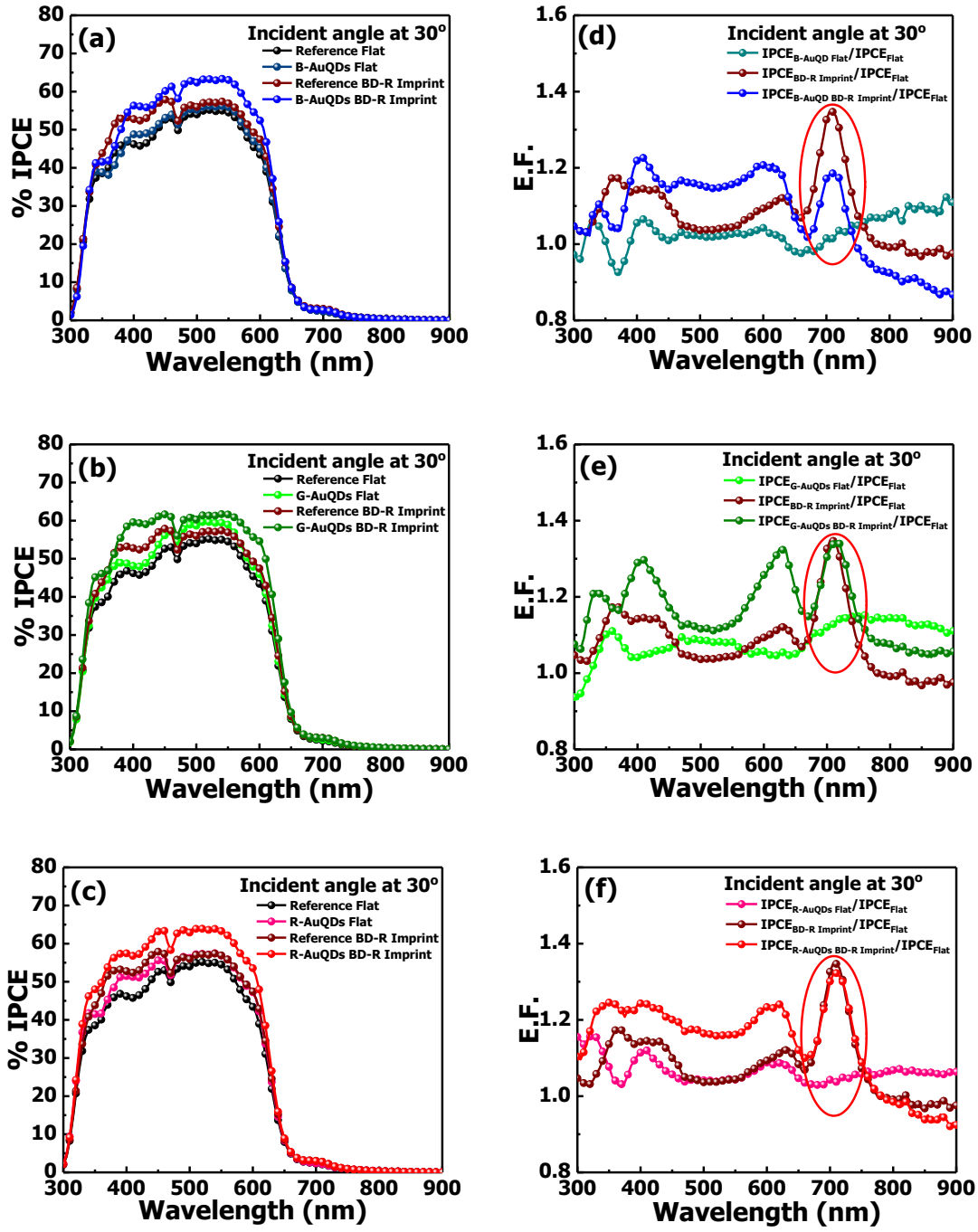


**Figure 3.9** IPCE spectra and E.F. spectra of AuQDs; B-AuQDs (a, d), G-AuQDs (b, e), and R-AuQDs (c, f) loaded photovoltaic devices with/without BD-R imprinting as compared to the reference OSCs, measured at fixed incident angles 30$^{o}$ under irradiation of non-polarized light.

As a result, an incorporating G-AuQDs into imprinting solar cell shows an E.F. greater than the solar cell without G-AuQDs in the ranges approximately of 550 - 660 nm. This improvement might be induced by the synergistic effect between the fluorescent property of AuQDs and the SPR property of Al grating. The SPR effect is originated from grating, leading to increase the light absorption at the wavelength region after 600 nm [14]. Moreover, AuQDs generate a strong fluorescence in visible regions (B-AuQDs; 430-670 nm, G-AuQDs; 450-700 nm, and R-AuQDs; 550-780 nm) [40, 41], promoting a higher number of photocarriers in the photoactive layer (300 - 700 nm). AuNPs formed from the agglomeration of AuQDs give LSPR property. Therefore, it could be reasoning in the enhancement of the E.F. within the device. Additionally, the overall IPCE of developing devices could be noticed that the addition of G-AuQDs into the both systematic devices (flat and grating devices) obviously showed the greatest IPCE improvement as same as the $J_{sc}$ and PCE enhancements, followed by the insertion of R-AuQDs and B-AuQDs, respectively as shown in appendix B Figure B3.5 (a-d).

To investigate the effect of grating structure, the IPCE of photovoltaic devices were further measured at different incident angle from $20^{o}$ to $60^{o}$ under non-polarized light illumination. In the comparison of E.F. between flat devices and BD-R imprinting devices indicating that the broadband enhancement of IPCE could be clearly observed for the entire wavelength in E.F. spectra (Figure 3.10). The SPR property from metallic grating generally demonstrate at the longer wavelength (after 600 nm), the E.F. of flat devices (Figure 3.10 (a-c)) exhibit an absence of resonance peaks. In contrast, the remarkable absorption enhancement could be achieve at the wavelength regions longer than 650 nm which is presented the SPR characteristic of grating structure from imprinting cells (Figure 3.10 (d-g)). The resonance peaks redshift are observed from 650 to 900 nm when the incident angle increases from $20^{o}$ to $60^{o}$, respectively.

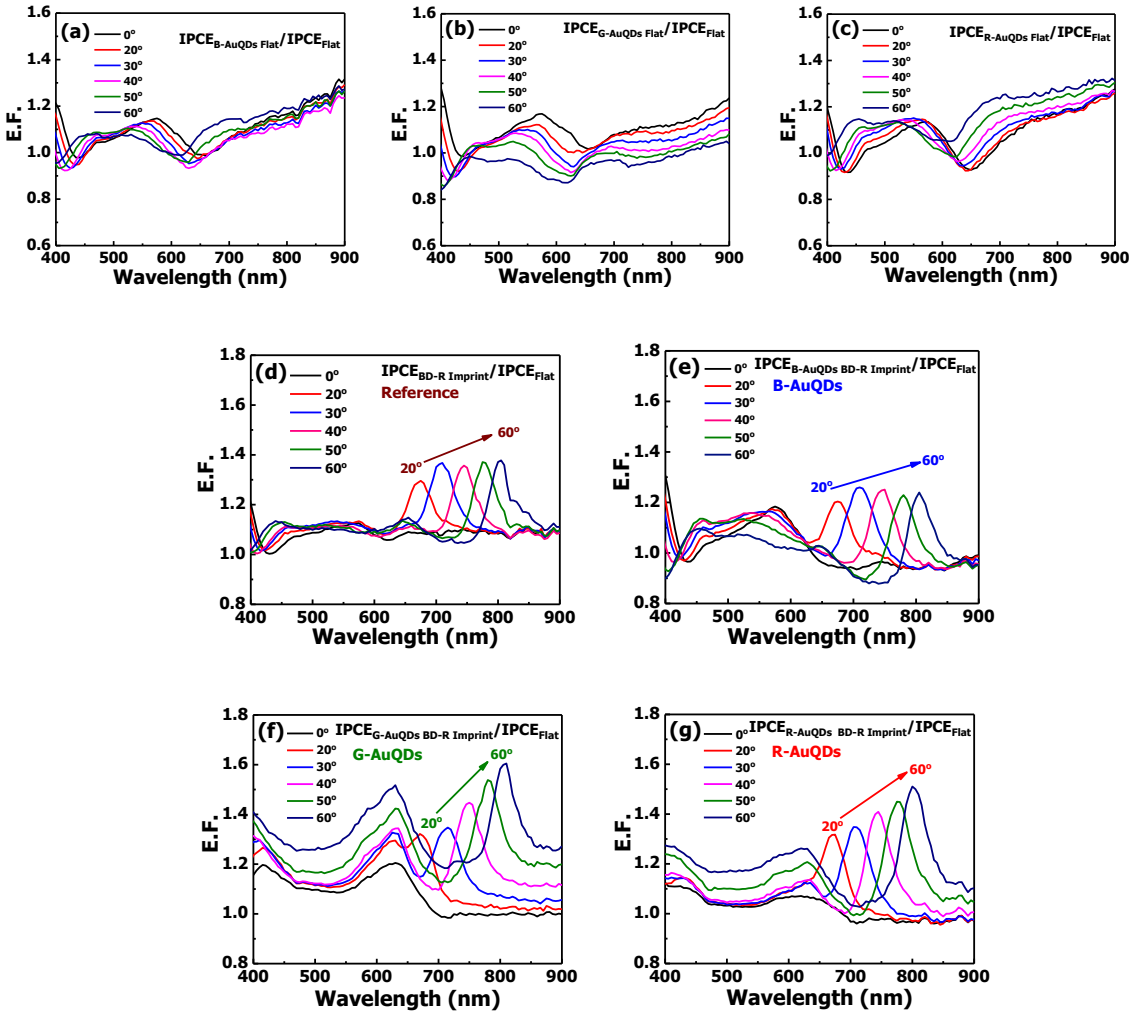


**Figure 3.10** IPCE E.F. spectra of flat devices and patterning devices incorporated AuQDs. Flat devices; B-AuQDs (a), G-AuQDs (b), and R-AuQDs (c), patterning devices; reference (d), B-AuQDs (e), G-AuQDs (f), and R-AuQDs (g), performed at fixed incident angles from 20° to 60° under irradiation of normal light.

It can be noticed that the IPCE E.F. of the plasmonic devices completely related with the SPR reflectivity spectra. These results suggesting that the presence of BD-R grating on the photoactive layer of the device offered the benefit of the improvement in OSCs performance due to efficient light harvesting, light scattering, and increased interfacial area [1]. The study of the optical absorption for both polarization modes (s and p polarization) of the plasmonic solar cells are shown in Figure 3.11.

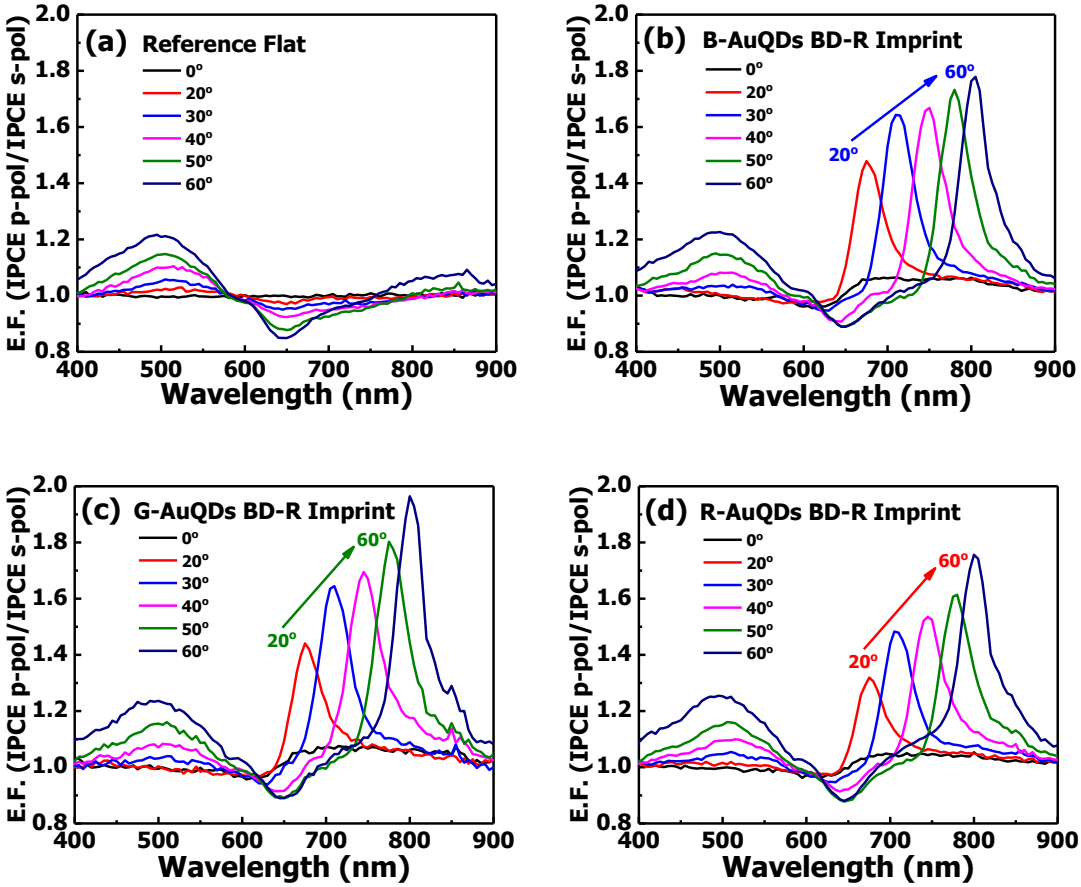


**Figure 3.11** IPCE E.F. spectra; (p-pol/s-pol) of reference cell (flat cell) (a), and BD-R imprinting cell incorporated with B-AuQDs (b), G-AuQDs (c), R-AuQDs (d), performed at fixed incident angles from 20° to 60° under irradiation of s- or p-polarized light.

Generally, the plasmonic effect is excited under p-pol light illumination, the IPCE E.F. data could be calculated from the dividing of IPCE value between p-pol (with excitation) and s-pol (without excitation) illumination (P/S; p-pol/s-pol). In Figure 3.11 (a), E.F. (P/S) spectra of flat reference cell cannot observe an enhancement peaks in the resonance wavelengths, indicating that the flat device did not enhance by GCSPR property. On the other hand, the grating devices incorporating with AuQDs (B-, G-, and R-AuQDs) considerably exhibit enhancement peaks from GCSPR at the wavelength above 600 nm (Figure 3.11 (b-d)) and the peak slightly shifted to longer wavelength when the incident angle increased as same as previous mentioned results, suggesting that the SP excitation could increase the absorption

of the irradiated light in the photoactive layer which can increase the $J_{sc}$ value [8]. As aforementioned, it can be noted that the fabricated devices are desirable success to achieve broadband absorption enhancement with prominent at the range between 650 to 900 nm, induced from metallic grating-nanostructure.

### 3.3.3 Impedance spectroscopy of fabricated OSCs

The introduction of AuQDs into patterned grating-nanostructure photovoltaic devices is not only expected to enhance the optical property but it is also supposed to increase the electrical property via increment of the interfacial area. The analysis of the charge transport resistance and the kinetics of electron transfer of the different device structures were investigated using electrochemical impedance spectroscopy (EIS) and the Nyquist plots are shown in Figure 3.12. From the fitting curves of the electron transport resistances, the Nyquist plots exhibit a single semicircular curve for all case and the data were modeled by the equivalent circuit as shown in the inset of Figures 3.12(a) and 3.12(b).

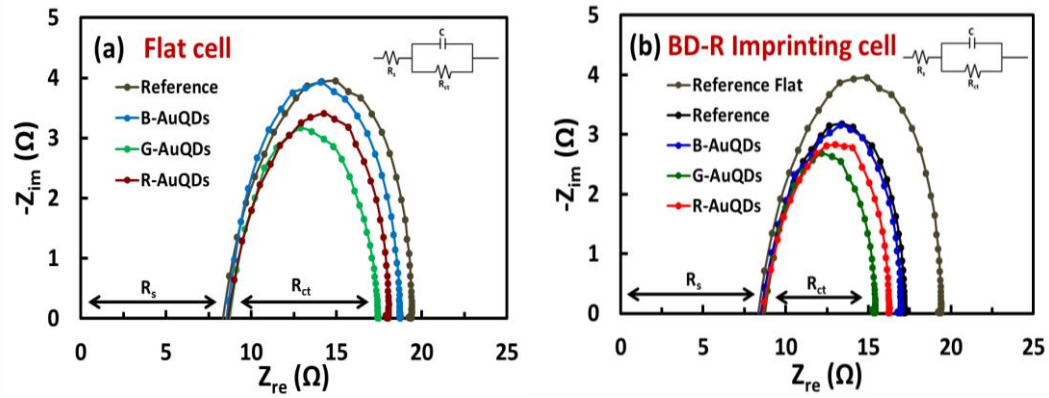


**Figure 3.12** Impedance spectroscopy of photovoltaic device, Nyquist plots of flat devices (a), BD-R imprinting device (b) incorporating with three types of AuQDs

In this model, $R_s$ or series resistance represents the resistive losses in the ITO and PEDOT:PSS, corresponding to the intersection of the semicircle with the $Z_{re}$ [7, 33]. The results indicate that the $R_s$ values of both flat and imprinting devices are insignificantly differences, it could be described that the addition of AuQDs into PEDOT:PSS layer have

minor effect on the contact resistance, resulting in the small changes in FF values. On the other hand, the capacitor (C) and the charge transfer resistance ($R_{ct}$) in a parallel are normally used to explain a recombination resistance and chemical capacitance within the donor/acceptor interfaces of polymer solar cell [7]. The introduction of AuQDs into photovoltaic device lead to decrease the $R_{ct}$ and addition of G-AuQDs resulted in the lowest of bulk resistance for both flat and grating devices. In flat devices, the presence of G-AuQDs exhibit the smallest $R_{ct}$ value of 8.4 Ω, following by R-AuQDs (9.1 Ω), B-AuQDs (9.7 Ω), and reference cell (10.4 Ω), respectively. In contrast, the patterning of BD-R grating-nanostructure on photoactive layer hugely induce the reduction of bulk resistance as presented a lower $R_{ct}$ values as compared to those of flat solar cells, which are 6.6 Ω, 7.5 Ω, 8.2 Ω, and 8.4 Ω for G-AuQDs, R-AuQDs, B-AuQDs, and non-AuQDs loading into grating device, respectively. As a result, it can be noted that the incorporation of AuQDs and a hybrid AuQDs-GCSPR into the solar cell can promote a positive effect on charge recombination enhancement in active layer, which is in agreement to the results from *J-V* measurements. The fluorescent emission from AuQDs could be capable to increase the number of photocarriers in P3HT:PCBM by absorption enhancement, likewise the plasmonic grating nanostructure could increase the interfacial areas resulted in the charge transport and photocarrier generation enhancement within the device. The characteristic frequency peaks are related to bulk resistance and electron lifetime in the photoactive layer [23, 50, 51]. Figures 3.13(a) and 3.13(b) represent the characteristic frequency peaks of Bode phase plots for AuQDs included in flat and grating OSCs, respectively.

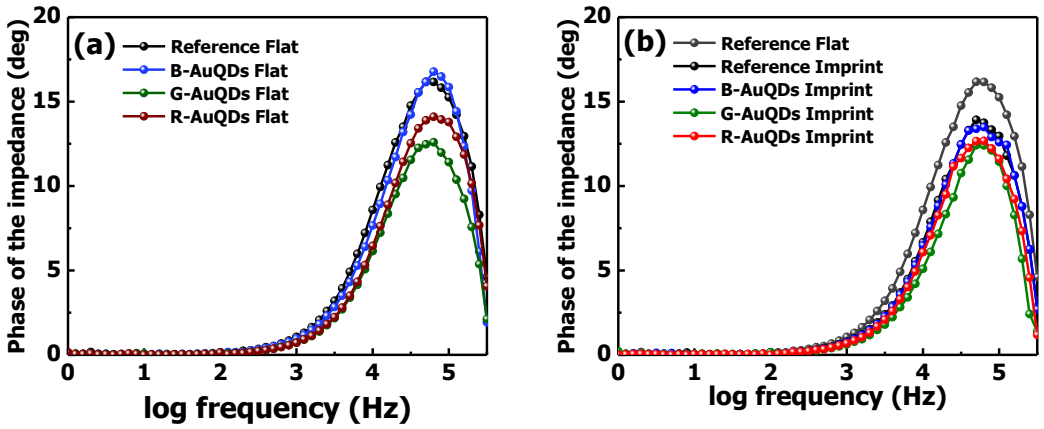


**Figure 3.13** Bode phase plots of flat devices (a) and BD-R imprinting device (b) incorporating with three types of AuQDs under solar light illumination.

The frequency peak features of flat device embedded AuQDs exhibit a slightly shift to higher frequency for all devices when compared to the reference cell as similar as the behavior of imprinting OSCs. According to lower frequency peak of OSCs cause a high $R_{ct}$ value [52], in this case could imply that the loading metallic nanostructure into OSCs can improve the charge transport which is correlated to the Nyquist plots. Additionally, the determination of the electron lifetime in OSCs was investigated from impedance spectroscopy [23, 53, 54]. The average electron lifetime ($\tau_{avg}$) are calculated from the characteristic frequency peak in Bode phase plots and summarized in appendix B Table B3.1. The results are insignificantly difference, indicating that the introduction of AuQDs into both flat and grating device would not affect the carrier lifetime. As aforementioned results suggest that the modification of OSCs with AuQDs and grating nanostructure provides a significant improvement of photovoltaic performances by increasing the optical and electrical properties due to their characteristic, including the specific fluorescence emission from AuQDs, the LSPR effect from AuQDs aggregation, and the GCSPR which contribute to higher OSCs efficiency for all of developed devices.

## 3.4. SUMMARY

This work has successfully demonstrated an enhancement of OSCs performances by addition of dual systematic metallic nanostructure into fabricated OSCs. The cell design, a structure of ITO/PEDOT:PSS:AuQDs/P3HT:PCBM/Al grating electrode, exhibited an excellent to increase the solar cell efficiency due to broadband absorption enhancement. Three types of AuQDs; B-AuQDs, G-AuQDs, and R-AuQDs significantly related to the size dependent of gold atoms, this implied that AuQDs can harvest the light in UV regions and convert it into visible light which different fluorescence emission. The device included dual systematic nanostructure offered a benefit to increase solar cell efficiency, especially increase $J_{sc}$ and PCE value. G-AuQDs with imprinting device provided the highest PCE of 3.91% with enhance the solar performance approximately 20% as compared to the reference cell. Based on the result, the metallic nanostructure can reduce the resistance and increase IPCE. Thus, the dual systematic structures are interesting materials, considered to use for improving the organic solar cell performances.

## 3.5 REFERENCES


[1] Jonas, W., B.D. Ricky, C.H. Holger, W. Wolfgang, and S.-M. Lukas, *Nanostructured organic and hybrid solar cells*. Advanced Materials, 2011. **23**(16): p. 1810-1828.

[2] Qiaoqiang, G., B.F. J., and K.Z. H., *Plasmonic-enhanced organic photovoltaics: breaking the 10% efficiency barrier*. Advanced Materials, 2013. **25**(17): p. 2385-2396.

[3] Kang, M.-G., M.-S. Kim, J. Kim, and L.J. Guo, *Organic solar cells using nanoimprinted transparent metal electrodes*. Advanced Materials, 2008. **20**(23): p. 4408-4413.

[4] Chou, C.-H. and F.-C. Chen, *Plasmonic nanostructures for light trapping in organic photovoltaic devices*. Nanoscale, 2014. **6**(15): p. 8444-8458.

[5] Li, X., W.C.H. Choy, L. Huo, F. Xie, W.E.I. Sha, B. Ding, X. Guo, Y. Li, J. Hou, J. You, and Y. Yang, *Dual plasmonic nanostructures for high performance inverted organic solar cells*. Advanced Materials, 2012. **24**(22): p. 3046-3052.

[6] Choy, W.C.H., *The emerging multiple metal nanostructures for enhancing the light trapping of thin film organic photovoltaic cells*. Chemical Communications, 2014. **50**(81): p. 11984-11993.

[7] Leever, B.J., C.A. Bailey, T.J. Marks, M.C. Hersam, and M.F. Durstock, In situ characterization of lifetime and morphology in operating bulk heterojunction organic photovoltaic devices by impedance spectroscopy. Advanced Energy Materials, 2012. **2**(1): p. 120-128.

[8] Nootchanat, S., A. Pangdam, R. Ishikawa, K. Wongravee, K. Shinbo, K. Kato, F. Kaneko, S. Ekgasit, and A. Baba, *Grating-coupled surface plasmon resonance enhanced organic photovoltaic devices induced by Blu-ray disc recordable and Blu-ray disc grating structures*. Nanoscale, 2017. **9**(15): p. 4963-4971.

[9] Notarianni, M., K. Vernon, A. Chou, M. Aljada, J. Liu, and N. Motta, *Plasmonic effect of gold nanoparticles in organic solar cells*. Solar Energy, 2014. **106**: p. 23-37.

[10] Brabec, C.J., S. Gowrisanker, J.J.M. Halls, D. Laird, S. Jia, and S.P. Williams, *Polymer-fullerene bulk-heterojunction solar cells*. Advanced Materials, 2010. **22**(34): p. 3839-3856.

[11] Yang, J., J. You, C.-C. Chen, W.-C. Hsu, H.-r. Tan, X.W. Zhang, Z. Hong, and Y. Yang, Plasmonic polymer tandem solar cell. ACS Nano, 2011. **5**(8): p. 6210-6217.

[12] Luo, G., X. Ren, S. Zhang, H. Wu, W.C.H. Choy, Z. He, and Y. Cao, *Recent advances in organic photovoltaics: device structure and optical engineering optimization on the nanoscale*. Small, 2011. **12**(12): p. 1547-1571.

[13] Li, X., W.C.H. Choy, H. Lu, W.E.I. Sha, and A.H.P. Ho, *Efficiency enhancement of organic solar cells by using shape-dependent broadband plasmonic absorption in metallic nanoparticles*. Advanced Functional Materials, 2013. **23**(21): p. 2728-2735.

[14] Li, X., X. Ren, F. Xie, Y. Zhang, T. Xu, B. Wei, and W.C.H. Choy, *High-performance organic solar cells with broadband absorption enhancement and reliable reproducibility enabled by collective plasmonic effects*. Advanced Optical Materials, 2015. **3**(9): p. 1220-1231.

[15] Atwater, H.A. and A. Polman, *Plasmonics for improved photovoltaic devices*. Nature Materials, 2010. **9**: p. 205-213.

[16] Wang, W., S. Wu, K. Reinhardt, Y. Lu, and S. Chen, *Broadband light absorption enhancement in thin-film silicon solar cells*. Nano Letters, 2010. **10**(6): p. 2012-2018.

[17] Aryal, M., K. Trivedi, and W. Hu, *Nano-confinement induced chain alignment in ordered P3HT nanostructures defined by nanoimprint lithography*. ACS Nano, 2009. **3**(10): p. 3085-3090.

[18] Park, J.Y., N.R. Hendricks, and K.R. Carter, *Solvent-assisted soft nanoimprint lithography for structured bilayer heterojunction organic solar cells*. Langmuir, 2011. **27**(17): p. 11251-11258.

[19] You, J., X. Li, F.-x. Xie, W.E.I. Sha, J.H.W. Kwong, G. Li, W.C.H. Choy, and Y. Yang, *Surface plasmon and scattering-enhanced low-bandgap polymer solar cell by a metal grating back electrode*. Advanced Energy Materials, 2012. **2**(10): p. 1203-1207.

[20] Baba, A., N. Aoki, K. Shinbo, K. Kato, and F. Kaneko, *Grating-coupled surface plasmon enhanced short-circuit current in organic thin-film photovoltaic cells*. ACS Applied Materials & Interfaces, 2011. **3**(6): p. 2080-2084.

[21] Hara, K., C. Lertvachirapaiboon, R. Ishikawa, Y. Ohdaira, K. Shinbo, K. Kato, F. Kaneko, and A. Baba, *Inverted organic solar cells enhanced by grating-coupled surface plasmons and waveguide modes*. Physical Chemistry Chemical Physics, 2017. **19**(4): p. 2791-2796.

[22] Baba, A., K. Wakatsuki, K. Shinbo, K. Kato, and F. Kaneko, *Increased short-circuit current in grating-coupled surface plasmon resonance field-enhanced dye-sensitized solar cells*. Journal of Materials Chemistry, 2011. **21**(41): p. 16436-16441.

[23] Nootchanat, S., H. Ninsonti, A. Baba, S. Ekgasit, C. Thammacharoen, K. Shinbo, K. Kato, and F. Kaneko, *Investigation of localized surface plasmon/grating-coupled surface plasmon enhanced photocurrent in $TiO_2$ thin films*. Physical Chemistry Chemical Physics, 2014. **16**(44): p. 24484-24492.

[24] Zhu, J., M. Xue, R. Hoekstra, F. Xiu, B. Zeng, and K.L. Wang, *Light concentration and redistribution in polymer solar cells by plasmonic nanoparticles*. Nanoscale, 2012. **4**(6): p. 1978-1981.

[25] Wang, C.C.D., W.C.H. Choy, C. Duan, D.D.S. Fung, W.E.I. Xie, F. Huang, and Y. Cao, *Optical and electrical effects of gold nanoparticles in the active layer of polymer solar cells*. Journal of Materials Chemistry, 2012. **22**(3): p. 1206-1211.

[26] Hsiao, Y.-S., S. Charan, F.-Y. Wu, F.-C. Chien, C.-W. Chu, P. Chen, and F.-C. Chen, *Improving the light trapping efficiency of plasmonic polymer solar cells through photon management*. The Journal of Physical Chemistry C, 2012. **116**(39): p. 20731-20737.

[27] Sharma, M., P.R. Pudasaini, F. Ruiz-Zepeda, E. Vinogradova, and A.A. Ayon, *Plasmonic effects of Au/Ag bimetallic multispiked nanoparticles for photovoltaic applications*. ACS Applied Materials & Interfaces, 2014. **6**(17): p. 15472-15479.

[28] Pangdam, A., S. Nootchanat, R. Ishikawa, K. Shinbo, K. Kato, F. Kaneko, C. Thammacharoen, S. Ekgasit, and A. Baba, *Effect of urchin-like gold nanoparticles in organic thin-film solar cells*. Physical Chemistry Chemical Physics, 2016. **18**(27): p. 18500-18506.

[29] Stratakis, E. and E. Kymakis, *Nanoparticle-based plasmonic organic photovoltaic devices*. Materials Today, 2013. **16**(4): p. 133-146.

[30] Liu, C.-M., C.-M. Chen, Y.-W. Su, S.-M. Wang, and K.-H. Wei, *The dual localized surface plasmonic effects of gold nanodots and gold nanoparticles enhance the performance of bulk heterojunction polymer solar cells*. Organic Electronics, 2013. **14**(10): p. 2476-2483.

[31] Lu, L., Z. Luo, T. Xu, and L. Yu, *Cooperative plasmonic effect of Ag and Au nanoparticles on enhancing performance of polymer solar cells*. Nano Letters, 2013. **13**(1): p. 59-64.

[32] Tseng, W.-H., C.-Y. Chiu, S.-W. Chou, H.-C. Chen, M.-L. Tsai, Y.-C. Kuo, D.-H. Lien, Y.-C. Tsao, K.-Y. Huang, C.-T. Yeh, J.-H. He, C.-I. Wu, M.H. Huang, and P.-T. Chou, *Shape-dependent light harvesting of 3D gold nanocrystals on bulk heterojunction solar cells: plasmonic or optical scattering effect?*. The Journal of Physical Chemistry C, 2015. **119**(14): p. 7554-7564.

[33] Ng, A., W.K. Yiu, Y. Foo, Q. Shen, A. Bejaoui, Y. Zhao, H.C. Gokkaya, A.B. Djurišić, J.A. Zapien, W.K. Chan, and C. Surya, *Enhanced performance of PTB7:$PC_{71}$BM solar cells via different morphologies of gold nanoparticles*. ACS Applied Materials & Interfaces, 2014. **6**(23): p. 20676-20684.

[34] Eustis, S. and M.A. El-Sayed, *Why gold nanoparticles are more precious than pretty gold: noble metal surface plasmon resonance and its enhancement of the radiative and nonradiative properties of nanocrystals of different shapes*. Chemical Society Reviews, 2006. **35**(3): p. 209-217.

[35] Kogo, A., Y. Takahashi, N. Sakai, and T. Tatsuma, *Gold cluster-nanoparticle diad systems for plasmonic enhancement of photosensitization*. Nanoscale, 2013. **5**(17): p. 7855-7860.

[36] Stamplecoskie, K.G. and P.V. Kamat, *Synergistic effects in the coupling of plasmon resonance of metal nanoparticles with excited gold clusters*. The Journal of Physical Chemistry Letters, 2015. **6**(10): p. 1870-1875.

[37] Stamplecoskie, K.G., Y.-S. Chen, and P.V. Kamat, *Excited-state behavior of luminescent glutathione-protected gold clusters*. The Journal of Physical Chemistry C, 2014. **118**(2): p. 1370-1376.

[38] Uddayasankar, U. and U.J. Krull, *Energy transfer assays using quantum dot–gold nanoparticle complexes: optimizing oligonucleotide assay configuration using monovalently conjugated quantum dots*. Langmuir, 2015. **31**(29): p. 8194-8204.

[39] Chen, L.-Y., C.-W. Wang, Z. Yuan, and H.-T. Chang, *Fluorescent gold nanoclusters: recent advances in sensing and imaging*. Analytical Chemistry, 2015. **87**(1): p. 216-229.

[40] Zheng, J., C. Zhang, and R.M. Dickson, *Highly fluorescent, water-soluble, size-tunable gold quantum dots*. Physical Review Letters, 2004. **93**(7): p. 077402.

[41] Pangdam, A., S. Nootchanat, C. Lertvachirapaiboon, R. Ishikawa, K. Shinbo, K. Kato, F. Kaneko, S. Ekgasit, and A. Baba, *Investigation of gold quantum dot enhanced organic thin film solar cells*. Particle & Particle Systems Characterization, 2017. **34**(11): p. 1700133.

[42] Nobuyuki, S. and T. Tetsu, *Photovoltaic properties of glutathione-protected gold clusters adsorbed on $TiO_2$ electrodes*. Advanced Materials, 2010. **22**(29): p. 3185-3188.

[43] Choi, H., Y.-S. Chen, K.G. Stamplecoskie, and P.V. Kamat, *Boosting the photovoltage of dye-sensitized solar cells with thiolated gold nanoclusters*. The Journal of Physical Chemistry Letters, 2015. **6**(1): p. 217-223.

[44] Abbas, M.A., T.-Y. Kim, S.U. Lee, Y.S. Kang, and J.H. Bang, *Exploring interfacial events in gold-nanocluster-sensitized solar cells: insights into the effects of the cluster size and electrolyte on solar cell performance*. Journal of the American Chemical Society, 2016. **138**(1): p. 390-401.

[45] Chen, X., L. Zuo, W. Fu, Q. Yan, C. Fan, and H. Chen, *Insight into the efficiency enhancement of polymer solar cells by incorporating gold nanoparticles*. Solar Energy Materials and Solar Cells, 2013. **111**: p. 1-8.

[46] Yang, Y., K. Mielczarek, M. Aryal, A. Zakhidov, and W. Hu, *Nanoimprinted polymer solar cell*. ACS Nano, 2012. **6**(4): p. 2877-2892.

[47] Leem, J.W., S. Kim, C. Park, E. Kim, and J.S. Yu, *Strong photocurrent enhancements in plasmonic organic photovoltaics by biomimetic nanoarchitectures with efficient light harvesting*. ACS Applied Materials & Interfaces, 2015. **7**(12): p. 6706-6715.

[48] Jeong, S., C. Cho, H. Kang, K.-H. Kim, Y. Yuk, J.Y. Park, B.J. Kim, and J.-Y. Lee, *Nanoimprinting-induced nanomorphological transition in polymer solar cells: enhanced electrical and optical performance*. ACS Nano, 2015. **9**(3): p. 2773-2782.

[49] Kumar, P.N., M. Deepa, and P. Ghosal, *Low-cost copper nanostructures impart high efficiencies to quantum dot solar cells*. ACS Applied Materials & Interfaces, 2015. **7**(24): p. 13303-13313.

[50] Hsu, C.-P., K.-M. Lee, J.T.-W. Huang, C.-Y. Lin, C.-H. Lee, L.-P. Wang, S.-Y. Tsai, and K.-C. Ho, *EIS analysis on low temperature fabrication of $TiO_2$ porous films for dye-sensitized solar cells*. Electrochimica Acta, 2008. **53**(25): p. 7514-7522.

[51] Wang, Q., J.-E. Moser, and M. Grätzel, *Electrochemical impedance spectroscopic analysis of dye-sensitized solar cells*. The Journal of Physical Chemistry B, 2005. **109**(31): p. 14945-14953.

[52] Nagamani, S., G. Kumarasamy, M. Song, C.S. Kim, D.-H. Kim, S.Y. Ryu, J.-W. Kang, and S.-H. Jin, *Optical absorption and electrical properties of enhanced efficiency in organic solar cells as interfacial layer with Au NPs*. Synthetic Metals, 2016. **217**: p. 117-122.

[53] Li, L., Y. Yang, R. Fan, X. Wang, Q. Zhang, L. Zhang, B. Yang, W. Cao, W. Zhang, Y. Wang, and L. Ma, *Photocurrent enhanced dye-sensitized solar cells based on $TiO_2$ loaded $K_6SiW_{11}O_{39}Co(ii)(H_2O)\cdot xH_2O$ photoanode materials*. Dalton Transactions, 2014. **43**(4): p. 1577-1582.

[54] Bisquert, J., F. Fabregat-Santiago, I. Mora-Seró, G. Garcia-Belmonte, and S. Giménez, *Electron lifetime in dye-sensitized solar cells: theory and interpretation of measurements*. The Journal of Physical Chemistry C, 2009. **113**(40): p. 17278-17290.

# CHAPTER IV

## Investigation of Gold Nanospheres-Gold Nanorods Hybrid/Metallic Grating Incorporated into Organic Solar Cells

**ABSTRACT**

The incorporation of plasmonic nanostructures in organic solar cells (OSCs) is one of key issues to increase light harvesting and the photocurrent. This study demonstrates the fabrication of hybrid plasmonic solar cells using gold nanoparticles (AuNPs): a mixture gold nanospheres (AuNSs) and gold nanorods (AuNRs) incorporated in a hole transport layer (PEDOT:PSS) with metallic grating electrode. The OSCs structure consists of ITO coated glass substrate/PEDOT:PSS:AuNSs:AuNRs/P3HT:PCBM/Al grating electrode. Loading of AuNPs can induce the localized surface plasmon resonance (LSPR) while nanoimprinting process was performed to make a grating nanostructure on the surface of photoactive layer. Compared to flat reference cell, the proposed OSCs exhibit higher photovoltaic property by increasing both the short-circuit current density ($J_{sc}$) and the power conversion efficiency (PCE) with large enhancement of 16.23% and 14.06%, respectively. As a result, the efficiency enhancement was induced by increasing broadband absorption and improving electrical property inside thin film devices. Therefore, the proposed OSCs could be further developed in practical application for OSCs.

**Keywords:** plasmonic solar cells, localized surface plasmon resonance, gold nanoparticles, gold nanorods, grating surface plasmon resonance

## 4.1 INTRODUCTION

Solar energy is considered as a promising alternative source for long term sustainable energy production [1]. Among developing solar technologies, organic solar cells (OSCs) are receiving as a potential candidate because of their attractive properties including light weight, flexibility, cost effective, and simplistic fabrication [2-4]. Currently, several researchers have demonstrated the great photovoltaic performances on bulk heterojunction OSCs with different device structures; however, the power conversion efficiency (PCE) of the proposed devices is limited as compared to those of the traditional silicon-based inorganic solar cells [5]. Commonly, the OSCs based on bulk heterojunction are consisted of conjugated polymers and fullerene derivatives which can promote an efficient exciton dissociation and tunable energy bands, leading to enhance the PCE of the devices [6]. The performances of OSCs are limited by insufficient light absorption, low carrier mobility and charge recombination due to a thinner film of photoactive layer [7, 8]. Increasing of photoactive layer thickness can enhance the light absorption but a thicker layer is possibly effective in a higher resistance and lower efficiency. Therefore, the improving of light management without increasing the active layer thickness is very important to reach high performance of OSCs. Metallic nanostructures have been considerable designed for light harvesting improvement of the photovoltaic devices. Especially, the use of plasmonic metallic nanoparticles such as gold nanoparticles (AuNPs) and silver nanoparticles (AgNPs) can promote light absorption of the device induced by increasing the scattering cross section and a near-field enhancement [9, 10]. It has been known that AuNPs typically enhance an electric field and optical absorption through the excitation of localized surface plasmon resonance (LSPR). AuNPs have been extensively introduced into hole transport layers or photoactive layers of OSCs and high photovoltaic improvement has been observed [6, 11-13]. Our group also reported the use of urchin-like AuNPs to improve the performance of OSCs [14]. Incorporation of mixed nanoparticles in

photovoltaic devices has also been applied for the PCE enhancement. The cooperation of AgNPs and AuNPs [15, 16], gold nanodots (AuNDs) and AuNPs [6], or gold nanospheres (AuNSs) and gold nanorods (AuNRs) [17] can promote a great improvement of devices efficiency. The introducing of gold quantum dots (AuQDs)/AuNPs into OSCs can also enhance the photovoltaic performances [18]. Additionally, several corrugated metallic nanostructures such as nanopillar, nanohole, honeycomb lattice, and grating nanostructure have been included on the surface to increase the optical property of OSCs [19]. Periodic grating nanostructures offer the surface plasmon polaritons (SPP) modes that the resonance wavelength can be tuned within the visible to near-infrared regions [3]. Also, it can increase donor/acceptor interface and exciton dissociation, enhancing the charge carrier transport in conjugated polymer. This property induces a better light harvesting within the OSCs [19]. The previous works reported the utilization of periodic based grating-coupled surface plasmon resonance (GCSPR) to enhance photocurrent of photovoltaic device and dye-sensitized solar cells [20-23]. Furthermore, the incorporation of dual plasmonic nanostructures has been investigated to boost the OSCs performances [24]. Therefore, the utilization of hybrid plasmonic nanostructures is the main concept for development of our devices according to their great property.

This work demonstrates the synergistic effect of hybrid plasmonic nanostructures on the OSCs performances. The OSC design was included plasmonic AuNPs incorporating with metallic grating nanostructure into thin-film photovoltaic device; a structure of ITO/PEDOT:PSS:AuNSs:AuNRs/P3HT:PCBM/Al grating electrode. The mixture solution of AuNPs (AuNSs and AuNRs) was added into hole transport layer (PEDOT:PSS) in order to generate the LSPR property within OSCs. The photoactive layer surface was imprinted with the pattern of blu-ray disc recordable (BD-R) via a thermal imprinting technique to obtain the grating structure at electrode. The synergistic effect between the LSPR and GCSPR was

expected to enhance the optical path length within the devices. Additionally, the proposed OSCs exhibit a great improvement in photovoltaic performances by increasing the $J_{sc}$ and the PCE with a large enhancement percentage of 16.23% and 14.06%, respectively in comparison with the flat reference device. Therefore, this systematic platform could be further developed in practical application for OSCs.

## 4.2 EXPERIMENTAL SECTION

### 4.2.1 Chemicals and materials

Poly(3-hexylthiophene-2,5-diyl) (P3HT), [6,6]-phenyl $C_{61}$ butyric acid methyl ester (PCBM), 1,2-dichlorobenzene, nitric acid ($HNO_3$), and gold nanospheres solution (AuNSs) were purchased from Sigma-Aldrich (Singapore). Gold nanorods solution (AuNRs) used was Au-WPP08-C Lot.160314, Dainippon Paint Co. Ltd. (Japan), Poly(3,4-ethylenedioxy thiophene):poly(styrenesulfonate) or PEDOT:PSS (Clevios$^{TM}$ HTL Solar) was obtained from Heraeus (Germany). The analytical grade of ethanol and acetone were obtained from Kanto Chemical Co. Ltd. (Japan). An indium tin oxide (ITO)-coated glass substrate with a conductivity of 10 Ω/cm$^2$ was purchased from Furuuchi chemical (Japan).

### 4.2.2 Preparation of PDMS molds

The polydimethylsiloxane (PDMS) was used as a master template. The PDMS mold was imitated nanopattern from periodic BD-R. First, small rectangular pieces of BD-R (2.5 cm x 4.0 cm) were immersed in conc. $HNO_3$ for 20 min to remove the dye coating layer on the polycarbonate grating side. Subsequently, they were cleaned with liquid detergent, tap water, and DI water using ultrasonic bath for 15 min of each step, respectively. Pieces of BD-R substrate were dried under $N_2$ stream and placed in clean petri dish. After that the PDMS solution was placed and covered on the BD-R grating substrates. Air bubble was eliminated by placing the petri dish in a vacuum chamber and then curing at 80 $^oC$ for 3 h to obtain the BD-R grating mold.

### 4.2.3 Fabrication of plasmonic photovoltaic devices

The plasmonic photovoltaic devices were constructed on ITO-coated glass substrates. ITO substrates were cleaned via a common process and were treated with ozone-ultraviolet cleaner before being used. PEDOT:PSS solution or hole transport layer (HTL) was mixed under optimized condition of AuNSs, AuNRs, or mixture of AuNSs:AuNRs solution with a ratio of 6:1 (v/v) following by ultrasonication for 1 h to homogenize the mixture solution. After that the mixture solution was spin coated at 1000 rpm for 90s on ITO substrate and was subsequently annealed at 120 $^{o}$C for 20 min before spin coating photoactive layer. The device in an absence of metal nanoparticles was used as the control device and the thickness of PEDOT:PSS layer was approximately 80 nm (Figure C4.1, appendix C). Polymeric mixture solution of P3HT:PCBM (ratio 1:0.8 in dichlorobenzene) was spin coated on the top of HTL at 1000 rpm for 10s and 1500 rpm for 60s, respectively. Then, the PDMS mold with BD-R pattern was carefully transferred on the surface of photoactive layer to construct nanograting on the surface and annealed at 100 $^{o}$C for 1 h. The substrate was cooled down to room temperature before removing the PDMS mold. The thickness of photoactive film was approximately 100 nm (Figure C4.2, appendix C). Finally, a 150 nm thick of aluminium electrode was deposited on top of the patterned photoactive layer by thermal evaporation to obtain fabricated OSCs. The schematic of fabrication of hybrid OSCs, a structure of ITO/AuNSs:AuNRs:PEDOT:PSS/ P3HT:PCBM/Al grating electrode, is shown in Figure 4.1.

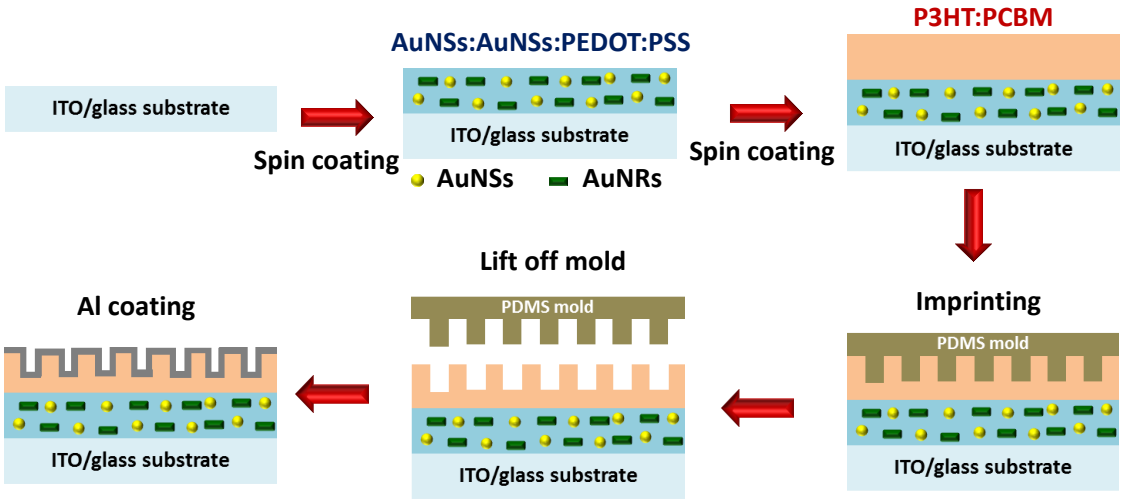


**Figure 4.1** Schematic illustration of the fabrication of hybrid plasmonic OSCs incorporated with metallic grating nanostructure.

### 4.2.4 Device characterizations

The current density-voltage characteristics ($J-V$ curve) of fabricated photovoltaic device were measured with a precision source/measure unit (B2901A, Agilent) under simulated sunlight illumination using solar simulator (HAL-C100, 100W compact xenon light source, Asahi Spectra, USA Inc.) at 75 mW/cm$^2$. The electrochemical impedance spectroscopy (EIS) measurement was evaluated by potentiostat (PARSTAT 4000, Princeton Applied Research) under 1 sun illumination with frequencies in the range of 1 Hz – 1 MHz. The surface morphology and the thickness of the device (PEDOT:PSS or P3HT:PCBM layer) were characterized by an atomic force microscopy (AFM, SPM-9600, Shimadzu, Japan). The UV–visible absorption spectra of AuNPs solution and PEDOT:PSS:AuNPs/P3HT:PCBM films on ITO glass were investigated using a UV-vis spectrometer (V-650, Jasco). The optical reflectivity of fabricated OSCs was measured by a homemade reflectrometer. The fabricated photovoltaic device was located on a $\theta$-$2\theta$ goniometer and was irradiated with the p-s polarized light (p-s pol) from a halogen lamp. SP excitation was obtained using an objective lens and the SPR reflectivity was characterized by UV–vis spectrometer (Ocean optic USB 2000).

## 4.3 RESULTS AND DISCUSSION

### 4.3.1 Optical properties and surface morphology of plasmonic solar cells

The incorporation of metallic plasmonic nanostructured within photovoltaic device can improve both of electrical and optical properties, inducing an enhancement of photocurrent in the device via SPR effect [24]. AuNPs with various sizes and shapes can generate different plasmonic behaviors which would influence on the performances of plasmonic solar cells. The UV-visible absorption spectra of AuNSs, AuNRs, and mixture AuNSs:AuNRs in solution exhibit the absorption band in the range from 470 to 800 nm as shown in Figure 4.2 (A). The characteristic absorption peaks of AuNSs (530 nm) and AuNRs (510 and 660 nm, transverse and longitudinal modes) reveal a good distribution of AuNPs in DI water. Interestingly, the mixture AuNSs:AuNSs solution exhibits two absorption bands (520 and 660 nm) with more light absorption in the region of 525 nm. The absorption enhancement was achieved by the LSPR property from AuNSs and the transverse mode from AuNRs. This result suggests that an incorporation of AuNSs and AuNRs can promote a wider light absorption which can increase the light harvesting in photovoltaic devices.

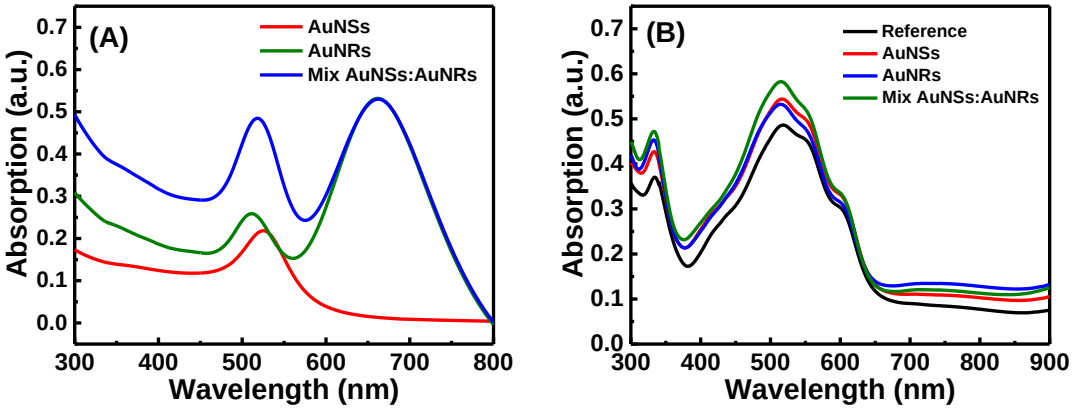


**Figure 4.2** UV-vis absorption spectra, (A) the solution of AuNPs, AuNRs and the mixture solution of AuNPs and AuNRs , (B) the photoactive layer film of fabricated solar cell: glass/AuNPs:PEDOT:PSS/P3HT:PCBM.

In order to study the LSPR effect of AuNSs:AuNRs on photovoltaic performance of the device, the optical absorption of P3HT:PCBM/PEDOT:PSS/ITO films with/without the insertion of AuNPs was investigated as shown in Figure 4.2 (B). The UV-vis absorption spectra illustrate the characteristic absorption peaks of P3HT:PCBM photoactive layer in two wavelength regions; an absorption peak at *ca.* 350 nm and an absorption broad peak from 400 to 700 nm for all of devices which is well consistent with the previous report [6, 25]. As compared to the pristine photoactive film, the absorption spectra of the device embedded AuNPs (AuNSs, AuNRs, or AuNSs:AuNRs) into PEDOT:PSS buffer layer do not significantly change when compared to the control device. On the other hand, the absorption intensity increases when AuNPs are incorporated into the HTL. Especially, the absorption of the hybrid AuNSs:AuNRs nanostructures film is being greater than those of devices due to the synergistic property. The enhanced light absorption of the P3HT:PCBM films could be resulted from the optical near field which was generated by LSPR from AuNPs, giving an effectiveness of solar light harvesting [6]. In fact, the incorporation of AuNPs into PEDOT:PSS solution is easy and straight forward because both components are dispersed in aqueous solution. Therefore, they can combine with a good uniformity and the plasmonic property of AuNPs could be retained in mixture solution which subsequently enhanced the absorption capability of the photoactive layer [9].

The surface morphology has influenced on the optical and electrical performances of photovoltaic devices. Therefore, AFM was applied for analysis of the surface of PEDOT:PSS film to study the morphology changes after the incorporation of AuNSs:AuNRs. Furthermore, amount of AuNSs:AuNRs would affect the performances of photovoltaic devices. The AFM images of the pristine PEDOT:PSS film and the PEDOT:PSS films with the insertion of different AuNSs:AuNRs concentrations are shown in Figure 4.3.

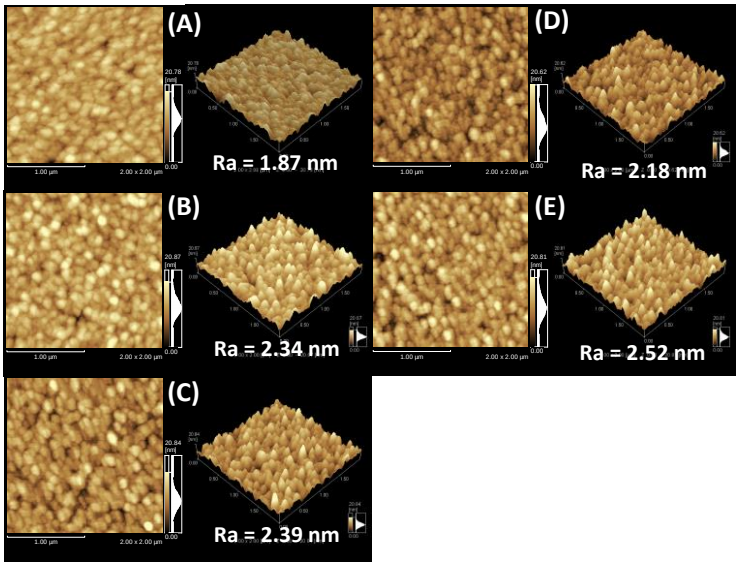


**Figure 4.3** AFM images of PEDOT:PSS films, pristine PEDOT:PSS (without AuNPs) (A), and PEDOT:PSS:AuNSs:AuNRs films containing different total concentrations of mixture AuNSs:AuNRs (1:1); 0.030 mM (B), 0.050 mM (C), 0.070 mM (D), and 0.100 (E) on ITO glass substrate.

The PEDOT:PSS films display a smooth surface morphology and no significant change on the surface are observed for all devices. Whereas, the surface roughness ($R_a$) of the PEDOT:PSS films slightly increase from 1.87 nm to 2.52 nm with the increment of different mixture AuNSs:AuNRs concentrations. The result can be implied that the incorporation of AuNSs:AuNRs into PEDOT:PSS can increase the surface roughness in the photovoltaic device via the distribution of AuNPs with various sizes. Additionally, the agglomeration of AuNPs can increase the roughness of the surface. High surface roughness can enlarge the interfacial area between PEDOT:PSS and P3HT:PCBM, resulting in a short route for holes to reach the anode and leading to enhance the holes collection efficiency [26]. However, the rougher surface from large particles embedded in the film may interrupt the exciton dissociation interfaces [25], resulting in the lower photocurrent in the device at a high concentration (AuNSs:AuNRs, 0.100 mM).

Under the optimal condition, the developed OSCs were incorporated with grating nanostructure. The surface morphology of P3HT:PCBM layer after patterning are presented in Figure 4.4. As a result, the pattern of the periodic BD-R nanostructure are clearly observed on the P3HT:PCBM film for all devices, which is indicating that the grating nanostructure was successfully constructed on the surface of device. In nanoimprinting process, the blended polymer can flow and align towards the grooves of the negative patterns of PDMS mold by the capillary force. Then, the inverse grating nanostructure retained on the polymer film after demolding [20]. Grating nanostructure can cause a roughness in the photovoltaic device, leading to increase in the interfacial area which can support the exciton dissociation and charge transport enhancement [27, 28].

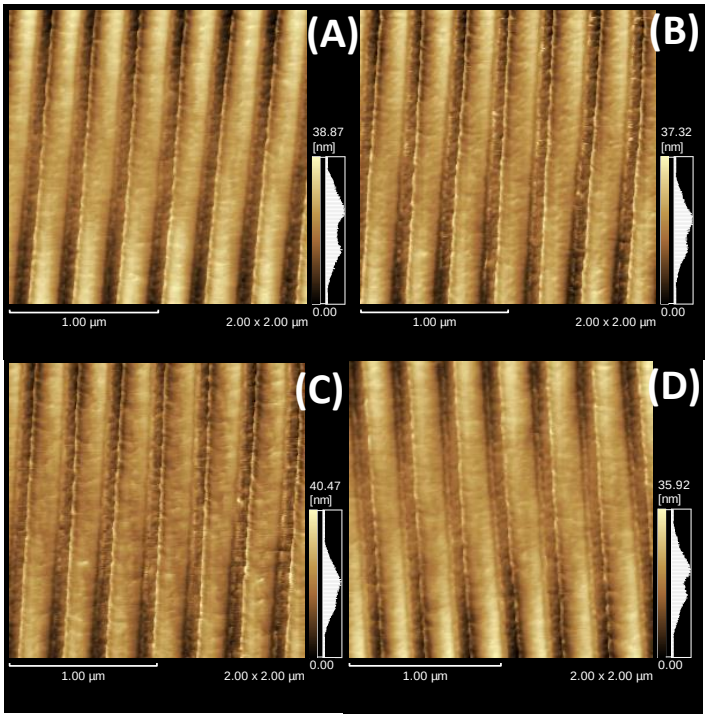


**Figure 4.4** Surface morphology of P3HT:PCBM layer coated on PEDOT:PSS layer after imprinting process, reference cell (A), AuNSs (B), AuNRs (C) and mix AuNSs:AuNRs (D).

To investigate the grating effect on the plasmonic absorption enhancement of the device, the SPR reflectivity was examined by setting the incident angles from $10^o$ to $60^o$ under p-pol (the excitation of SP) or s-pol (the non-excitation of SP) white light illumination. The reflectivity curves of each device present the relative reflectivity calculated by dividing with the reflectivity of flat reference cell. The light absorption inside of the devices would be improved, if the reflectivity values are less than 1. The reflectivity spectra of the developed OSCs are shown in Figure 4.5. Both s-pol and p-pol light were scattered and reflected by the grating surface. The phenomena could increase the light traveling path in the photoactive layer, which can promote the light management in the OSCs in the region of 400 - 600 nm (Figure 4.5 (A-D)).

The absorption enhancement peaks from metallic grating nanostructures can be observed as dip peaks at fixed incident angles in the resonant wavelength [20]. As seen in Figure 4.5 (C), the resonant peaks are demonstrated at the wavelengths above 600 nm under p-pol light illumination and the peaks slightly shift toward longer wavelengths from 650 to 820 nm when increase the incident angles from $10^o$ to $60^o$, respectively. It is indicated that the enhancement of the electric fields in fabricated device would be obtained [22]. Whereas, no dip peaks at longer wavelength are observed under s-pol light illumination. It is known that the SPR is not occurred without the SP excitation. Also, we cannot observe the resonant peaks at flat device for both of p-pol and s-pol illumination (Figure 4.5 (D)). The results suggest that the surface plasmons enhancement can be originated by grating nanostructure and GCSPR would enhance the photovoltaic efficiency in the developed devices. Additionally, similar reflectivity spectra are observed for other devices under p-pol and s-pol as shown in Figures 4.6 and 4.7, respectively. The incorporation of metallic grating nanostructure on the surface of photoactive layer exhibits an improvement of light management and increase the interfacial area without expanding the thickness of absorber layers [21, 24]. Therefore, the combination

of plasmonic AuNSs:AuNRs with BD-R grating-nanostructure in the devices is expected to improve the photovoltaic performance of devices.

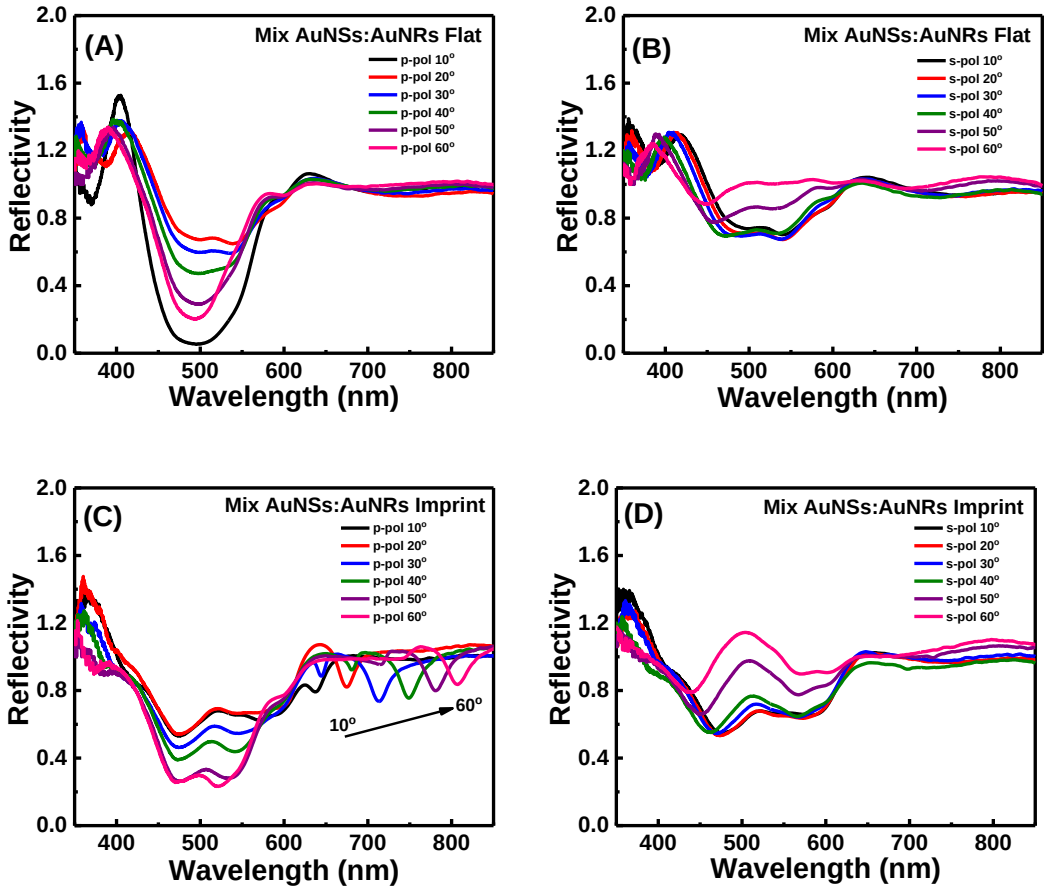


**Figure 4.5** SPR reflectivity curves of the plasmonic OSCs adding AuNSs:AuNRs, (A and B) without BD-R grating (flat device) and (C and D) with BD-R grating under p-pol or s-pol illumination, measured at fixed incident angles from 10° to 60°.

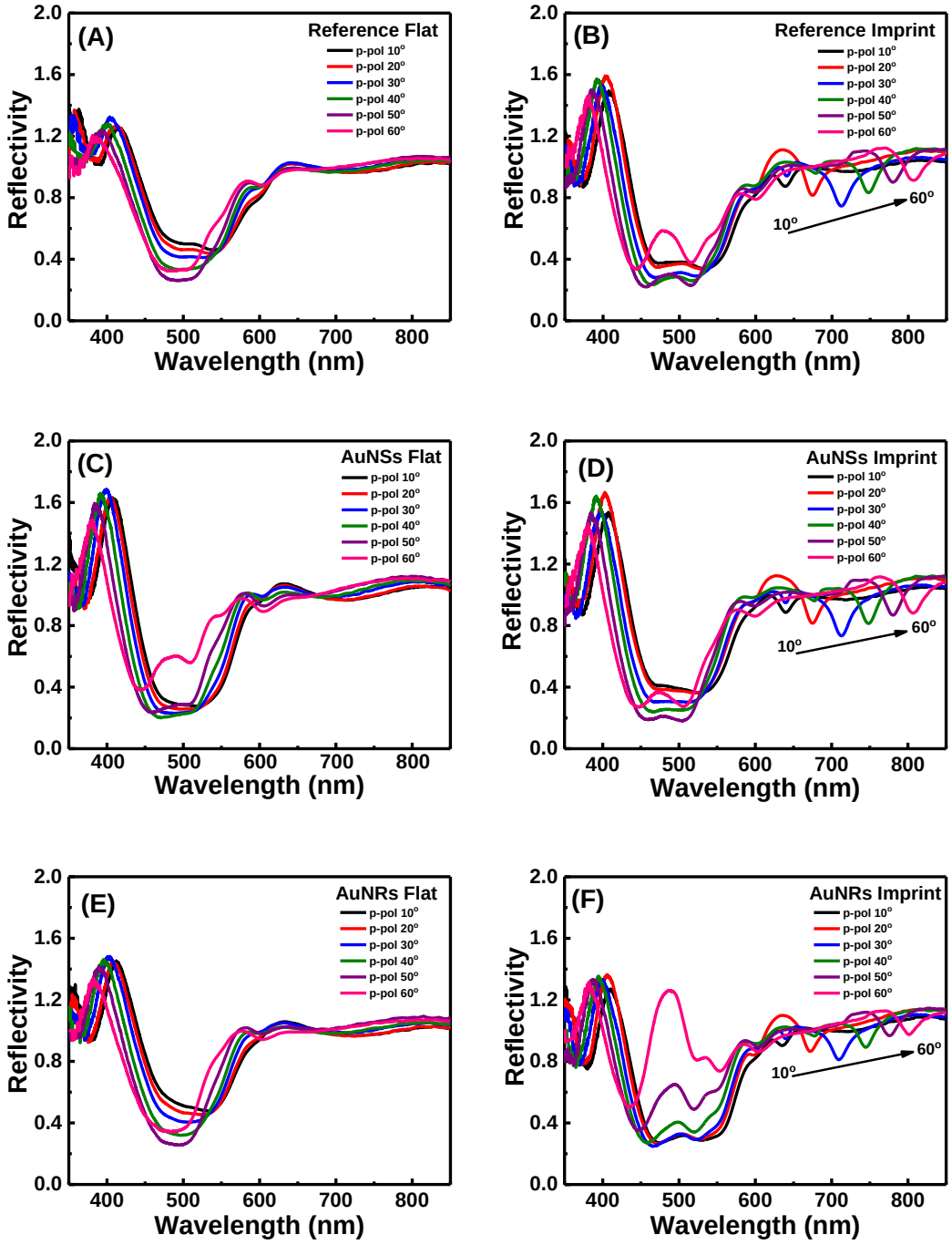


**Figure 4.6** SPR reflectivity curves of the fabricated OSCs (A) reference flat, (B) reference BD-R, (C) AuNSs flat, (D) AuNSs BD-R, (E) AuNRs flat, and (F) AuNRs BD-R. The reflectivity curves were recorded at various incident angles under illumination of p-pol light.

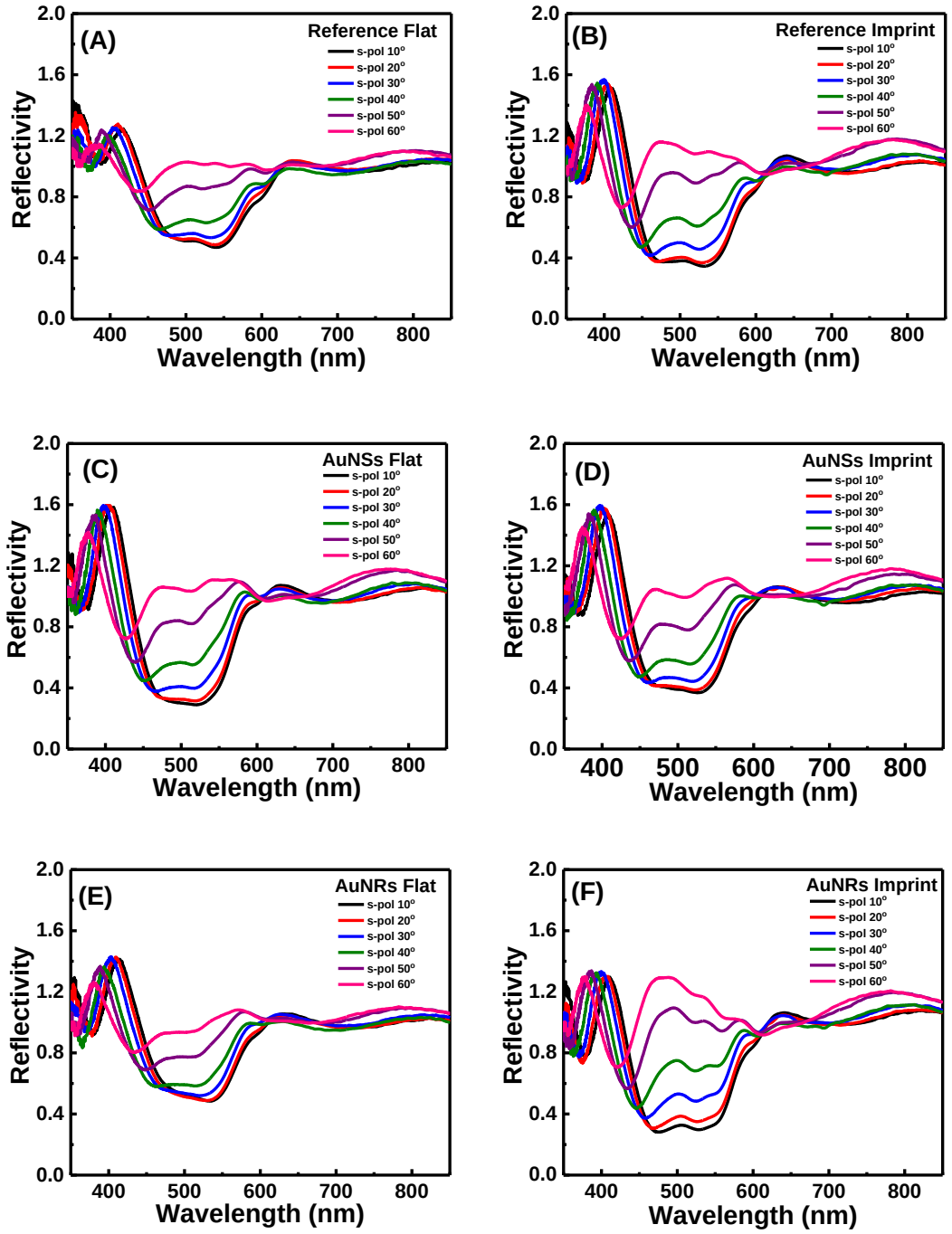


**Figure 4.7** SPR reflectivity curves of the fabricated OSCs (A) reference flat, (B) reference BD-R, (C) AuNSs flat, (D) AuNSs BD-R, (E) AuNRs flat, and (F) AuNRs BD-R. The reflectivity curves were recorded at various incident angles under illumination of s-pol light.

### 4.3.2 The electrical performances of hybrid plasmonic solar cells

The device performance is highly sensitive to the concentration of the mixture AuNSs:AuNRs blended into the HTL. Therefore, the optimal concentrations of mixture AuNSs:AuNRs solution was examined in order to gain the OSCs provided a great efficiency. The current density versus voltage (*J-V*) characteristic and the photovoltaic parameters of the fabricated OSCs are shown in Figure 4.8 and Table 4.1, respectively.

**Table 4.1** Photovoltaic parameters of the OSCs

| **Devices** | **Parameters** | | | | |
|---|---|---|---|---|---|
| | $J_{sc}$ **(mA·cm$^{-2}$)** | $V_{oc}$ **(V)** | **FF (%)** | **PCE (%)** | **Enhancement (%)** |
| Reference Flat | 6.84±0.02 | 0.59 | 0.60 | 3.20±0.03 | - |
| AuNSs Flat | 7.07±0.15 | 0.59 | 0.60 | 3.34±0.02 | 4.37 |
| AuNRs Flat | 6.99±0.07 | 0.59 | 0.60 | 3.27±0.04 | 2.19 |
| AuNSs:AuNRs (1:1) Flat | | | | | |
| 0.030 mM | 7.01±0.00 | 0.59 | 0.60 | 3.31±0.04 | 3.44 |
| 0.050 mM | 7.11±0.02 | 0.58 | 0.62 | 3.41±0.01 | 6.56 |
| 0.070 mM | 7.16±0.04 | 0.59 | 0.61 | 3.45±0.03 | 7.81 |
| 0.100 mM | 7.05±0.0 | 0.59 | 0.61 | 3.39±0.01 | 5.94 |

All devices incorporating with AuNSs:AuNRs exhibit an enhancement of $J_{sc}$ and PCE when compared to the reference device without the addition of AuNPs. The $V_{oc}$ and the FF are found to be insignificant change. While, the $J_{sc}$ value of the device increase by 4.68% from 6.84 mA·cm$^{-2}$ to 7.16 mA·cm$^{-2}$ and the PCE is improved by 7.81% from 3.20% to 3.45%, when the concentration of AuNSs:AuNRs increased up to 0.070 mM. After increasing the concentration of AuNSs:AuNRs (0.100 mM), the $J_{sc}$ and PCE values drop to 7.05 mA·cm$^{-2}$ and 3.39%, respectively. Generally, the high density of AuNPs will easily aggregate which

will form undesired conducting paths between the ITO and the metal contact [13]. Thus, the lower efficiency at high concentration might be resulting from the aggregation of AuNPs, resulted in the decreasing in electrical property of the device.

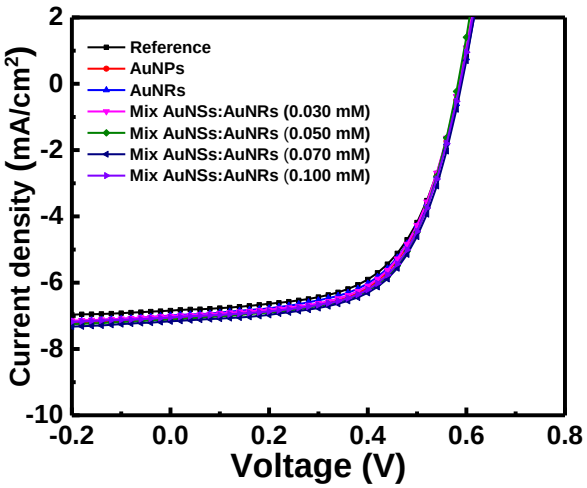


**Figure 4.8** *J-V* characteristics of the developed photovoltaic devices with different concentrations and the reference cell.

Furthermore, the EIS was also applied for analysis the interfacial properties in the OSCs under solar light illumination. The Nyquist plots of the impedance spectra of the developed OSCs and the simple equivalent circuit model (inset) are shown in Figure 4.9. Single semicircular curves are observed at all devices. The series resistance ($R_s$) value represents the resistive loss in the ITO and PEDOT:PSS, corresponding to the intersection of the semicircles [13]. From the result, the $R_s$ values of the devices incorporating AuNSs:AuNRs are slightly smaller than that of the reference cell, indicating that the reduction of interfacial contact resistance in the fabricated devices.

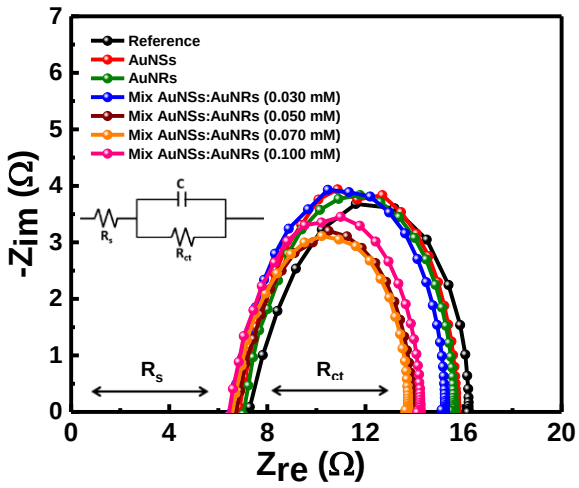


**Figure 4.9** Impedance spectroscopy of photovoltaic device, Nyquist plots of flat devices incorporating with AuNSs:AuNRs.

In the case of CPE in parallel with a $R_{ct}$, it is corresponding to the chemical capacitance which is used to describe a distribution of relaxation times at the donor/acceptor interfaces [29]. The bulk resistance of the device is decreased when the AuNSs:AuNRs was included in the fabricated OSCs. Which is related to an increasing in the number of charge carriers in the P3HT:PCBM layers or lower contact resistance between organic layer [12]. The $R_{ct}$ value of each OSCs are presented as follows: reference OSCs (8.9 Ω), developed OSCs incorporating AuNSs:AuNRs; (8.7 Ω, 0.030 mM), (7.1 Ω, 0.050 mM), (6.9 Ω, 0.070 mM), and (7.4 Ω, 0.100 mM). The improvement of photovoltaic properties is attributed to the decrease in electrical resistance and the enhancement of optical property of AuNPs embedded in the OSCs. As the results, the OSCs incorporating AuNSs:AuNRs with the concentration of 0.070 mM exhibits the highest efficiency enhancement and the lowest resistance; therefore, this condition is selected for further study.

The hybrid plasmonic OSCs were also constructed by incorporation of AuNSs:AuNRs with metallic grating nanostructure in order to enhance the efficiency. The BD-R grating nanopattern was imprinted on the surface of photoactive layer and the device was coated with Al as the back electrode. The effect of dual metallic nanostructure on the photovoltaic

properties of developed OSCs was investigated under the same experiment. The corresponding *J-V* characteristics of the optimal OSCs with and without metallic grating are shown in Figure 4.10 and the photovoltaic parameters are summarized in Table 4.2.

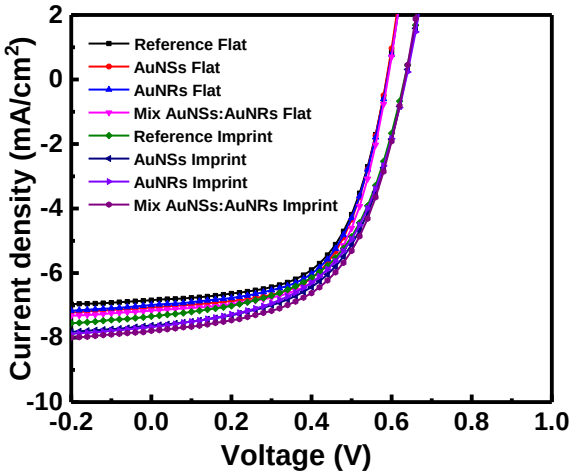


**Figure 4.10** *J-V* characteristics of the developed photovoltaic devices; flat and BD-R imprinting cells.

As seen in the *J-V* plots, the devices covered with grating-nanostructure clearly exhibit higher $J_{SC}$ compared to the flat devices. In the case of flat devices performances, the dual AuNSs:AuNRs OSC shows a great efficiency improvement higher than those of OSCs incorporated with AuNSs and AuNRs. The photovoltaic enhancements are particularly induced by the synergistic of between AuNSs and AuNRs due to the localized surface plasmon effect, which enhanced the optical path lengths via light scattering as well as increasing light absorption by the photoactive layer [17, 18].

**Table 4.2** Photovoltaic parameters of the hybrid plasmonic OSCs with and without metallic grating nanostructures under solar light illumination.

| Fabricated devices | Parameters | | | | |
|---|---|---|---|---|---|
| | $J_{sc}$ (mA·cm$^{-2}$) | $V_{oc}$ (V) | FF (%) | PCE (%) | Enhancement (%) |
| Reference Flat | 6.84±0.02 | 0.59 | 0.60 | 3.20±0.03 | - |
| AuNSs Flat | 7.07±0.15 | 0.59 | 0.60 | 3.34±0.02 | 4.37 |
| AuNRs Flat | 6.99±0.07 | 0.59 | 0.60 | 3.27±0.04 | 2.19 |
| Mix AuNSs:AuNRs Flat | 7.16±0.04 | 0.59 | 0.61 | 3.45±0.03 | 7.81 |
| Reference BD-R Imprint | 7.50±0.05 | 0.63 | 0.54 | 3.42±0.04 | 6.88 |
| AuNSs BD-R Imprint | 7.68±0.08 | 0.63 | 0.55 | 3.56±0.01 | 11.25 |
| AuNRs BD-R Imprint | 7.84±0.11 | 0.63 | 0.53 | 3.52±0.08 | 10.00 |
| Mix AuNSs:AuNRs BD-R Imprint | 7.95±0.05 | 0.63 | 0.54 | 3.65±0.01 | 14.06 |

All of the plasmonic OSCs with metallic grating indeed exhibit the improvement of performances. The grating devices incorporated with only AuNSs and AuNRs exhibit great $J_{sc}$ values of 7.68 mA·cm$^{-2}$ and 7.84 mA·cm$^{-2}$, indicating large $J_{sc}$ enhancements of approximately 12.28% and 14.62%, respectively. The improvement attributed to increase the PCE values of 3.56 % and 3.52 % which is a considerable PCE enhancement percentage of 11.25% and 10.0 %, respectively. Interestingly, the dual AuNSs:AuNRs reveals the best enhancement which is enormously improved the $J_{sc}$ of up to 16.23% (from 6.84 mA·cm$^{-2}$ to 7.95 mA·cm$^{-2}$) and enhanced the PCE of 14.06% (from 3.20% to 3.65%), respectively, compared to the corresponding values from the reference cell without a grating structure. In this study, aqueous solutions of AuNPs (AuNSs and AuNRs) were directly blended in the PEDOT:PSS layer. Due to water solubility, they can merge in HTL with a good distribution.

An enhancement of performances in solar cell was indeed originated from AuNPs within our devices via broadening the light absorption in visible region. Additionally, the combination of plasmonic OSCs with GCSPR leads to increase the photocurrent via the efficient light trapping and the reduction of electrical resistance.

### 4.3.3 The incident photon-to-current efficiency (IPCE)

To study the cooperative effects between AuNPs (AuNSs and AuNRs) and metallic grating nanostructure in the OSC performances, especially photocurrent responses or $J_{sc}$, the IPCE was characterized at the wavelength from 300 to 800 nm as shown in Figure 4.11.

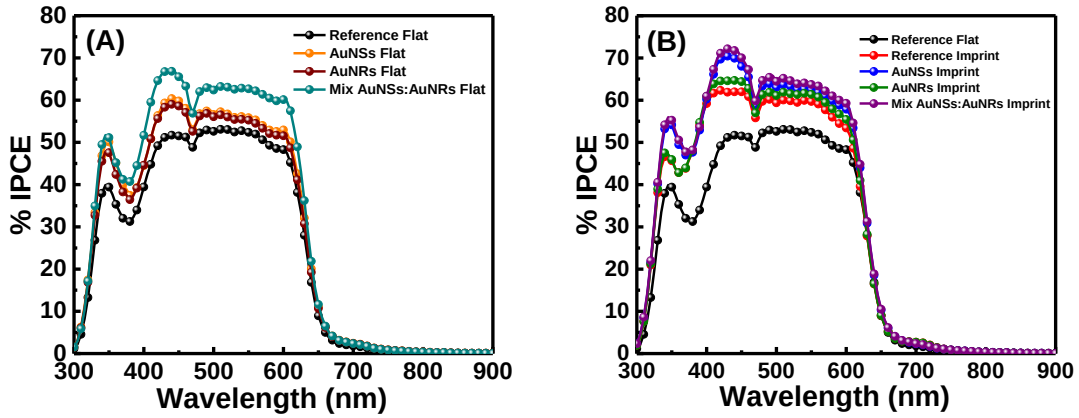


**Figure 4.11** IPCE spectra compared to the reference cell, (A) Flat OSCs and (B) BD-R imprinting OSCs incorporated with AuNSs, AuNRs, and mix AuNSs:AuNRs, respectively, measuring under irradiation of non-pol light.

Compared to the flat reference cell, the developed OSCs demonstrate an improvement in the IPCE spectra over the broad wavelength range of 300-800 nm. (Here, the dip peak at around 450 nm is not related to the device performance, it is produced from the characteristic of light source.) Interestingly, the hybrid plasmonic solar cells incorporated with grating nanostructures obviously enhance the IPCE. The IPCE of grating OSCs were further measured at different incident angle from $30^{o}$ to $50^{o}$ under non-polarized light illumination in order to study the effect of grating nanostructure on photovoltaic performance enhancement.

To understand the metallic nanostructure enhanced the IPCE of fabricated device, the E.F. of the extracted IPCE between flat reference cell and hybrid plasmonic device was calculated and the results are shown in Figure 4.12. The photovoltaic devices incorporated with BD-R grating pattern clearly exhibit an enhancement over a wide wavelength range with a similar fashion. The patterning devices remarkably exhibit the broadband absorption enhancement at the wavelength regions longer than 650 nm, which are represented the SPR characteristic of grating structure inside OSCs. The enhancement peaks gradually redshift when the incident angle increased from $30^{o}$ to $50^{o}$, respectively. Additionally, the E.F. of the plasmonic devices from the region from 650 to 800 nm is related to the SPR reflectivity spectra. The comparison of E.F. of developing device at each incident angle ($0^{o}$ – $50^{o}$) is shown in Figure 4.13. As compared to the reference device, the addition of AuNPs into the OSCs reveal IPCE E.F. in the visible wavelength regions particularly around 450-650 nm, inducing from the absorption of AuNPs within the device. Furthermore, the device incorporated with mixed AuNSs:AuNRs shows the highest enhancement.

AuNPs-induced LSPR effect can enhance the effective absorption cross-section by coupling the plasmonic near field to the active layer, which can enhance the absorption capability of the devices [30]. These suggesting that the corporation of AuNPs in HTL and construction of BD-R grating on the photoactive layer of the device offers the beneficial to enhance the OSCs performance due to efficient light harvesting, light scattering, and increase in interfacial area.

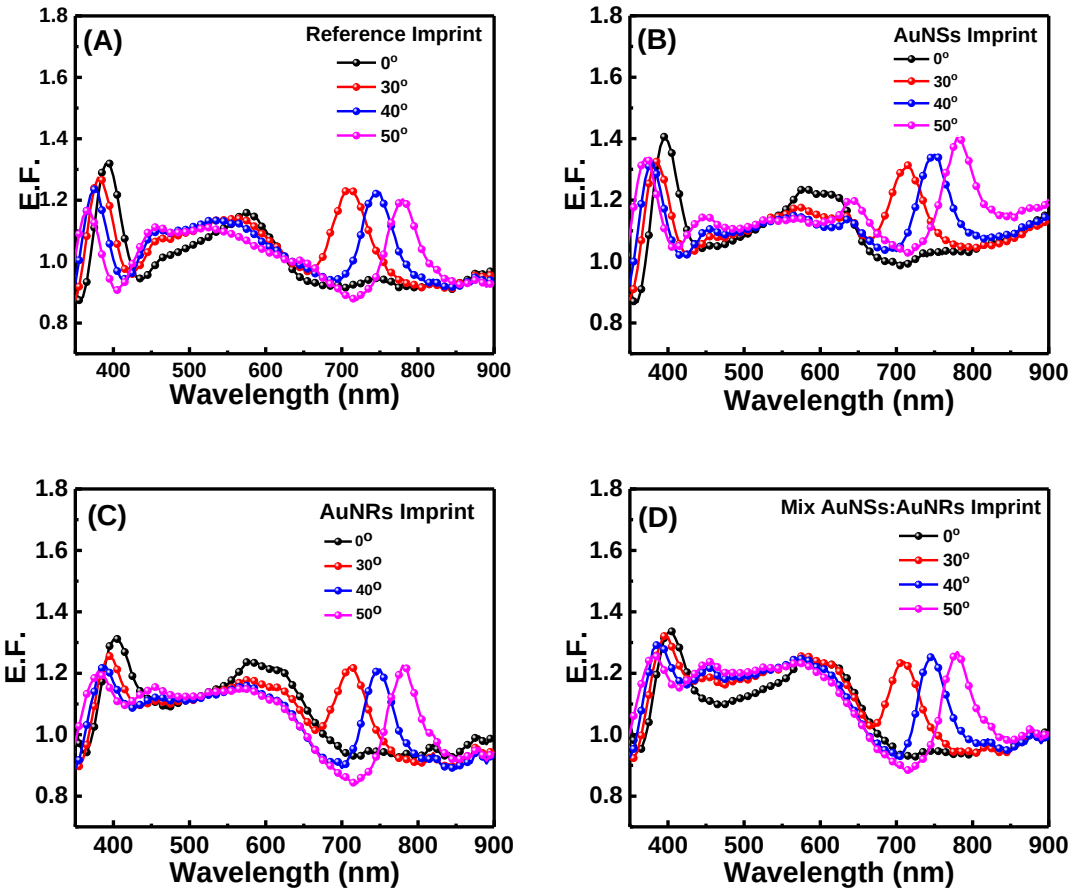


**Figure 4.12** IPCE E.F. spectra of patterning devices, reference imprinting cell without the insertion of AuNPs (A), the developing cell incorporated AuNSs (B), AuNRs (C), and mixed AuNSs:AuNRs (D), performed at fixed incident angles from 30° to 50° under irradiation of normal light.

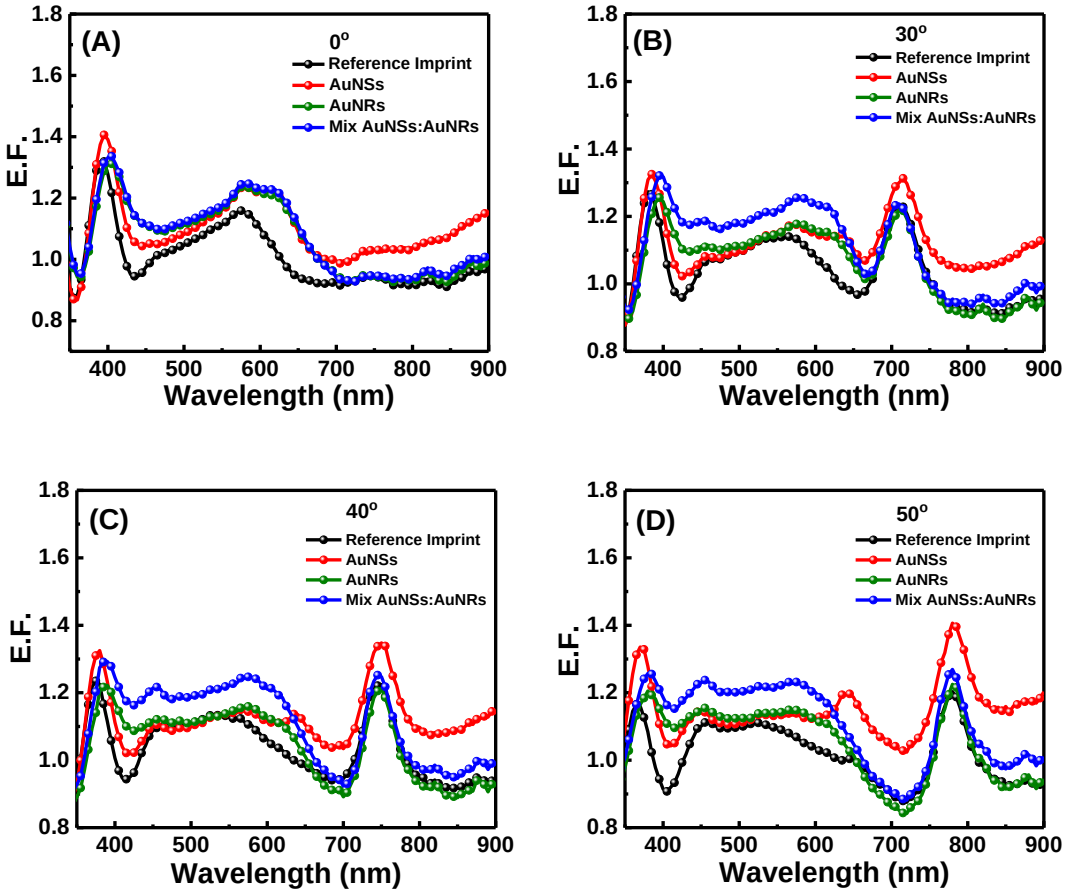


**Figure 4.13** IPCE E.F. spectra of different patterning devices including reference cell, AuNSs, AuNRs, and mixed AuNSs:AuNRs at the incident angle of 0° (A), 30° (B), 40° (C) and 50° (D), respectively. The experiment was measured at fixed incident angles from 0° to 50° under irradiation of non-polarized light.

## 4.4 SUMMARY

The hybrid plasmonic OSCs incorporating GCSPR were successfully fabricated in this work. A device structure, ITO/AuNSs:AuNRs:PEDOT:PSS/P3HT:PCBM/Al grating electrode, exhibited an excellent improvement in photovoltaic performances. As compared to the control, almost 15% enhancement on PCE value (3.65%) was obtained from the AuNSs:AuNRs with grating platform. Different LSPR bands between AuNSs and AuNRs broadened light absorption while GCSPR induced the light scattering within photovoltaic device. Thus, the synergistic effect of both LSPR and GCSPR enormously increase the optical

property. In addition, the device included dual systematic nanostructure, giving the best improvement in solar cell efficiency. Therefore, this systematic platform would be used as an alternative way toward higher efficiency OSCs.

## 4.5 REFERENCES


[1] Stratakis, E. and E. Kymakis, *Nanoparticle-based plasmonic organic photovoltaic devices*. Materials Today, 2013. **16**(4): p. 133-146.

[2] Kang, M.-G., M.-S. Kim, J. Kim, and L.J. Guo, *Organic solar cells using nanoimprinted transparent metal electrodes*. Advanced Materials, 2008. **20**(23): p. 4408-4413.

[3] Chou, C.-H. and F.-C. Chen, *Plasmonic nanostructures for light trapping in organic photovoltaic devices*. Nanoscale, 2014. **6**(15): p. 8444-8458.

[4] Borchert, H., *Elementary processes and limiting factors in hybrid polymer/nanoparticle solar cells*. Energy & Environmental Science, 2010. **3**(11): p. 1682-1694.

[5] Park, J.Y., N.R. Hendricks, and K.R. Carter, *Solvent-assisted soft nanoimprint lithography for structured bilayer heterojunction organic solar cells*. Langmuir, 2011. **27**(17): p. 11251-11258.

[6] Liu, C.-M., C.-M. Chen, Y.-W. Su, S.-M. Wang, and K.-H. Wei, *The dual localized surface plasmonic effects of gold nanodots and gold nanoparticles enhance the performance of bulk heterojunction polymer solar cells*. Organic Electronics, 2013. **14**(10): p. 2476-2483.

[7] Wang, W., S. Wu, K. Reinhardt, Y. Lu, and S. Chen, *Broadband light absorption enhancement in thin-film silicon solar cells*. Nano Letters, 2010. **10**(6): p. 2012-2018.

[8] You, J., X. Li, F.-x. Xie, W.E.I. Sha, J.H.W. Kwong, G. Li, W.C.H. Choy, and Y. Yang, *Surface plasmon and scattering-enhanced low-bandgap polymer solar cell by a metal grating back electrode*. Advanced Energy Materials, 2012. **2**(10): p. 1203-1207.

[9] Notarianni, M., K. Vernon, A. Chou, M. Aljada, J. Liu, and N. Motta, *Plasmonic effect of gold nanoparticles in organic solar cells*. Solar Energy, 2014. **106**: p. 23-37.

[10] Li, X.H., W.E.I. Sha, W.C.H. Choy, D.D.S. Fung, and F.X. Xie, *Efficient inverted polymer solar cells with directly patterned active layer and silver back grating*. The Journal of Physical Chemistry C, 2012. **116**(12): p. 7200-7206.

[11] Zhu, J., M. Xue, R. Hoekstra, F. Xiu, B. Zeng, and K.L. Wang, *Light concentration and redistribution in polymer solar cells by plasmonic nanoparticles*. Nanoscale, 2012. **4**(6): p. 1978-1981.

[12] Nagamani, S., G. Kumarasamy, M. Song, C.S. Kim, D.-H. Kim, S.Y. Ryu, J.-W. Kang, and S.-H Jin, *Optical absorption and electrical properties of enhanced efficiency in organic solar cells as interfacial layer with Au NPs*. Synthetic Metals, 2016. **217**: p. 117-122.

[13] Ng, A., W.K. Yiu, Y. Foo, Q. Shen, A. Bejaoui, Y. Zhao, H.C. Gokkaya, A.B. Djurišić, J.A. Zapien, W.K. Chan, and C. Surya, *Enhanced performance of PTB7:$PC_{71}$BM solar cells via different morphologies of gold nanoparticles*. ACS Applied Materials & Interfaces, 2014. **6**(23): p. 20676-20684.

[14] Pangdam, A., S. Nootchanat, R. Ishikawa, K. Shinbo, K. Kato, F. Kaneko, C. Thammacharoen, S. Ekgasit, and A. Baba, *Effect of urchin-like gold nanoparticles in organic thin-film solar cells*. Physical Chemistry Chemical Physics, 2016. **18**(27): p. 18500-18506.

[15] Lu, L., Z. Luo, T. Xu, and L. Yu, *Cooperative plasmonic effect of Ag and Au nanoparticles on enhancing performance of polymer solar cells*. Nano Letters, 2013. **13**(1): p. 59-64.

[16] Sharma, M., P.R. Pudasaini, F. Ruiz-Zepeda, E. Vinogradova, and A.A. Ayon, *Plasmonic effects of Au/Ag bimetallic multispiked nanoparticles for photovoltaic applications*. ACS Applied Materials & Interfaces, 2014. **6**(17): p. 15472-15479.

[17] Hsiao, Y.-S., S. Charan, F.-Y. Wu, F.-C. Chien, C.-W. Chu, P. Chen, and F.-C. Chen, *Improving the light trapping efficiency of plasmonic polymer solar cells through photon management*. The Journal of Physical Chemistry C, 2012. **116**(39): p. 20731-20737.

[18] Phetsang, S., A. Phengdaam, C. Lertvachirapaiboon, R. Ishikawa, K. Shinbo, K. Kato, P. Mungkornasawakul, K. Ounnunkad, and A. Baba, *Investigation of a gold quantum dot/plasmonic gold nanoparticle system for improvement of organic solar cells*. Nanoscale Advances, 2019. **1**(2): p. 792-798.

[19] Yang, Y., K. Mielczarek, M. Aryal, A. Zakhidov, and W. Hu, *Nanoimprinted polymer solar cell*. ACS Nano, 2012. **6**(4): p. 2877-2892.

[20] Nootchanat, S., A. Pangdam, R. Ishikawa, K. Wongravee, K. Shinbo, K. Kato, F. Kaneko, S. Ekgasit, and A. Baba, *Grating-coupled surface plasmon resonance enhanced organic photovoltaic devices induced by Blu-ray disc recordable and Blu-ray disc grating structures*. Nanoscale, 2017. **9**(15): p. 4963-4971.

[21] Hara, K., C. Lertvachirapaiboon, R. Ishikawa, Y. Ohdaira, K. Shinbo, K. Kato, F. Kaneko, and A. Baba, *Inverted organic solar cells enhanced by grating-coupled surface plasmons and waveguide modes*. Physical Chemistry Chemical Physics, 2017. **19**(4): p. 2791-2796.

[22] Baba, A., N. Aoki, K. Shinbo, K. Kato, and F. Kaneko, *Grating-coupled surface plasmon enhanced short-circuit current in organic thin-film photovoltaic cells*. ACS Applied Materials & Interfaces, 2011. **3**(6): p. 2080-2084.

[23] Baba, A., K. Wakatsuki, K. Shinbo, K. Kato, and F. Kaneko, *Increased short-circuit current in grating-coupled surface plasmon resonance field-enhanced dye-sensitized solar cells*. Journal of Materials Chemistry, 2011. **21**(41): p. 16436-16441.

[24] Li, X., W.C.H. Choy, L. Huo, F. Xie, W.E.I. Sha, B. Ding, X. Guo, Y. Li, J. Hou, J. You, and Y. Yang, *Dual plasmonic nanostructures for high performance inverted organic solar cells*. Advanced Materials, 2012. **24**(22): p. 3046-3052.

[25] Tseng, W.-H., C.-Y. Chiu, S.-W. Chou, H.-C. Chen, M.-L. Tsai, Y.-C. Kuo, D.-H. Lien, Y.-C. Tsao, K.-Y. Huang, C.-T. Yeh, J.-H. He, C.-I. Wu, M.H. Huang, and P.-T. Chou, *Shape-dependent light harvesting of 3D gold nanocrystals on bulk heterojunction solar cells: plasmonic or optical scattering effect?*. The Journal of Physical Chemistry C, 2015. **119**(14): p. 7554-7564.

[26] Wang, C.C.D., W.C.H. Choy, C. Duan, D.D.S. Fung, W.E.I. Sha, F.-X. Xie, F. Huang, and Y. Cao, *Optical and electrical effects of gold nanoparticles in the active layer of polymer solar cells*. Journal of Materials Chemistry, 2012. **22**(3): p. 1206-1211.

[27] Luo, G., X. Ren, S. Zhang, H. Wu, W.C.H. Choy, Z. He, and Y. Cao, *Recent advances in organic photovoltaics: device structure and optical engineering optimization on the nanoscale*. Small, 2016. **12**(12): p. 1547-1571.

[28] Jeong, S., C. Cho, H. Kang, K.-H. Kim, Y. Yuk, J.Y. Park, B.J. Kim, and J.-Y. Lee, *Nanoimprinting-induced nanomorphological transition in polymer solar cells: enhanced electrical and optical performance*. ACS Nano, 2015. **9**(3): p. 2773-2782.

[29] Leever, B.J., C.A. Bailey, T.J. Marks, M.C. Hersam, and M.F. Durstock, *In situ characterization of lifetime and morphology in operating bulk heterojunction organic photovoltaic devices by impedance spectroscopy*. Advanced Energy Materials, 2012. **2**(1): p. 120-128.

[30] Jonas, W., D.R. B., H.H. C., W. Wolfgang, and S.-M. *Lukas, Nanostructured organic and hybrid solar cells*. Advanced Materials, 2011. **23**(16): p. 1810-1828.

# CHAPTER V

# CONCLUSIONS

Incorporation of plasmonic nanostructures into OSCs was successfully demonstrated to enhance the photovoltaic performances. Three types of AuQDs (B-AuQDs, G-AuQDs, and R-AuQDs) and AuNPs (AuNSs and AuNRs) were introduced into OSCs in order to increase the optical and electrical properties. Furthermore, the synergistic effect of metallic nanostructures namely AuQDs/AuNPs, AuQDs/GCSPR, and AuNSs:AuNRs/GCSPR was illustrated in this work. All of developed OSCs exhibited an enhancement of photovoltaic efficiency observed with increasing the $J_{sc}$ and PCE in comparison with those of reference OSCs. Typically, AuNPs with a particle size from 2 to 100 nm provided LSPR property which was matching with the photon excitation of photoactive layer in OSCs, promoting the better photocurrent and the solar cell efficiency. When the size of AuNPs is less than 2 nm, known as AuQDs, it contributes no localized plasmons. AuQDs are excited by absorption of UV light and then emit fluorescence light in the visible region. In this study, the use of AuQDs can promote broadband absorption in UV region in OSCs. Also, their fluorescence emission in visible regions can be harvested within the device.

Moreover, dual systems, including AuQDs/AuNPs, AuQDs/GCSPR, and AuNSs:AuNRs/GCSPR, showed the synergistic effect as found with greater improvements in OSCs efficiency. Enhancements of photovoltaic performances in AuQDs/plasmonic OSCs resulted from the harvesting of UV absorption and the emitted visible light from AuQDs available in the cells, in which the higher photogenerated carrier could be obtained due to the additional absorption of visible light by active layer. Furthermore, the energy/electron transfer from the AuQDs to the AuNPs could occur, in turn, promoting a better PCE improvement. In

cases of AuQDs/GCSPR and AuNSs:AuNRs/GCSPR, the imprinted pattern can increase a roughness within the OSCs, leading to increase in the interfacial area and photocurrent. Additionally, the GCSPR property offers the electromagnetic fields enhancement, enhancing the photocurrent of the device. Moreover, the incorporation of metallic grating nanostructure on the surface of photoactive layer has been carried out for light trapping enhancement. Therefore, all dual systems introduced into our OSCs are important for better light harvesting.

**RECOMENDATION FOR FUTURE WORK**

The combination of metallic nanostructures into the devices strongly enhances the OSCs properties. To achieve more light harvesting within OSCs, the incorporation of three types of AuQDs together with other plasmonic NPs like AgNPs with different sizes and shapes should be investigated. In addition, the synergistic effect from the combination of AuQDs (B-, G-, R-AuQDs) into the devices for light harvesting should be also examined.

# APPENDICES

# APPENDIX A

SUPPORTING INFORMATION FOR CHAPTER II

Investigation of Gold Quantum Dot/Plasmonic Gold Nanoparticle System Incorporated into Organic Solar Cells

**Table A2.1** Optimization of AuQDs contents in our OSCs

| **Devices** | $J_{sc}$ **(mA/cm$^2$)** | $V_{oc}$ **(V)** | **FF (%)** | **PCE (%)** |
|---|---|---|---|---|
| **Reference** | 6.85 | 0.59 | 0.59 | 3.24 |
| **AuNPs 0.1 mM** | 7.28 | 0.59 | 0.60 | 3.42 |
| **B-AuQDs/AuNPs** | | | | |
| 0.0100 mM | 6.83 | 0.58 | 0.61 | 3.28 |
| 0.0050 mM | 7.20 | 0.59 | 0.60 | 3.44 |
| 0.0025 mM | 7.11 | 0.59 | 0.62 | 3.43 |
| 0.0012 mM | 7.08 | 0.59 | 0.61 | 3.43 |
| **G-AuQDs/AuNPs** | | | | |
| 0.0100 mM | 7.00 | 0.58 | 0.60 | 3.37 |
| 0.0050 mM | 7.61 | 0.60 | 0.60 | 3.66 |
| 0.0025 mM | 7.48 | 0.59 | 0.61 | 3.59 |
| 0.0012 mM | 7.11 | 0.59 | 0.61 | 3.45 |
| **R-AuQDs/AuNPs** | | | | |
| 0.0100 mM | 7.20 | 0.59 | 0.60 | 3.46 |
| 0.0050 mM | 7.38 | 0.60 | 0.60 | 3.54 |
| 0.0025 mM | 7.14 | 0.58 | 0.61 | 3.42 |
| 0.0012 mM | 7.06 | 0.59 | 0.61 | 3.41 |

**Table A2.2** Power conversion efficiency (PCE), short circuit current density ($J_{sc}$), the average electron lifetime ($\tau_{avg}$) and the maximum frequency ($f_{max}$) of fabricated OSCs

| Devices | PCE (%) | $J_{SC}$ (mA/cm$^2$) | $\tau_{avg}$ (μs) | $f_{max}$ (kHz) |
|---|---|---|---|---|
| Reference | 3.24±0.03 | 6.85±0.08 | 5.05 | 31.62 |
| AuNPs | 3.42±0.02 | 7.28±0.05 | 5.05 | 31.62 |
| B-AuQDs | 3.32±0.02 | 7.05±0.15 | 4.48 | 35.48 |
| G-AuQDs | 3.50±0.01 | 7.33±0.02 | 4.00 | 39.81 |
| R-AuQDs | 3.45±0.04 | 7.21±0.07 | 4.00 | 39.81 |
| B-AuQDs/AuNPs | 3.44±0.04 | 7.20±0.11 | 4.48 | 35.48 |
| G-AuQDs/AuNPs | 3.66±0.03 | 7.61±0.04 | 4.00 | 39.81 |
| R-AuQDs/AuNPs | 3.54±0.01 | 7.38±0.05 | 4.00 | 39.81 |

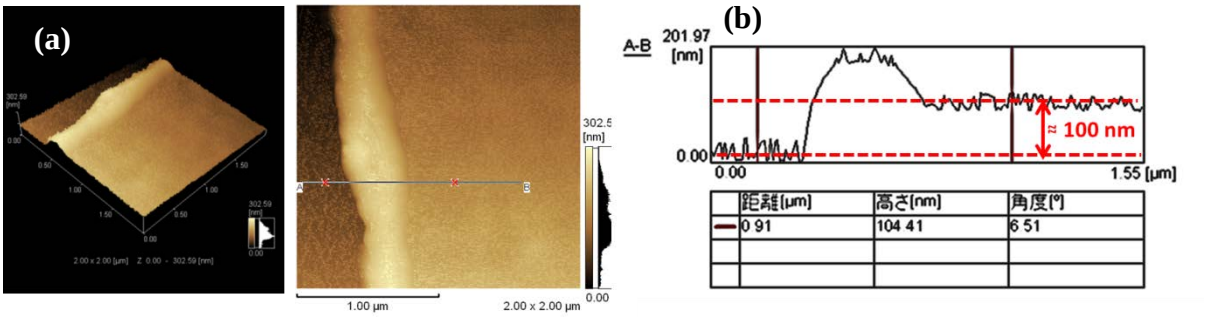


**Figure A2.1** (a) AFM image and (b) its cross-section profile of a AuQDs/PEDOT:PSS film on an substrate indicating the thickness of the film (100 nm).

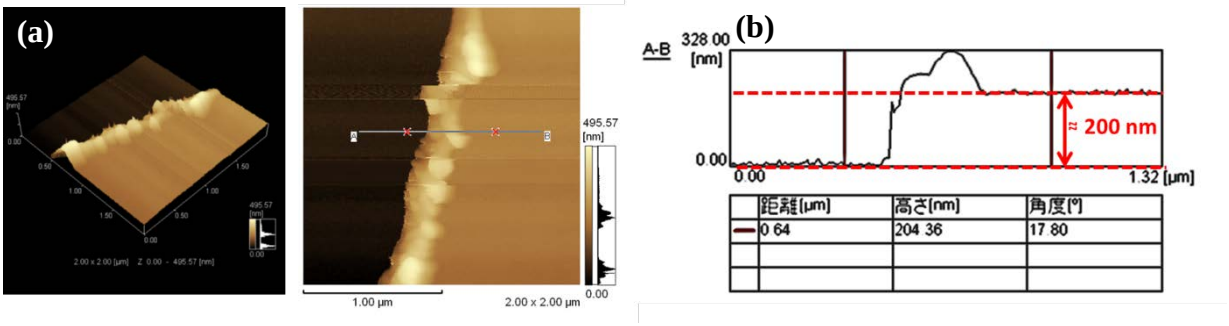


**Figure A2.2** (a) AFM image and (b) its cross-section profile of a AuQDs/PEDOT:PSS/ P3HT:PCBM film on an substrate indicating the thickness of the film (200 nm).

# APPENDIX B

SUPPORTING INFORMATION FOR CHAPTER III

Investigation of Gold Quantum Dots/Metallic Grating System Incorporated into Organic Solar Cells

**Table B3.1** Power conversion efficiency (PCE), short circuit current density ($J_{sc}$), the average electron lifetime ($\tau_{avg}$) and the maximum frequency ($f_{max}$) of fabricated OSCs

| Devices | PCE (%) | $J_{SC}$ (mA/cm$^2$) | $\tau_{avg}$ (µs) | $f_{max}$ (kHz) |
|---|---|---|---|---|
| Reference Flat | 3.27±0.03 | 7.37±0.08 | 2.52 | 63.10 |
| B-AuQDs Flat | 3.31±0.02 | 7.57±0.15 | 2.52 | 63.10 |
| G-AuQDs Flat | 3.54±0.04 | 7.83±0.07 | 2.52 | 63.10 |
| R-AuQDs Flat | 3.49±0.03 | 7.61±0.04 | 2.52 | 63.10 |
| Reference BD-R imprint | 3.61±0.02 | 7.89±0.05 | 2.52 | 63.10 |
| B-AuQDs BD-R imprint | 3.62±0.01 | 8.35±0.02 | 2.52 | 63.10 |
| G-AuQDs BD-R imprint | 3.91±0.04 | 8.41±0.11 | 2.52 | 63.10 |
| R-AuQDs BD-R imprint | 3.81±0.01 | 8.42±0.05 | 2.52 | 63.10 |

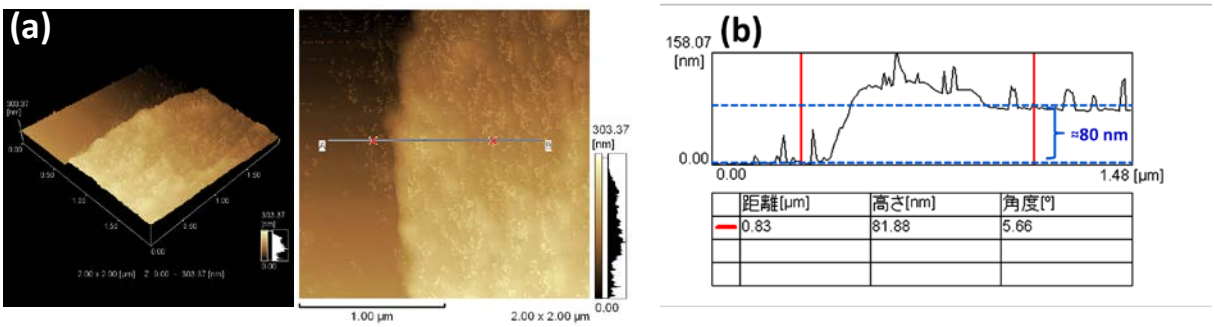


**Figure B3.1** AFM image (a) and its cross-section profile (b) of a PEDOT:PSS:AuQDs film on a substrate indicating the thickness of the film (80 nm).

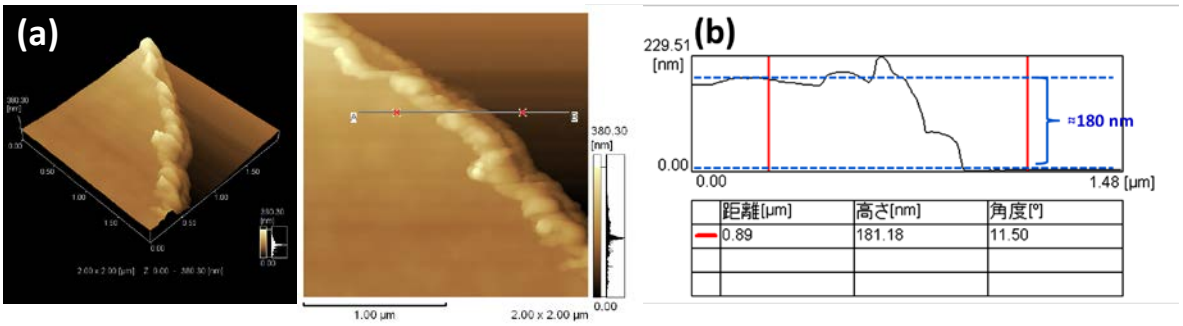


**Figure B3.2** AFM image (a) and its cross-section profile (b) of a PEDOT:PSS:AuQDs/ P3HT:PCBM film on a substrate indicating the thickness of the whole film (180 nm).

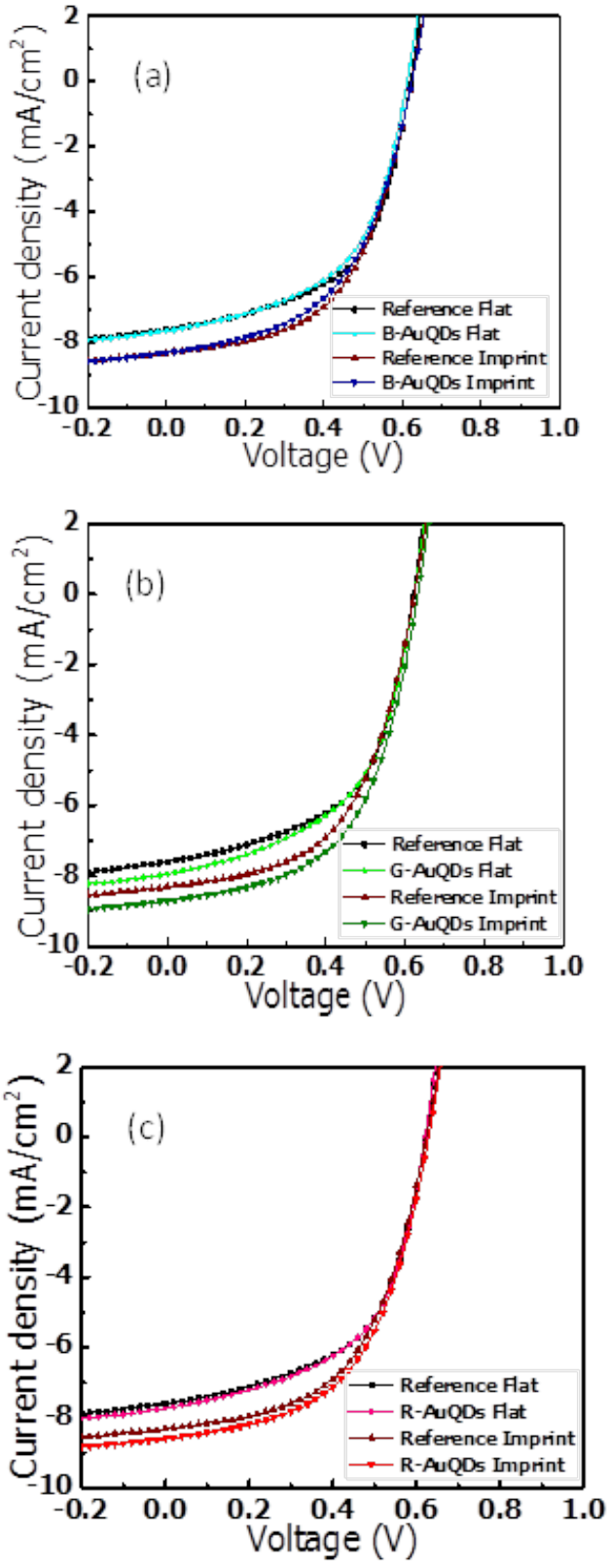


**Figure B3.3** *J-V* characteristics of the developed photovoltaic devices compared to the reference cell, including with B-AuQDs (a), G-AuQDs (b), and R-AuQDs (d), respectively.

# APPENDIX C

SUPPORTING INFORMATION FOR CHAPTER IV

Investigation of Gold Nanospheres-Gold Nanorods Hybrid/Metallic Grating Incorporated into Organic Solar Cells

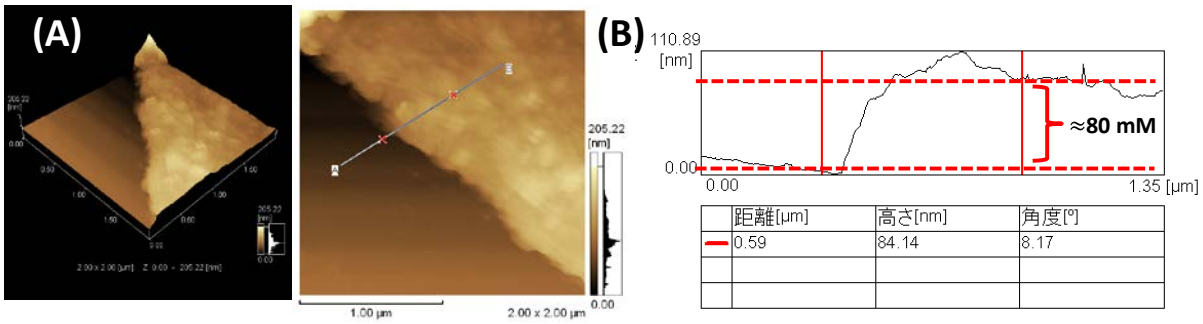


**Figure C4.1** AFM image (A) and its cross-section profile (B) of a AuNSs:AuNRs:PEDOT:PSS film on a substrate indicating the thickness of the film (80 nm).

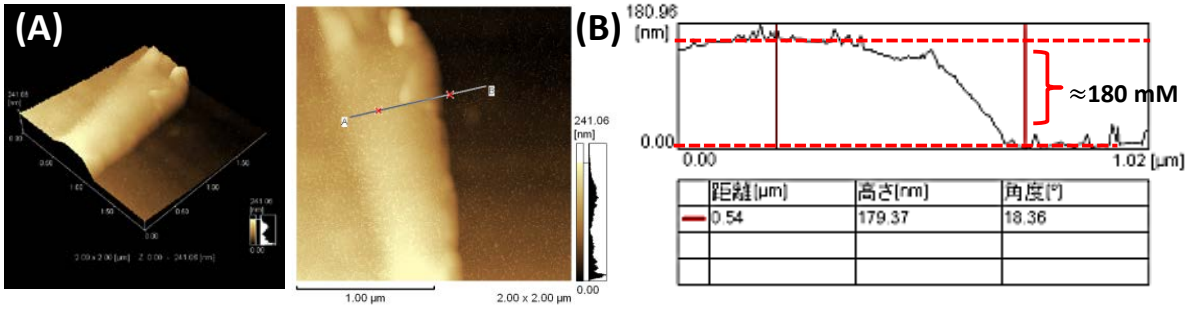


**Figure C4.2** AFM image (A) and its cross-section profile (B) of a AuNSs:AuNRs:PEDOT:PSS/P3HT:PCBM film on a substrate indicating the thickness of the whole film (180 nm).

# VITAE


**Author's Name** Miss Sopit Phetsang

**Date of Birth** 23 December 1989

**Address** 169/4 Panitsampan road Pakphanang district Nakhon Si Thammarat 80140 Thailand

**Email** phetsang_sp@hotmail.com


**Education**

| | |
|---|---|
| 2008-2012 | B.S. (Chemistry), Chiang Mai University, Chiang Mai, Thailand |
| 2012-2014 | M.S. (Chemistry), Chiang Mai University, Chiang Mai, Thailand |
| 2014-2019 | Ph.D. (Chemistry), Chiang Mai University, Chiang Mai, Thailand |
| 2016-2019 | Ph.D. (Electrical and Electronic Engineering), Niigata University, Niigata, Japan |

**Scholarship**

| | |
|---|---|
| 2012-2017 | Human Resource Development in Science Project (Science Achievement Scholarship of Thailand, SAST) |
| 2016-2017 | Graduate School of Science and Technology, Niigata University, Niigata, Japan (Double Degree Program, DDP) |

**Short visit** Campus France of Cergy-pontoise University, France (Franco-Thai) (4 September 2017 – 27 October 2017)

**Publication**


1. Phetsang, S., Phengdaam, A., Lertvachirapaiboon, C., Ishikawa, R., Shinbo, K., Kato, K., Mungkornasawakul, P., Ounnunkad, K., and Baba, A., "Investigation of a gold quantum dot/ plasmonic gold nanoparticle system for improvement of organic solar cells," Nanoscale Advances, 1, 2019, 792-798.

**Conferences**

1. Phetsang, S., pangdam, A., Mungkornasawakul, P., Ounnunkad, K., Lertvachirapaiboon, C., Shinbo, K., Kato, K., Kaneko, F., and Baba, A., "Plasmonic-enhanced polymer thin film solar cells fabricated by nanoimprinting technique," The KJF International Conference on Organic Materials for Electronics and Photonics (KJF-ICOMEP 2016), Poster Presentation, September 2016, Fukuoka, Japan.
2. Putnin, T., Phetsang, S., pangdam, A., Mungkornasawakul, P., Ounnunkad, K., Lertvachirapaiboon, C., Shinbo, K., Kato, K., Kaneko, F., and Baba, A., "Effect of metal nanoparticles on metallic grating electrodes in organic thin-film solar cells," The 77$^{th}$ Japan Society of Applied Physics Autumn Meeting, 2016 (JSAP, Autumn Meeting, 2016), Oral Presentation, September 2016, Niigata, Japan.
3. Phetsang, S., pangdam, A., Mungkornasawakul, P., Ounnunkad, K., Lertvachirapaiboon, C., Shinbo, K., Kato, K., Kaneko, F., and Baba, A., "Effect of hybrid localized surface plasmon resonances on organic thin-film solar cells," JSAP Hokuriku Shinetsu Chapter, Oral Presentation, December 2016, Toyama, Japan.
4. Phetsang, S., pangdam, A., Mungkornasawakul, P., Ounnunkad, K., Lertvachirapaiboon, C., Shinbo, K., Kato, K., Kaneko, F., and Baba, A., "Enhanced performances of organic thin-film solar cells with gold quantum dots-gold nanoparticles," The 64$^{th}$ Japan Society of Applied Physics Spring Meeting, 2017 (JSAP, Spring Meeting, 2017), Poster Presentation, March 2017, Yokohama, Japan.
5. Phetsang, S., pangdam, A., Mungkornasawakul, P., Ounnunkad, K., Lertvachirapaiboon, C., Shinbo, K., Kato, K., Kaneko, F., and Baba, A., "Investigation of gold quantum dots-gold nanoparticles enhanced organic thin-film solar cells," The Institute of Electrical Engineers of Japan (IEEJ), Oral Presentation, March 2017, Toyama, Japan.

**Award**

"Excellent paper presentation award," in the Institute of Electrical Engineers of Japan (IEEJ) annual meeting 2017, Toyama, Japan